Hierarchy of quasisymmetries and degeneracies in the CoSi family of chiral crystal materials

Lun-Hui Hu [1,2,*] Chunyu Guo [3,*] Yan Sun,[4] Claudia Felser,[4] Luis Elcoro,[5,6] Philip J. W. Moll,[3]
Chao-Xing Liu,[1,†] and B. Andrei Bernevig[7,8,9,‡]

[1]*Department of Physics, The Pennsylvania State University, University Park, Pennsylvania 16802, USA*
[2]*Department of Physics and Astronomy, University of Tennessee, Knoxville, Tennessee 37996, USA*
[3]*Laboratory of Quantum Materials (QMAT), Institute of Materials (IMX),*
École Polytechnique Fédérale de Lausanne (EPFL), CH-1015 Lausanne, Switzerland
[4]*Max Planck Institute for Chemical Physics of Solids, 01187 Dresden, Germany*
[5]*Department of Physics, University of the Basque Country UPV/EHU, Apdo. 644, 48080 Bilbao, Spain*
[6]*EHU Quantum Center, University of the Basque Country UPV/EHU*
[7]*Department of Physics, Princeton University, Princeton, New Jersey 08544, USA*
[8]*Donostia International Physics Center, P. Manuel de Lardizabal 4, 20018 Donostia-San Sebastian, Spain*
[9]*IKERBASQUE, Basque Foundation for Science, Bilbao, Spain*

In materials, certain approximated symmetry operations can exist in a lower-order approximation of the effective model but are good enough to influence the physical responses of the system, and these approximated symmetries were recently dubbed "quasisymmetries" [Nat. Phys. **18**, 813 (2022)]. In this paper, we reveal a hierarchy structure of the quasisymmetries and the corresponding nodal structures that they enforce via two different approaches of the perturbation expansions for the effective model in the chiral crystal material CoSi. In the first approach, we treat the spin-independent linear momentum (k) term as the zero-order Hamiltonian. Its energy bands are fourfold degenerate due to an $SU(2) \times SU(2)$ quasisymmetry. We next consider both the k-independent spin-orbit coupling (SOC) and full quadratic k terms as the perturbation terms and find that the first-order perturbation leads to a model described by a self-commuting "stabilizer code" Hamiltonian with a U(1) quasisymmetry that can protect nodal planes. In the second approach, we treat the SOC-free linear k term and k-independent SOC term as the zero order. They exhibit an SU(2) quasisymmetry, which can be reduced to U(1) quasisymmetry by a choice of quadratic terms. Correspondingly, a twofold degeneracy for all the bands due to the SU(2) quasisymmetry is reduced to twofold nodal planes that are protected by the U(1) quasisymmetry. For both approaches, including higher-order perturbation will break the U(1) quasisymmetry and induce a small gap ∼1 meV for the nodal planes. These quasisymmetry protected near degeneracies play an essential role in understanding recent quantum oscillation experiments in CoSi.

I. INTRODUCTION

Symmetry describes the invariance of a system under certain operations and plays a fundamental role in almost all branches of physics. In condensed matter physics, different quantum states of matter and the phase transition between them can be characterized via the principle of spontaneous symmetry breaking, as formulated in the Landau-Ginzburg theory [1]. For example, the crystallization of a solid breaks continuous translation to discrete translation and the formation of ferromagnetism in a magnet breaks the full rotation symmetry, even though the microscopic interaction in these systems has full translation and rotation symmetries [2].

In the scenario of spontaneous symmetry breaking, the high-symmetry states appear at a high-energy scale (or high temperature); when the energy scale is lowered, symmetry-breaking states start appearing. However, the opposite scenario also exists, and a high-symmetry state can emerge in the low-energy sector of a system [3,4]. For example, the Lorentz symmetry is accompanied by the emergence of the two-dimensional Dirac equation as a low-energy effective theory in graphene or at the surface of topological insulators, although both systems are nonrelativistic [5–11]. The existence of Dirac fermions and Lorentz symmetry leads to several exotic physical properties of graphene and topological insulators, making them appealing platforms to test quantum relativistic phenomena in table-top experiments [12]. Besides the space-time symmetry, emergent symmetries can also exist for the internal degree of freedom. For example, due to the spin and valley degrees, graphene has an additional SU(4) symmetry, which leads to intriguing physical phenomena, such as SU(4) quantum Hall ferromagnets [13–15].

Recently, we introduce the concept of "quasisymmetry" to describe such emergent internal symmetry [16]. More precisely, we refer to quasisymmetry as a symmetry

---
*These authors contributed equally to this work.
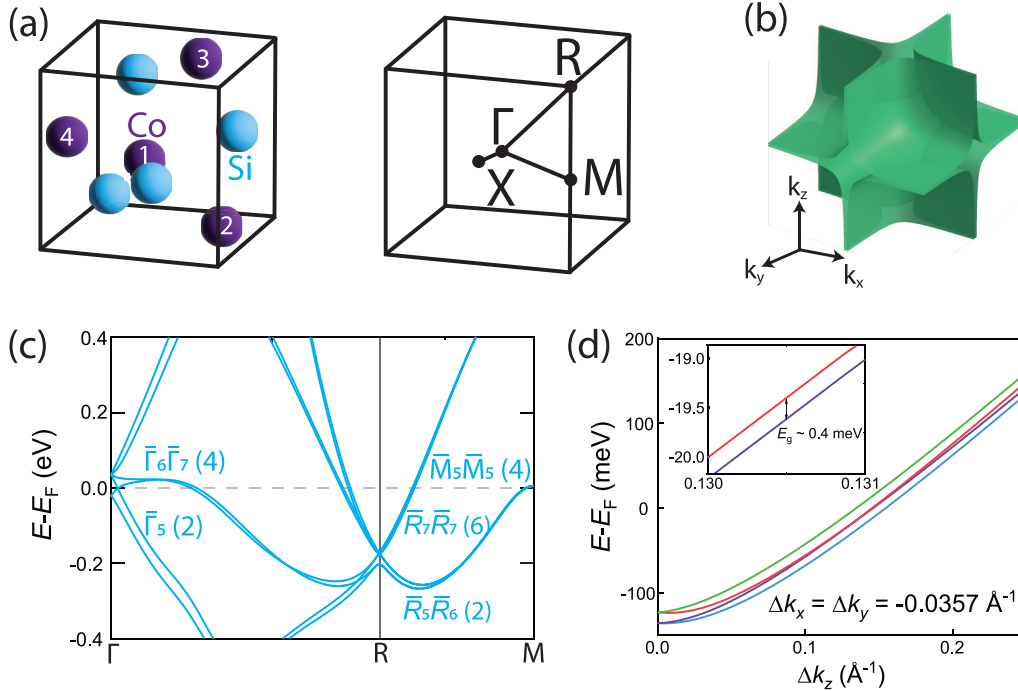†cxl56@psu.edu
‡bernevig@princeton.edu

125145-1

FIG. 1. (a) One unit cell with four Co and Si atoms, and the Brillouin zone with high-symmetry points (Γ, R, X, M). (b) Shows the quasisymmetry protected nodal planes. (c) Electronic band structure of CoSi along $\Gamma - R - M$ lines. The irreps of the energy states at high-symmetry points are labeled. (d) The DFT bands along the $(-0.0357, -0.0357, k_z)$ direction and the inset shows the tiny gap ~ 0.4 meV.

operator that only exists in a lower-order approximation of the effective Hamiltonian but is good enough to influence the physical responses of the material. The crystalline symmetry of solid material without magnetic order, described by 17 space groups in two dimensions (2D) and 230 space groups in 3D [17], gives a strong constraint on the form of the low-energy effective model (in the spirit of $\mathbf{k} \cdot \mathbf{p}$ type of Hamiltonian) around high symmetry momenta in the Brillouin zone [18–22]. As a consequence, if one only keeps lower-order k terms in the expansion, the effective Hamiltonian can generally possess additional symmetries, beyond the crystalline symmetry itself. With keeping further powers of $\mathbf{k}$ in the $\mathbf{k} \cdot \mathbf{p}$ expansion, these additional symmetries will gradually be broken by the higher-order $\mathbf{k}$ terms or other perturbations [e.g., spin-orbit coupling (SOC)], thus forming a hierarchy structure of quasisymmetry groups.

This paper aims in revealing such a hierarchy structure of quasisymmetries in the low-energy effective Hamiltonian expansion for different orders of the momentum $\mathbf{k}$ for the material compound CoSi with a chiral crystal structure (space group No. 198). Recent experimental and theoretical work [16] has shown that the quasisymmetry exists in this compound and leads to the near-nodal-planes that are located at non-high-symmetric momenta, which are essential in understanding the transport measurement of quantum oscillations in CoSi. In this paper, we will systematically discuss two approaches to constructing the effective Hamiltonian perturbatively for CoSi, and reveal the hierarchy structure of quasisymmetries in different orders of the perturbation expansion. As discussed in Fig. 2 (see below), our first approach treats the SOC-free linear k term as the zero order, which leads to a fourfold degeneracy protected by SU(2) × SU(2)

quasisymmetry. Then we consider both the k^2 terms and SOC as the perturbation and project them into the subspace of these fourfold degenerate bands. The resulting effective Hamiltonian shows a striking "self-commuting" feature that results in a U(1) quasisymmetry for the protection of nodal planes in non-high-symmetric momenta [Fig. 1(b), see below]. Our second approach (Fig. 3, see below) treats both linear k term and SOC as the zero-order Hamiltonian and shows all the bands are doubly degenerate due to the orbital SU(2) quasisymmetry. We then consider k^2 terms as a perturbation and classify them into three different groups with each group selectively breaking the SU(2) quasisymmetry into U(1) quasisymmetry along a certain direction, which can also protect nodal planes. In both approaches, the second-order perturbation can induce a tiny gap (~ 1 meV for CoSi). In this sense, we dubbed these quasisymmetry protected nodal planes to be near-nodal planes.

II. EFFECTIVE k · p MODEL FOR COSI

The crystal CoSi family crystallizes in a chiral cubic structure of space group (SG) $P2_1 3$ (No. 198) without a center of inversion [23]. Its cubic lattice with the lattice constant $a_0 = 4.433$ Å, as shown in Fig. 1(a), contains four Si atoms and four Co atoms in one unit cell. The corresponding Brillouin zone (BZ) is shown in Fig. 1(c), where high-symmetry points including Γ, R, and M are marked. With the Seitz notation for the nonsymmorphic symmetry operations, the three generators of SG 198 are $S_{2x} = \{C_{2x} | \frac{1}{2} \frac{1}{2} 0\}$, $S_{2y} = \{C_{2y} | 0 \frac{1}{2} \frac{1}{2}\}$, and $C_3 = \{C_{3,(111)} | 000\}$. The system has also time-reversal symmetry $\mathcal{T}$. With the density function theory (DFT) calculations, we obtain the electronic band structure with SOC, as shown

TABLE I. The parameters for the $\mathbf{k} \cdot \mathbf{p}$ Hamiltonian $\mathcal{H}_R$.

Parameter	C_0	B_1	A_1	C_1	C_2	C_3	λ_0
Value	−0.18	2.123	0.853	−0.042	0.546	3.345	0.0075
Unit	eV	eV × Å²	eV × Å	eV × Å²	eV × Å²	eV × Å²	eV

in Fig. 1(c) along the $\Gamma - R - M$ lines. Hole Fermi pockets are found around Γ while electron Fermi pockets exist around R, $\mathbf{k}_R = (\pi, \pi, \pi)$. Here we focus on the electronic bands around R. For the SOC-free band structures, there are fourfold degenerate states (without spin degeneracy) at the R point, which disperse linearly around R and give rise to the electron Fermi pockets. The corresponding single-valued irreducible representation (irrep) is $R_1 R_3$ based on the notations in the Bilbao Crystallographic Server [24–26]. Taking into account the spin degree of freedom, the eightfold degenerate states at R are split by SOC into higher-energy sixfold degenerate states [27] (double-valued irrep $\bar{R}_7 \bar{R}_7$) and lower-energy twofold degenerate states (double-valued irrep $\bar{R}_5 \bar{R}_6$) with a gap ∼30 meV.

As described in Ref. [16] and Appendix A, the effective model to describe the energy bands around R is constructed based on the little group at R point generated by S_{2x}, S_{2y}, C_3, and $\mathcal{T}$. Up to k^2 order, the Hamiltonian contains three parts

$$\mathcal{H}_R = \mathcal{H}_1 + \mathcal{H}_{\text{soc}} + \mathcal{H}_2, \tag{1}$$

where $\mathcal{H}_1 = C_0 + 2A_1 s_0 (\mathbf{k} \cdot \mathbf{L})$ includes a constant and linear k term, and $\mathcal{H}_{\text{soc}} = 2\lambda_0 (\mathbf{s} \cdot \mathbf{L})$. Here we define the operators

$$L_x = \tfrac{1}{2}\sigma_y \tau_0, \quad L_y = \tfrac{1}{2}\sigma_x \tau_y, \quad L_z = -\tfrac{1}{2}\sigma_z \tau_y, \tag{2}$$

which satisfies the angular momentum commutation relation $[L_i, L_j] = i\epsilon_{ijk} L_k$ with Levi-Civita symbol ϵ_{ijk} and $i = x, y, z$. $\mathbf{s}$ represents the Pauli matrix in the spin space and both σ, τ for the Pauli matrices in the orbital space. The basis for four orbitals of the σ, τ matrices are mainly (>80%) composed of the mixing between the t_{2g} and e_g orbitals of the four Co atoms, as justified by the DFT calculations. And the detailed forms of the wave functions are shown in Appendix .B

In addition, the k^2 order effective Hamiltonian $\mathcal{H}_2$ in Eq. (1) shows an intriguing structure and can be grouped into three classes,

$$\mathcal{H}_2 = \mathcal{H}_{2,\mathcal{M}_1} + \mathcal{H}_{2,\mathcal{M}_2} + \mathcal{H}_{2,\mathcal{M}_3}, \tag{3}$$

where $\mathcal{H}_{2,\mathcal{M}_i} = \mathbf{g}_i \cdot \mathbf{J}_i$ for i=1,2,3. Here we define

$$\mathbf{g}_1 = (C_2 k_x k_y, -C_3 k_x k_z, C_1 k_y k_z), \tag{4a}$$

$$\mathbf{g}_2 = (C_3 k_x k_y, C_1 k_x k_z, -C_2 k_y k_z), \tag{4b}$$

$$\mathbf{g}_3 = (C_1 k_x k_y, C_2 k_x k_z, -C_3 k_y k_z). \tag{4c}$$

and

$$\mathbf{J}_1 = (\sigma_x \tau_x, -\sigma_z \tau_x, \sigma_0 \tau_z), \tag{5a}$$

$$\mathbf{J}_2 = (\sigma_x \tau_z, \sigma_z \tau_z, \sigma_0 \tau_x), \tag{5b}$$

$$\mathbf{J}_3 = (\sigma_z \tau_0, \sigma_x \tau_0, \sigma_y \tau_y). \tag{5c}$$

The parameters for CoSi are obtained by fitting with the DFT bands [16] and listed in Table I. It should be noted that all the bands at the $k_i = \pi$ planes ($i = x, y, z$) are doubly

degenerate as a consequence of the anti-unitary symmetries $S_{2x}\mathcal{T}$, $S_{2y}\mathcal{T}$, and $S_{2z}\mathcal{T}$ in these planes [16,28,29]. Furthermore, the DFT calculations show near-nodal planes with tiny gaps ∼0.5 meV at non-high-symmetry momenta shown in Fig. 1(d), and we next discuss how to apply the perturbation theory to the model Hamiltonian $\mathcal{H}_R$ in Eq. (1) to understand these near-nodal planes, as well as the underlying quasisymmetries.

Below, we consider two approaches to understand the underlying reason of nearly degenerate nodal planes.

III. APPROACH I: SELF-COMMUTING HAMILTONIAN

We now precisely formulate the hidden quasisymmetry that may appear at low-energy in the physics of the model Hamiltonian, and start with the linear k-order Hamiltonian, SOC-free $\mathcal{H}_1$ in Eq. (1), which is invariant under the spin $\text{SU}_s(2)$ symmetry group. Moreover, an additional hidden $\text{SU}_o(2)$ symmetry also exists for $\mathcal{H}_1$ in the orbital space, and can be generated by the operators

$$\mathcal{M}_{1,2,3} = \tfrac{1}{2}\{s_0 \sigma_y \tau_z, s_0 \sigma_y \tau_x, s_0 \sigma_0 \tau_y\}, \tag{6}$$

which all commute with $\mathcal{H}_1$ and satisfy the commutation relations $[\mathcal{M}_i, \mathcal{M}_j] = i\epsilon_{i,j,k}\mathcal{M}_k$. Thus, we refer to it as the $\text{SU}_o(2)$ quasisymmetry group for $\mathcal{H}_1$. As a result, the $\text{SU}_s(2) \times \text{SU}_o(2)$ quasisymmetry group protects the fourfold degeneracy for each band $[E_{\pm}(k) = \pm A_1 k + C_0]$ at any nonzero $\mathbf{k}$ [see Fig. 2(a)]. Hereafter, we absorb the constant energy C_0 into Fermi energy E_F.

We now consider the perturbation from $\mathcal{H}_{\text{soc}}$ and $\mathcal{H}_2$. Without loss of generality, we choose four degenerate bands with positive energy $[E_+(k) = A_1 k]$ as the basis, $\{|\Psi_{+,s,i}\rangle\}$ with $s = \uparrow, \downarrow$ and i=1,2, and project $\mathcal{H}_{\text{soc}}$ and $\mathcal{H}_2$ into this subspace. Shown in Appendix C, the projected four-band model is given by

$$\mathcal{H}_P^{\text{eff}(1)}(\mathbf{k}) = E_0 + \mathcal{H}_{\text{soc}}^{\text{eff}(1)}(\mathbf{k}) + \mathcal{H}_2^{\text{eff}(1)}(\mathbf{k}), \tag{7}$$

where

$$E_0 = C_0 + A_1 k + B_1 k^2, \tag{8a}$$

$$\mathcal{H}_{\text{soc}}^{\text{eff}(1)}(\mathbf{k}) = \lambda_0 (\mathbf{k} \cdot \mathbf{s}) \omega_0, \tag{8b}$$

$$\mathcal{H}_2^{\text{eff}(1)}(\mathbf{k}) = \tilde{C} k^2 s_0 (d_{x,\mathbf{k}} \omega_x + d_{y,\mathbf{k}} \omega_y + d_{z,\mathbf{k}} \omega_z), \tag{8c}$$

with $\tilde{C} = C_1 - C_2 + C_3$. Here ω_0 is identity matrix and ω_i ($i = x, y, z$) are the Pauli matrices for the two spinless bands. The coefficients $d_{i,\mathbf{k}}$ depend on $\mathbf{k}$, and the detailed forms are given in Appendix C. Such perturbation process can be well justified by satisfying both $A_1 k \gg \lambda_0$ and $A_1 k \gg \frac{\sqrt{3}}{4}\tilde{C} k^2$, which results in the valid momentum range $0.01 < k < 1$ (Å⁻¹), corresponding to a wide Fermi energy range $8.5 \ll E_F \ll 850$ (meV). Thus, the obtained effective model is relevant for the realistic experimental situations (E_F in CoSi is 180 meV). Strikingly, we notice that the two terms in this effective Hamiltonian are self-commuting, namely,

$$\left[\mathcal{H}_{\text{soc}}^{\text{eff}(1)}(\mathbf{k}_1), \mathcal{H}_2^{\text{eff}(1)}(\mathbf{k}_2)\right] = 0, \tag{9}$$

which implies that Hamiltonian (7) is a stabilizer code Hamiltonian [30–33]. The commutation relation in Eq. (9) can be easily seen since $\mathcal{H}_{\text{soc}}^{\text{eff}(1)}$ ($\mathcal{H}_2^{\text{eff}(1)}$) contains an identity matrix
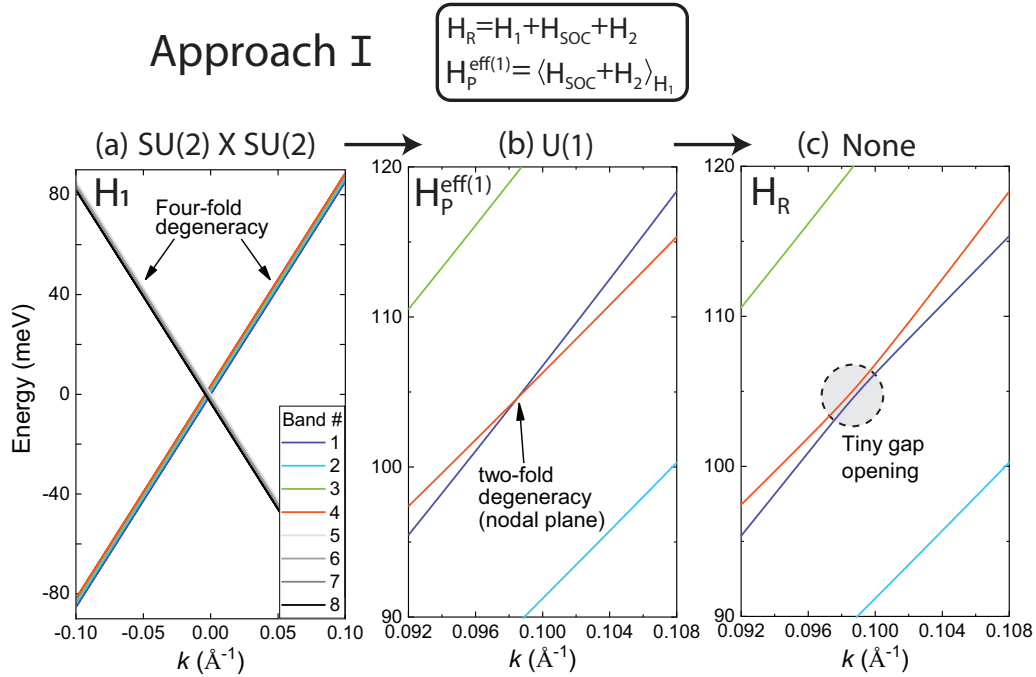
FIG. 2. The summary of the hierarchy of quasisymmetry with the Approach I (self-commuting Hamiltonian). We plot the band splitting along the non-high-symmetry direction within the spherical coordinate ($\theta = \phi = \pi/3$). The left panel shows the SU(2) × SU(2) quasisymmetry protect the fourfold degeneracy. In the middle panel, all the bands split but there exists the U(1) quasisymmetry protecting the nodal plane. The right panel shows a tiny gap appears once high-order perturbation corrections are involved.

in the ω space (spin **s** space). The self-commuting property implies the existence of a unitary symmetry operator $S_{\text{eff}} = \frac{\mathbf{k} \cdot \mathbf{s}}{|\mathbf{k}|} \omega_0$ that commutes with the whole Hamiltonian $\mathcal{H}_P^{\text{eff}(1)}$ for any momentum. S_{eff} describes an internal symmetry and can be viewed as the generator of a U(1) group.

Due to the self-commuting nature, the eigenstate of the Hamiltonian in Eq. (7) can be explicitly solved with its eigenenergy given by

$$E_{\alpha,\beta} = E_0 + \alpha\lambda_0 + \beta\sqrt{3}\tilde{C}|k_x k_y k_z|/k, \quad (10)$$

with $\alpha, \beta = \pm 1$, where α labels the eigenvalues of S_{eff}. We notice that two eigenenergies $E_{+,-}$ and $E_{-,+}$ can be equal when the condition

$$\lambda_0 = \sqrt{3}\tilde{C}|k_x k_y k_z|/k \quad (11)$$

is satisfied. It determines nodal planes of the effective model in Eq. (7) in the whole momentum space. Figure 2(b) shows the U(1) quasisymmetry protected twofold degeneracy along a non-high-symmetry line ($\theta = \phi = \pi/3$), where the spherical coordinator (k, θ, ϕ) is used with polar angle θ and azimuthal angle ϕ. The Fermi sphere crosses the nodal planes to form nodal rings at the Fermi energy, which can be extracted by combining $E_F = E_{+,-}$ with Eq. (11). Explicitly, the nodal rings at a fixed Fermi energy E_F can be determined by

$$f_N(\theta, \phi) = \frac{2A_1^2\lambda_0}{\sqrt{3}\tilde{C}E_F^2}\left[1 + \frac{2B_1E_F}{A_1^2} + \sqrt{1 + \frac{4B_1E_F}{A_1^2}}\right], \quad (12)$$

where $f_N(\theta, \phi) = |\sin 2\phi \sin 2\theta \sin \theta|$. We notice that Eq. (12) has solution only when $E_F \geqslant E_W$ with $E_W = \frac{2}{\sqrt{3}\tilde{C}}(A_1\sqrt{\sqrt{3}\tilde{C}\lambda_0} + 2B_1\lambda_0)$. It coincides to the energy

of Weyl point $E_W \approx 114.4$ meV, smaller than E_F in CoSi. Thus, we expect the Fermi energy crosses the nodal plane in a ring form for CoSi. Therefore, up to the first-order perturbation, we obtain a hierarchy of quasisymmetry for CoSi, represented by (Fig. 2)

$$\text{SU}_s(2) \times \text{SU}_o(2) \xrightarrow{\langle\mathcal{H}_{\text{soc}} + \mathcal{H}_2\rangle_{\mathcal{H}_1}} \text{U}(1), \quad (13)$$

and the corresponding energy bands are split from fourfold degeneracies at any momenta down to twofold degeneracies that form nodal planes. Including further second-order perturbation corrections generate a tiny gap for the near-nodal planes, as shown in Fig. 2(c). At $E_F = E_W$, the near-nodal rings at the Fermi energy shrink into nodal points, the Weyl points, which are stable to any order and do not rely on quasisymmetries.

The quasisymmetry S_{eff} is essential in protecting the gapless nature of the near-nodal planes in the four-band effective model. To see that, we may consider a generic four-band Hamiltonian commuting with S_{eff} for any momenta, which can only include the following terms

$$\mathcal{H}_S = \mu_0 s_0 \omega_0 + \mu_1[(\mathbf{k} \cdot \mathbf{s})\omega_0]$$
$$+ \mu_2[s_0(\mathbf{f} \cdot \boldsymbol{\omega})] + \mu_3[(\mathbf{k} \cdot \mathbf{s})(\mathbf{g} \cdot \boldsymbol{\omega})]. \quad (14)$$

Here $\mu_{0,1,2,3}$ are all positive constants, $\mathbf{f}(\mathbf{k}) = (f_1(\mathbf{k}), f_2(\mathbf{k}), f_3(\mathbf{k}))$ and $\mathbf{g}(\mathbf{k}) = (g_1(\mathbf{k}), g_2(\mathbf{k}), g_3(\mathbf{k}))$ are two vectors of generic functions of $\mathbf{k}$. $\mathcal{H}_S$ contains all the terms in Eq. (7). The eigenenergies of $\mathcal{H}_S$ are

$$E_{\alpha,\beta}(\mathbf{k}) = \mu_0 + \alpha(\mu_1 k) + \beta|\mu_2\mathbf{f}(\mathbf{k}) + \alpha\mu_3 k\mathbf{g}(\mathbf{k})| \quad (15)$$
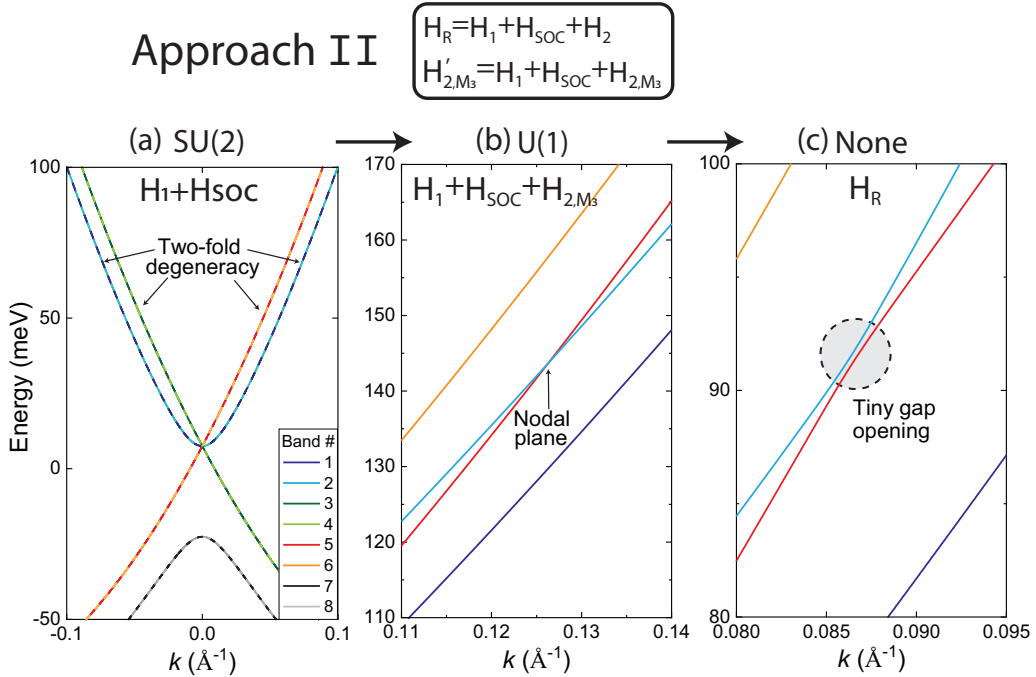
FIG. 3. The hierarchy of quasisymmetries by the Approach II. Here we plot the band splitting along a non-high-symmetry line with $\theta = \phi = \pi/3$. The left panel shows the band splitting of $\mathcal{H}_1 + \mathcal{H}_{\text{soc}}$ is shown and each band is twofold degeneracy required by the $\text{SU}_o(2)$ quasisymmetry. In the middle panel, all the bands split but there still exists a twofold degeneracy, which is protected by the U(1) quasisymmetry. The right panel shows all the quasisymmetries are broken and a tiny gap appears.

with $\alpha, \beta = \pm$. Generally, all the bands are nondegenerate at generic momenta $\mathbf{k}$ once $\mathbf{f}(\mathbf{k})$ and $\mathbf{g}(\mathbf{k})$ are nonzero. Accidental degeneracy can occur when (1) $\mu_2 \mathbf{f}(\mathbf{k}) = \alpha \mu_3 k \mathbf{g}(\mathbf{k})$ for $E_{\alpha,+} = E_{\alpha,-}$, which gives a nodal point, and (2) $2\mu_1 k - \sum_{\alpha=\pm} |\mu_2 \mathbf{f}(\mathbf{k}) + \alpha \mu_3 k \mathbf{g}(\mathbf{k})| = 0$ for $E_{+,-}(\mathbf{k}) = E_{-,+}(\mathbf{k})$, which defines plane solutions for the degenerate subspace in 3D momentum space. In our model, the former corresponds to the degeneracy at $\mathbf{k} = 0$, while the latter gives the nodal planes. It should be noted that a two-level degeneracy usually requires three constraint equations (codimension 3), and thus only Weyl nodes are stable in 3D momentum space [34,35]. The presence of quasisymmetry S_{eff} reduces the number of the constraint equation to 1 (codimension 1), making the nodal planes stable. This can be viewed as a generalization of the Wigner-Von Neumann codimension theory.

IV. APPROACH II

In our second approach, $\mathcal{H}_1 + \mathcal{H}_{\text{soc}}$ is treated as the zeroth-order Hamiltonian and $\mathcal{H}_2$ as the perturbation. For $\mathcal{H}_1 + \mathcal{H}_{\text{soc}}$, we find that the spin $\text{SU}_s(2)$ symmetry is broken by SOC while the orbital $\text{SU}_o(2)$ symmetry generated by $\mathcal{M}_{1,2,3}$ remains. The existence of $\text{SU}_o(2)$ is due to the fact that spin $\mathbf{s}$ as a pseudo-vector behaves exactly the same as a vector due to the lack of inversion, mirror, etc., in chiral crystals, so $\mathcal{H}_{\text{soc}}$ can be obtained by replacing $\mathbf{k}$ by $\mathbf{s}$ in $\mathcal{H}_1$. The corresponding energy bands are given by $E_{1,\pm}(\mathbf{k}) = \pm A_1 k + \lambda_0$ and $E_{2,\pm}(\mathbf{k}) = \pm\sqrt{A_1^2 k^2 + 4\lambda_0^2} - \lambda_0$, and each band has twofold degeneracy, as required by $\text{SU}_o(2)$. The SOC-induced splitting between the $E_{1,\pm}(k)$ and $E_{2,\pm}(k)$ is $2\lambda_0$ for a large momentum k, which is depicted along the non-high-symmetry line ($\theta = \phi = \pi/3$) in Fig. 3(a).

Generally, the k^2 terms of $\mathcal{H}_2$ break the $\text{SU}_o(2)$ quasisymmetry and lead to the splitting of all bands. One can show $[\mathbf{J}_i, \mathcal{M}_i] = 0$ and $\{\mathbf{J}_i, \mathcal{M}_j\} = 0$ for $i \neq j$, so that $[\mathcal{H}_{2,\mathcal{M}_i}, \mathcal{M}_i] = 0$. Without loss of generality, we can pick up one term, say $\mathcal{H}_{2,\mathcal{M}_3}$, which commutes with $\mathcal{M}_3$ but anticommutes with $\mathcal{M}_1$ and $\mathcal{M}_2$. We show such choice of specific k^2 terms are general in Appendix D. As a result, the term $\mathcal{H}_{2,\mathcal{M}_3}$ breaks the $\text{SU}_o(2)$ quasisymmetry group down into a $\text{U}_o(1)$ group generated by $\mathcal{M}_3$. Thus, the twofold degenerate bands $E_{1,+}(\mathbf{k})$ and $E_{2,+}(\mathbf{k})$ are split by $\mathcal{H}_{2,\mathcal{M}_3}$, as shown in Fig. 3(b). The new eigenstates $|E_{i,\alpha,\beta}(\mathbf{k})\rangle$ with $i = 1, 2$ are the common eigenstates of $\mathcal{H}_1 + \mathcal{H}_{\text{soc}} + \mathcal{H}_{2,\mathcal{M}_3}$ and $\mathcal{M}_3$,

$$
\begin{aligned}
E_{1,\alpha,\beta} &= E_0 + \alpha\sqrt{f_{k^2} + 2\beta A_1 \tilde{C} k_x k_y k_z} + \lambda_0, \\
E_{2,\alpha,\beta} &= E_0 + \alpha\sqrt{f_{k^2} + 2\beta A_1 \tilde{C} k_x k_y k_z + 4\lambda_0^2} - \lambda_0,
\end{aligned}
\tag{16}
$$

where $\alpha, \beta = \pm$, $E_0 = B_1 k^2$ and $f_{k^2} = A_1^2 k^2 + C_1^2 k_x^2 k_y^2 + C_2^2 k_x^2 k_z^2 + C_3^2 k_y^2 k_z^2$. The index β labels the eigenvalues of the $\mathcal{M}_3$ operators (see details in Appendix D). When the splitting $2A_1 \tilde{C} k_x k_y k_z / \sqrt{f_{k^2}}$ by $\mathcal{H}_{2,\mathcal{M}_3}$ reaches the SOC-induced splitting $2\lambda_0$, the condition

$$
E_{1,+,-}(\mathbf{k}) = E_{2,+,+}(\mathbf{k}), \quad \forall \mathbf{k} \in k_x k_y k_z > 0
\tag{17}
$$

is satisfied and leads to the band crossings that form nodal planes. Since $\mathcal{H}_{2,\mathcal{M}_3}$ increases with k^2 while the SOC-induced splitting $2\lambda_0$ is independent of $\mathbf{k}$, the condition (17) can

always be satisfied at large enough k. As the two bands that form the nodal planes possess the opposite β values ($\mathcal{M}_3$ parities), we expect the nodal planes are protected by quasisymmetry. Turning on all the remaining k^2 terms break the U(1) quasisymmetry and generates a tiny gap of nodal planes, as shown in Fig. 3(c). The hierarchy structure of quasisymmetries for the Approach II is summarized in Fig. 3 as

$$\mathrm{SU}_s(2) \times \mathrm{SU}_o(2) \xrightarrow{\mathcal{H}_{\mathrm{soc}}} \mathrm{SU}_o(2) \xrightarrow{\mathcal{H}_{2,\mathcal{M}_i}} \mathrm{U}_o(1). \quad (18)$$

V. CONCLUSIONS AND OUTLOOKS

In this paper, we describe two different perturbation approaches to reveal the hierarchy structure of quasisymmetry and near-degeneracy in electronic band structures of chiral crystal materials CoSi. Both approaches describe the physical consequence of near-nodal planes and thus are physically equivalent. The Approach I reveals a self-commuting Hamiltonian in the first-order perturbation, while the Approach II treats both the SOC and linear k term as the zeroth order. We anticipate such a hierarchy structure of quasisymmetry in the context of $\mathbf{k} \cdot \mathbf{p}$ expansion of the effective models can generally appear in 230 space groups [20,21], which will be left for the future work. The hierarchy structure of quasisymmetry also provides a natural starting point to discuss physical phenomena in different energy scales of the effective models. For example, in CoSi, the smallest energy scale ~ 1 meV of the gap for near-nodal planes will easily be overcome by perturbations, e.g., disorder, and thus not be felt by electrons that take the cyclotron motion under magnetic fields, which is crucial in understanding the nearly angle-independent quantum oscillation spectrum in CoSi [16], as well as other experiments [28,36–39]. It is worth to note that the isostructural compounds PtGa [40–42], PdAl [43], PdGa [44,45], and RhSi [46,47] share the similar electronic band structure. Therefore, quasisymmetry is also expected to play a major role in understanding their physical properties, which require further experimental and theoretical attentions.

ACKNOWLEDGMENTS

APPENDIX A: THE EFFECTIVE k · p HAMILTONIAN AROUND THE *R* POINT

In this paper, we mainly focus on the electronic bands of cobalt silicide (CoSi) around the R point $\mathbf{k}_R = (\pi, \pi, \pi)$ [band structure is shown in Fig. 1 in the main text], specifically, the four electron-type Fermi surfaces (FSs) around the Fermi energy. To understand the low-energy physics, we construct the effective Hamiltonian. For this purpose, in this Appendix, we first discuss the space group 198 and its symmetry operators' matrix representations at the R point. Then, we use the $\mathbf{k} \cdot \mathbf{p}$ theory to construct the effective model with the parameters fitting to the DFT bands.

Figure 4(a) summarizes the general routines to construct the effective models with/without spin degree of freedom. First, we obtain the spin-orbit coupling (SOC)-free four-band spinless model. Secondly, the spin degree of freedom is taken into account by considering the on-site atomic SOC, resulting a eight-band spinful model. This is valid when SOC is relatively weak. Based on this eight-band model, we then discuss the emergent internal quasisymmetries and the corresponding hierarchy structure by using two approaches (discussed in the main text), illustrated in Fig. 4(b). The details of the Approach I will be discussed in Appendix C, and the details of the second approach will be discussed in Appendix D.

1. The Crystalline space group no. 198 and representations

As described in the main text, the CoSi crystallizes in a chiral cubic structure of space group (SG) $P2_13$ (No. 198) without a center of inversion. Its lattice structure with lattice constant $a_x = a_y = a_z = 4.433$ Å, containing four Si atoms and four Co atoms in one unit cell. The corresponding Brillouin zone (BZ) is also cubic. The SG 198 has 12 symmetry operations in addition to the translation subgroup. The three generators of SG 198 are: one threefold rotation symmetry along the (111) axis and two twofold screw rotation symmetries along the x and y axis. Hereafter, the Seitz notation is taken for the nonsymmorphic symmetry operations, i.e., a point group operation $\mathcal{O}$ followed by a translation $\mathbf{v} = v_i\mathbf{t}_i$, labeled as $\hat{\mathcal{O}} = \{\mathcal{O}|\mathbf{v}\}$ or $\hat{\mathcal{O}} = \{\mathcal{O}|v_1v_2v_3\}$, with $\mathbf{t}_i$ ($i = 1, 2, 3$) representing three basis vectors for a Bravais lattice in three dimensions. The rules for multiplication and inversion are defined as

$$\{\mathcal{O}_2|\mathbf{v}_2\}\{\mathcal{O}_1|\mathbf{v}_1\} = \{\mathcal{O}_2\mathcal{O}_1|\mathbf{v}_2 + \mathcal{O}_2\mathbf{v}_1\},$$
$$\{\mathcal{O}|\mathbf{v}\}^{-1} = \{\mathcal{O}^{-1}| - \mathcal{O}^{-1}\mathbf{v}\}. \quad (A1)$$

In addition to the translation operator $E_\mathbf{v} = \{E|\mathbf{v}\}$, the three symmetry generators of SG 198 are

$$S_{2x} = \{C_{2x}|\tfrac{1}{2}\tfrac{1}{2}0\}, \quad S_{2y} = \{C_{2y}|0\tfrac{1}{2}\tfrac{1}{2}\}, \quad C_3 = \{C_{3,(111)}|000\},$$
$$(A2)$$

defined by $S_{2x} : (x, y, z) \rightarrow (x + \tfrac{1}{2}, -y + \tfrac{1}{2}, -z)$, $S_{2y} : (x, y, z) \rightarrow (-x, y + \tfrac{1}{2}, -z + \tfrac{1}{2})$, and $C_3 : (x, y, z) \rightarrow$

(a) The effective *R*-model

```
┌─────────────────────┐       ┌─────────────────────┐           ┌─────────────────────┐
│  Spinless fermions  │       │  Spinful fermions   │    SOC    │  Spinful fermions   │
│    Without SOC      │  ───▶ │    Without SOC      │  ───────▶ │     With SOC        │
│  4-fold degeneracy  │       │  8-fold degeneracy  │           │  6-fold ⊕ 2-fold    │
│     at R point      │       │     at R point      │           │     at R point      │
└─────────────────────┘       └─────────────────────┘           └─────────────────────┘
```

(b) The perturbative models with quasi-symmetry

```
                                                        ┌────────────────────────────────────┐
                                                        │        4-band P-model              │
                                           Approach I   │     SU(2)×SU(2) → U(1)              │
                                          ───────────▶  │ H_P^eff(1) = ⟨H_soc + H_2⟩_{H_1}   │
┌──────────────────────────────┐    ⎧                   └────────────────────────────────────┘
│      Spinful fermions        │   ⎧
│        With SOC              │  ⎨
│      8-band R-model          │   ⎨                    ┌────────────────────────────────────┐
│  H_R = H_1 + H_soc + H_2     │    ⎩                   │        8-band R′-model             │
│  H_2 = H_{2,M_1} + H_{2,M_2} │        Approach II     │          SU(2) → U(1)              │
│         + H_{2,M_3}          │      ───────────────▶  │ H_{R′} = H_1 + H_soc + H_{2,M_3}   │
└──────────────────────────────┘                        └────────────────────────────────────┘
```
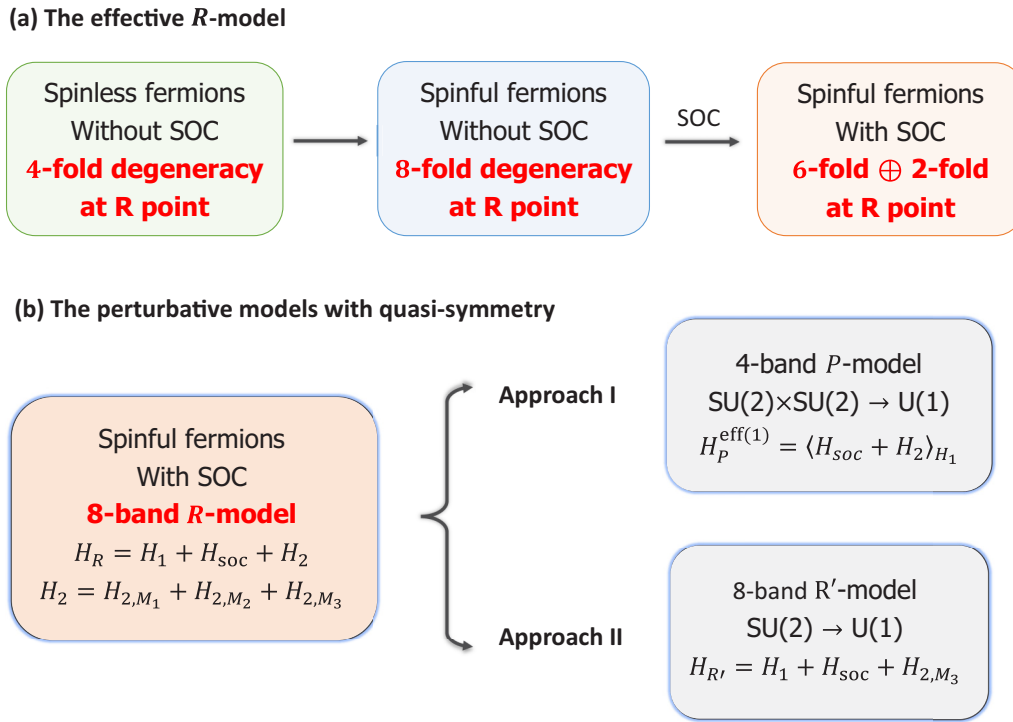
FIG. 4. A brief summary of model analysis for the hierarchy of quasisymmetry groups. (a) Shows the schematic process to construct the eight-band $\mathbf{k} \cdot \mathbf{p}$ effective Hamiltonian, labeled as R model. At R point, a four-dimensional single-valued irreducible representation (Irrep) is our starting point, specifically, the basis for the four-band spinless model. With the electron's spin degeneracy, it becomes a eightfold degeneracy, which is split into a sixfold degeneracy and a twofold degeneracy by the on-site atomic SOC. (b) Shows the two approaches used in the main text to identify the quasisymmetry with the perturbation theory. In the "Approach I", we use first-order perturbation theory to project the effective low-energy four-band P model, and find the hierarchy of quasisymmetry from SU(2) × SU(2) down to U(1). In the "Approach II", we add specially selected terms of the k^2-order Hamiltonian into the $\mathcal{H}_1 + \mathcal{H}_{\text{soc}}$ to identify the hierarchy of quasisymmetry from SU(2) down to U(1).

(y, z, x). Thus, one can check that $S_{2z} = \{C_{2z}|\frac{1}{2}0\frac{1}{2}\}$ can be given by the combination of S_{2x} and S_{2y},

$$S_{2x}S_{2y} = \{E|00\bar{1}\}S_{2z} \triangleq E_{00\bar{1}}S_{2z}. \tag{A3}$$

In addition, the threefold rotation can also be along $(11\bar{1})$, $(1\bar{1}1)$, and $(\bar{1}11)$ axis. Therefore, the lattice of CoSi has three twofold and four threefold rotation or screw axes.

Next, we use the commutation relations of the symmetry group generators to directly construct the corresponding matrix representations. Alternatively, they can be found on the on the notations in the Bilbao Crystallographic Server [24–26]. The band calculation based on the density-functional theory (DFT) without SOC shows that all states are fourfold degenerate at R point, which should belong to one 4D irreducible representation (Irrep). As mentioned in the main text, the 4D Irrep for the fourfold degenerate states close to the Fermi energy can be denoted as the single-valued Irrep R_1R_3 on the Bilbao [24–26]. Below, we discuss how this 4D Irrep can be established by considering the twofold screw rotations S_{2x}, S_{2y}, and time reversal (TR) symmetry $\mathcal{T}$. At R point, we have

$$S_{2x}^2 = S_{2y}^2 = -1, \quad S_{2x}S_{2y} = -S_{2y}S_{2x},$$
$$[S_{2x}, \mathcal{T}] = [S_{2y}, \mathcal{T}] = 0. \tag{A4}$$

Without loss of generality, for the spinless fermions, the TR symmetry operator can be chosen as $\mathcal{T} = \mathcal{K}$. Based on the above commutation relations, we construct the matrix representations denoted as $G_{1,2,3}$ for the twofold screw rotations S_{2x}, S_{2y}, and the threefold rotation C_3, respectively. Let us choose Ψ as the eigenstate of G_1 with eigenvalue λ, and the eigenvalues for different states at the R point constructed from Ψ are given in the following table.

	Ψ	$G_2\Psi$	$\mathcal{T}\Psi$	$G_2\mathcal{T}\Psi$
G_1	λ	$-\lambda$	$\lambda^* = -\lambda$	$-\lambda^* = \lambda$

With $G_1^2 = -1$, λ is a purely imaginary number. By using $(G_2\mathcal{T})^2 = -1$, $G_2\mathcal{T}$ is an anti-unitary symmetry operator, leading to the Kramer's degeneracy, namely, $\langle\Psi|G_2\mathcal{T}\Psi\rangle = 0$. This leads to two orthogonal states: Ψ and $G_2\mathcal{T}\Psi$. We now apply G_2 on these two states to generate the other two states, $G_2\Psi$ and $\mathcal{T}\Psi$, which are also eigenstates of G_1 with the eigenvalue $-\lambda$. The G_2-generated states have opposite G_1-eigenvalues compared with that of Ψ or $G_2\mathcal{T}\Psi$. Therefore, $G_2\Psi$ and $\mathcal{T}\Psi$ are orthogonal to Ψ and $G_2\mathcal{T}\Psi$, so

$$\langle\Psi|G_2\Psi\rangle = \langle\Psi|\mathcal{T}\Psi\rangle = \langle G_2\mathcal{T}\Psi|G_2\Psi\rangle = \langle G_2\mathcal{T}\Psi|\mathcal{T}\Psi\rangle = 0. \tag{A5}$$

Therefore, the fourfold degeneracy is formed by the four eigenstates at R,

$$\{\Psi, G_2\Psi, \mathcal{T}\Psi, G_2\mathcal{T}\Psi\}. \tag{A6}$$

In principle, a general basis of this 4D Irrep at R point can be presented as

$$\{|\Psi_1\rangle, |\Psi_2\rangle, |\Psi_3\rangle, |\Psi_4\rangle\}^T, \tag{A7}$$

which serves as the basis for the effective SOC-free four-band $\mathbf{k} \cdot \mathbf{p}$ Hamiltonian denoted as $\mathcal{H}_{\text{no-soc,R}}(\mathbf{k})$. Hereafter, $\mathbf{k}$ is the relative momentum to R point. In this work, we construct it up to k^2 order. Without loss of generality, we assume $|\Psi_i\rangle$ with $i = 1, 2, 3, 4$ are all real so that the representation for TR symmetry in this basis is given by

$$\mathcal{T} = I_{4\times 4}\mathcal{K}, \tag{A8}$$

where $I_{4\times 4}$ is the 4-by-4 identity matrix and $\mathcal{K}$ is the complex conjugate.

Next, we construct the matrix representations denoted as G_1, G_2, G_3 (4-by-4 matrices) for the twofold screw rotations S_{2x}, S_{2y}, and the threefold rotation C_3, respectively. For the spinless case, their commutation relations are summarized as

$$G_3^3 = 1, \quad G_1^2 = G_2^2 = -1, \quad G_1G_2 = -G_2G_1,$$

$$G_3^{-1}G_1G_3 = G_2, \quad G_3^{-1}G_2G_3 = -G_1G_2, \tag{A9}$$

because of $[\mathcal{T}, G_1] = [\mathcal{T}, G_2] = 0$, we have $G_1 = G_1^*$ and $G_2 = G_2^*$. Moreover, $G_1^2 = G_2^2 = -1$, and then both G_1 and G_2 are antisymmetric matrices, $G_{1,2} = -G_{1,2}^T$. Thus, G_1, G_2 can only be chosen from the following matrix set:

$$\{i\sigma_y\tau_0, i\sigma_y\tau_x, i\sigma_y\tau_z, i\sigma_0\tau_y, i\sigma_x\tau_y, i\sigma_z\tau_y\}, \tag{A10}$$

where both $\sigma_{x,y,z}$ and $\tau_{x,y,z}$ represent the Pauli matrices, and σ_0, τ_0 are two-by-two identity matrices. Considering $\{G_1, G_2\} = -1$, one can choose the representations as

$$G_1 = i\sigma_y\tau_0 \quad \text{and} \quad G_2 = i\sigma_x\tau_y. \tag{A11}$$

Similarly, we now discuss how to construct G_3. According to the Bilbao [24–26], there are two 4D single-valued Irreps: R_1R_3 and R_2R_2 of the little group at R point. It also shows the trace of G_3 for the R_1R_1-Irrep (R_2R_2-Irrep) is 1 (-2). According to the DFT calculation without SOC (see the Appendix B below), we find that the four states at R point of CoSi near the Fermi energy are belonging to the R_1R_3-Irrep, because of

$$\text{Tr}[C_3] = 1 + 1 + e^{i\omega_0} + e^{-i\omega_0} = 1, \tag{A12}$$

where $\omega_0 = 2\pi/3$, since we numerically check that these four states carry angular momentum $0, 0, 1, -1$ of C_3. To further satisfy both $\text{Tr}[C_3] = 1$ and the commutation relations

TABLE II. The classification of the Pauli matrices under the space group symmetry operators and time-reversal symmetry.

$\sigma_\mu\tau_\nu$	$S_{2x} = i\sigma_y\tau_0$	$S_{2y} = i\sigma_x\tau_y$	$\mathcal{T} = \mathcal{K}$	C_3 in Eq. (A13)
$\sigma_0\tau_0$	$+$	$+$	$+$	$\sigma_0\tau_0$
$\sigma_0\tau_x, \sigma_0\tau_z$	$+$	$-$	$+$	$-\sigma_x\tau_0, \sigma_z\tau_z$
$\sigma_0\tau_y$	$+$	$+$	$-$	$-\sigma_y\tau_z$
$\sigma_x\tau_0$	$-$	$+$	$+$	$\sigma_x\tau_x$
$\sigma_x\tau_x, \sigma_x\tau_z$	$-$	$-$	$+$	$-\sigma_0\tau_x, -\sigma_y\tau_y$
$\sigma_x\tau_y$	$-$	$+$	$-$	$-\sigma_z\tau_y$
$\sigma_y\tau_0$	$+$	$-$	$-$	$\sigma_x\tau_y$
$\sigma_y\tau_x, \sigma_y\tau_z$	$+$	$+$	$-$	$-\sigma_0\tau_y, \sigma_y\tau_x$
$\sigma_y\tau_y$	$+$	$-$	$+$	$\sigma_z\tau_x$
$\sigma_z\tau_0$	$-$	$-$	$+$	$\sigma_0\tau_z$
$\sigma_z\tau_x, \sigma_z\tau_z$	$-$	$+$	$+$	$-\sigma_x\tau_z, \sigma_z\tau_0$
$\sigma_z\tau_y$	$-$	$-$	$-$	$-\sigma_y\tau_0$

in Eq. (A9), we can choose

$$G_3 = \begin{pmatrix} 1 & 0 & 0 & 0 \\ 0 & 0 & -1 & 0 \\ 0 & 0 & 0 & 1 \\ 0 & -1 & 0 & 0 \end{pmatrix}. \tag{A13}$$

Please note that the choice of G_3 is not unique in the symmetry construction, while different choices of representation matrices just correspond to unitary transformation between different basis. For instance, the representation matrices G_1, G_2, G_3, and $\mathcal{T}$ are different form those on the Bilbao. This matrix chosen here is simple enough to make the construction of the effective $\mathbf{k} \cdot \mathbf{p}$ Hamiltonian become simper. Besides, in the Supplemental Material [48] [see Appendix A], we try to construct the basis made of the five $3d$ orbitals of the four Co atoms for the 4D Irrep R_1R_3. And the orbital basis can be explicitly shown by comparing to the Wannier functions from the DFT calculations.

2. The spin-independent effective four-band R model

In this section, we construct the spin-independent four-band $\mathbf{k} \cdot \mathbf{p}$ model Hamiltonian denoted as $\mathcal{H}_{\text{no-soc,R}}(\mathbf{k})$ by using the matrix representations G_1, G_2, G_3, and TR symmetry $\mathcal{T}$ of the R_1R_3-Irrep. The general 4-by-4 SOC-free Hamiltonian $\mathcal{H}_{\text{no-soc,R}}(\mathbf{k})$ is give by

$$\mathcal{H}_{\text{no-soc,R}}(\mathbf{k}) = \sum_{\mu\nu} h_{\mu\nu}(\mathbf{k})\sigma_\mu\tau_\nu, \tag{A14}$$

which should be invariant with any symmetry operators $g \in \{S_{2x}, S_{2y}, C_3, \mathcal{T}\}$ at the R point. Here $\mathbf{k}$ is the momentum with reference to $\mathbf{k}_R = (\pi, \pi, \pi)$. Therefore, the Hamiltonian should satisfy

$$\Delta^\dagger(g)[\mathcal{H}_{\text{no-soc,R}}(g\mathbf{k})]\Delta(g) = \mathcal{H}(\mathbf{k}), \tag{A15}$$

where $\Delta(g)$ is the matrix representation for symmetry g, specifically, G_1, G_2, G_3, and $\mathcal{T}$. The classification of matrices ($\sigma_\mu\tau_\nu$ with $\mu, \nu = 0, x, y, z$) and momentums (k_i, k_ik_j with $i, j = x, y, z$) are summarized in Table II and Table III, respectively, from which the 4-by-4 Hamiltonian to the leading order

TABLE III. The momentums and spin operators under the space group symmetry operators and time-reversal symmetry.

Momentums	C_{2x}	C_{2y}	$\mathcal{T}$	$C_{3,(111)}$
k_x	$+$	$-$	$-$	k_y
k_y	$-$	$+$	$-$	k_z
k_z	$-$	$-$	$-$	k_x
k_x^2, k_y^2, k_z^2	$+$	$+$	$+$	k_y^2, k_z^2, k_x^2
$k_x k_y$	$-$	$-$	$+$	$k_y k_z$
$k_x k_z$	$-$	$+$	$+$	$k_y k_x$
$k_y k_z$	$+$	$-$	$+$	$k_z k_x$
s_x	$+$	$-$	$-$	s_y
s_y	$-$	$+$	$-$	s_z
s_z	$-$	$-$	$-$	s_x

becomes

$$\mathcal{H}_1(\mathbf{k}) = C_0 \sigma_0 \tau_0 + A_1(k_x \sigma_y \tau_0 + k_y \sigma_x \tau_y - k_z \sigma_z \tau_y). \quad \text{(A16)}$$

The sign of A_1 is related to chirality of the crystal, which is chosen to be positive in this paper. Moreover, we notice that the spin-independent Hamiltonian $\mathcal{H}_1(\mathbf{k})$ in Eq. (A16) is isotropic with the full rotation symmetry. To see that, we could define the emergent angular momentum operators as

$$L_x = \tfrac{1}{2}\sigma_y \tau_0, \quad L_y = \tfrac{1}{2}\sigma_x \tau_y, \quad L_z = -\tfrac{1}{2}\sigma_z \tau_y, \quad \text{(A17)}$$

which satisfies the commutation relation $[L_i, L_j] = i\epsilon_{ijk} L_k$ with Levi-Civita symbol ϵ_{ijk} and $i = x, y, z$. Therefore, $\mathcal{H}_1(\mathbf{k})$ can be rewritten as

$$\mathcal{H}_1(\mathbf{k}) = C_0 \sigma_0 \tau_0 + 2A_1(\mathbf{k} \cdot \mathbf{L}). \quad \text{(A18)}$$

It is the linear k Hamiltonian presented in the main text [below Eq. (1)]. In addition, by similar symmetry analysis, the k^2-order effective Hamiltonian is given by

$$
\begin{aligned}
\mathcal{H}_2(\mathbf{k}) = {}& B_1\left(k_x^2 + k_y^2 + k_z^2\right) \\
& + C_1(k_x k_y \sigma_z \tau_0 + k_y k_z \sigma_0 \tau_z + k_x k_z \sigma_z \tau_z) \\
& + C_2(k_x k_y \sigma_x \tau_x - k_y k_z \sigma_0 \tau_x + k_x k_z \sigma_x \tau_0) \\
& + C_3(k_x k_y \sigma_x \tau_z - k_y k_z \sigma_y \tau_y - k_x k_z \sigma_z \tau_x), \quad \text{(A19)}
\end{aligned}
$$

which can be reorganized into a compact way as presented in the main text, by noticing that the k^2-order effective Hamiltonian $\mathcal{H}_2$ shows an intriguing structure and can be grouped into three classes,

$$\mathcal{H}_2(\mathbf{k}) = \mathcal{H}_{2,\mathcal{M}_1}(\mathbf{k}) + \mathcal{H}_{2,\mathcal{M}_2}(\mathbf{k}) + \mathcal{H}_{2,\mathcal{M}_3}(\mathbf{k}), \quad \text{(A20)}$$

where

$$\mathcal{H}_{2,\mathcal{M}_i}(\mathbf{k}) = \mathbf{g}_i(\mathbf{k}) \cdot \mathbf{J}_i, \quad \text{(A21)}$$

for i = 1, 2, 3. Here we define the parameter-momentum vectors

$$\mathbf{g}_1(\mathbf{k}) = (C_2 k_x k_y, -C_3 k_x k_z, C_1 k_y k_z), \quad \text{(A22a)}$$

$$\mathbf{g}_2(\mathbf{k}) = (C_3 k_x k_y, C_1 k_x k_z, -C_2 k_y k_z), \quad \text{(A22b)}$$

$$\mathbf{g}_3(\mathbf{k}) = (C_1 k_x k_y, C_2 k_x k_z, -C_3 k_y k_z). \quad \text{(A22c)}$$

And the operator vectors are

$$\mathbf{J}_1 = (\sigma_x \tau_x, -\sigma_z \tau_x, \sigma_0 \tau_z), \quad \text{(A23a)}$$

$$\mathbf{J}_2 = (\sigma_x \tau_z, \sigma_z \tau_z, \sigma_0 \tau_x), \quad \text{(A23b)}$$

$$\mathbf{J}_3 = (\sigma_z \tau_0, \sigma_x \tau_0, \sigma_y \tau_y). \quad \text{(A23c)}$$

The meaning of the subscript $\mathcal{M}_i$ is to be the role of quasisymmetry operators, which has been explained in the main text and will be also discussed later in Appendix C with details.

Combining Eq. (A16) and Eq. (A19), we finally get the effective 4-by-4 SOC-free Hamiltonian up to k^2 order,

$$\mathcal{H}_{\text{no-soc,R}}(\mathbf{k}) = \mathcal{H}_1(\mathbf{k}) + \mathcal{H}_2(\mathbf{k}), \quad \text{(A24)}$$

which is called the SOC-free R-model Hamiltonian for short in the following discussions.

Moreover, we notice that the linear k Hamiltonian $\mathcal{H}_1(\mathbf{k})$ in Eq. (A18) has a full rotational symmetry. This rotation is a combined rotation in both $\mathbf{k}$ space and orbital space simultaneously. To show that, without loss of generality, we can first define a rotation in the momentum space to make

$$R(\theta, \phi)(k_x, k_y, k_z)^T = k(0, 0, 1)^T, \quad \text{(A25)}$$

where $\mathbf{k} = k(\sin\theta\cos\phi, \sin\theta\sin\phi, \cos\theta)$, and the rotation in the momentum space is

$$
R(\theta, \phi) \triangleq R_y(-\theta) R_z(-\phi) = \begin{pmatrix} \cos\theta & 0 & -\sin\theta \\ 0 & 1 & 0 \\ \sin\theta & 0 & \cos\theta \end{pmatrix} \begin{pmatrix} \cos\phi & \sin\phi & 0 \\ -\sin\phi & \cos\phi & 0 \\ 0 & 0 & 1 \end{pmatrix} = \begin{pmatrix} \cos\theta\cos\phi & \cos\theta\sin\phi & -\sin\theta \\ -\sin\phi & \cos\phi & 0 \\ \sin\theta\cos\phi & \sin\theta\sin\phi & \cos\theta \end{pmatrix}.
$$
$$\text{(A26)}$$

To keep $\mathbf{k} \cdot \mathbf{L}$ invariant under rotations, we then define the associated rotation for the orbital subspace,

$$
\mathcal{R}(\theta, \phi) \triangleq e^{-i\theta L_y} e^{-i\phi L_z} = \begin{pmatrix} \cos\left(\frac{\theta}{2}\right)\cos\left(\frac{\phi}{2}\right) & \cos\left(\frac{\theta}{2}\right)\sin\left(\frac{\phi}{2}\right) & \sin\left(\frac{\theta}{2}\right)\sin\left(\frac{\phi}{2}\right) & -\sin\left(\frac{\theta}{2}\right)\cos\left(\frac{\phi}{2}\right) \\ -\cos\left(\frac{\theta}{2}\right)\sin\left(\frac{\phi}{2}\right) & \cos\left(\frac{\theta}{2}\right)\cos\left(\frac{\phi}{2}\right) & \sin\left(\frac{\theta}{2}\right)\cos\left(\frac{\phi}{2}\right) & \sin\left(\frac{\theta}{2}\right)\sin\left(\frac{\phi}{2}\right) \\ -\sin\left(\frac{\theta}{2}\right)\sin\left(\frac{\phi}{2}\right) & -\sin\left(\frac{\theta}{2}\right)\cos\left(\frac{\phi}{2}\right) & \cos\left(\frac{\theta}{2}\right)\cos\left(\frac{\phi}{2}\right) & -\cos\left(\frac{\theta}{2}\right)\sin\left(\frac{\phi}{2}\right) \\ \sin\left(\frac{\theta}{2}\right)\cos\left(\frac{\phi}{2}\right) & -\sin\left(\frac{\theta}{2}\right)\sin\left(\frac{\phi}{2}\right) & \cos\left(\frac{\theta}{2}\right)\sin\left(\frac{\phi}{2}\right) & \cos\left(\frac{\theta}{2}\right)\cos\left(\frac{\phi}{2}\right) \end{pmatrix},
$$
$$\text{(A27)}$$

Since **k** is rotated to the z axis, we only need to compute the $L_z(\theta, \phi)$ after the rotation,

$$L_z(\theta, \phi) = \mathcal{R}(\theta, \phi) L_z \mathcal{R}^{-1}(\theta, \phi) = \frac{1}{2} \begin{pmatrix} 0 & i\cos(\theta) & -i\sin(\theta)\cos(\phi) & -i\sin(\theta)\sin(\phi) \\ -i\cos(\theta) & 0 & i\sin(\theta)\sin(\phi) & -i\sin(\theta)\cos(\phi) \\ i\sin(\theta)\cos(\phi) & -i\sin(\theta)\sin(\phi) & 0 & -i\cos(\theta) \\ i\sin(\theta)\sin(\phi) & i\sin(\theta)\cos(\phi) & i\cos(\theta) & 0 \end{pmatrix}, \quad \text{(A28a)}$$

$$= [\sin(\theta)\cos(\phi)L_x + \sin(\theta)\sin(\phi)L_y + \cos(\theta)L_z], \quad \text{(A28b)}$$

$$= \mathbf{L} \cdot \vec{n}_{\mathbf{k}}. \quad \text{(A28c)}$$

Here $\vec{n}_{\mathbf{k}} = \frac{\mathbf{k}}{k}$ is the direction of **k**. Therefore, the linear k Hamiltonian becomes $\mathcal{H}_1(k, \theta, \phi) = C_0 + 2A_1 k L_z(\theta, \phi)$, which indicates the invariant of this Hamiltonian under the combined rotation $R(\theta, \phi)$ in the momentum space and $\mathcal{R}(\theta, \phi)$ in the orbital space keeps. Note that the helicity operator for low-energy Dirac fermions in spin-momentum coupled crystals is defined as $\mathcal{P}_{\mathbf{k}}^{\mathbf{S}} = \mathbf{S} \cdot \vec{n}_{\mathbf{k}}$ with **S** the spin matrix. For Hamiltonian that commutes with $\mathcal{P}_{\mathbf{k}}^{\mathbf{S}}$, such as, $\mathcal{H} \sim \mathbf{S} \cdot \mathbf{k}$, whose eigenstates at fixed **k** can be labeled by the eigenvalues $p = \pm 1/2$ of $\mathcal{P}_{\mathbf{k}}^{\mathbf{S}}$, $(\mathbf{S} \cdot \mathbf{k})|p\rangle = pk|p\rangle$, and these two states $|\pm 1/2\rangle$ represent left-handed or right-handed states. Following this spirit, we define a similar helicity operator $\mathcal{P}_{\mathbf{k}}^{\mathbf{L}} = \mathbf{L} \cdot \vec{n}_{\mathbf{k}}$ to reveal the angular momentum polarization along the moving direction in the absence of spin-orbit coupling. Thus, we obtain

$$\mathcal{H}_1(k, \theta, \phi)\left|\pm\tfrac{1}{2}\right\rangle = (C_0 \pm A_1 k)\left|\pm\tfrac{1}{2}\right\rangle. \quad \text{(A29)}$$

Here, $\pm\frac{1}{2}$ are the eigenvalues of $\mathcal{P}_{\mathbf{k}}^{\mathbf{L}}$. Each state has fourfold degeneracy if spin degeneracy is accounted. And, the explicit form of the eigen wavefunctions will be given in Appendix C.

3. The spinful eight-band R model with spin-orbit coupling

In this section, we further take spin degree of freedom into account and derive the effective 8-by-8 Hamiltonian with SOC. With the spin degree of freedom $\{\uparrow, \downarrow\}$, the spinful basis becomes

$$\{|\Psi_{1,\uparrow}\rangle, |\Psi_{2,\uparrow}\rangle, |\Psi_{3,\uparrow}\rangle, |\Psi_{4,\uparrow}\rangle\}^T$$
$$\oplus \{|\Psi_{1,\downarrow}\rangle, |\Psi_{2,\downarrow}\rangle, |\Psi_{3,\downarrow}\rangle, |\Psi_{4,\downarrow}\rangle\}^T, \quad \text{(A30)}$$

where $|\Psi_{i,\sigma}\rangle = |\Psi_i\rangle \otimes |\sigma\rangle$ with $i = 1, 2, 3, 4$ and $\sigma = \uparrow, \downarrow$. Thus, the spinful R model consists of two parts,

$$\mathcal{H}_R(\mathbf{k}) = s_0 \otimes \mathcal{H}_{\text{no-soc,R}}(\mathbf{k}) + \mathcal{H}_{\text{soc}}, \quad \text{(A31)}$$

where the spin-independent part $\mathcal{H}_{\text{no-soc,R}}(\mathbf{k})$ is given by Eq. (A24) and $\mathcal{H}_{\text{soc}}$ represents the k-independent SOC Hamiltonian. Here $\mathcal{H}_{\text{soc}}$ is also constructed from the symmetry principle, and is in a similar form as $\mathcal{H}_1(\mathbf{k})$. To show that, we need to consider the full rotation operators acting in both spin and orbital spaces,

$$S_{2x} = (is_x) \otimes (i\sigma_y\tau_0), \quad \text{(A32)}$$

$$S_{2y} = (is_y) \otimes (i\sigma_x\tau_y), \quad \text{(A33)}$$

$$C_3 = e^{i\frac{\pi}{3\sqrt{3}}(s_x + s_y + s_z)} \otimes \begin{pmatrix} 1 & 0 & 0 & 0 \\ 0 & 0 & -1 & 0 \\ 0 & 0 & 0 & 1 \\ 0 & -1 & 0 & 0 \end{pmatrix}, \quad \text{(A34)}$$

$$\mathcal{T} = (is_y) \otimes \sigma_0\tau_0\mathcal{K}. \quad \text{(A35)}$$

We use $s_{x,y,z}$ to be the Pauli matrices acting on the spin subspace, which obey

$$C_3 : (s_x, s_y, s_z) \to (s_y, s_z, s_x), \quad \text{(A36)}$$

which is the same as the transformation as momentum (k_x, k_y, k_z) under C_3. It is because the material CoSi is a chiral crystal, so that the electron spin (pseudovector) behaves the same as the **k** vector (see their classifications in Table III). Therefore, the lowest-order SOC Hamiltonian reads

$$\mathcal{H}_{\text{soc}} = \lambda_0(s_x\sigma_y\tau_0 + s_y\sigma_x\tau_y - s_z\sigma_z\tau_y) = 4\lambda_0(\mathbf{S} \cdot \mathbf{L}), \quad \text{(A37)}$$

which is obtained by just replacing (k_x, k_y, k_z) by (s_x, s_y, s_z). Here we take the notation: the spin operators $\mathbf{S} = \frac{1}{2}(s_x, s_y, s_z)$ and the angular momentum operators **L** given by Eq. (A17). The SU(2) algebra for the angular momentum operators is represented as

$$[S_i, S_j] = i\epsilon_{ijk}S_k, \quad \text{(A38a)}$$

$$[L_i, L_j] = i\epsilon_{ijk}L_k. \quad \text{(A38b)}$$

Moreover, in the next Appendix B, we will use two approaches for the justification of the above SOC Hamiltonian.

In addition to the on-site SOC in Eq. (A37), the linear k SOC Hamiltonian generally reads

$$\begin{aligned}\mathcal{H}_{k,\text{soc}}(\mathbf{k}) = &\; \lambda_1(k_x s_x + k_y s_y + k_z s_z) \otimes \sigma_0\tau_0 \\ &+ \lambda_2(k_x s_y \sigma_x\tau_x - k_y s_z \sigma_0\tau_x + k_z s_x \sigma_x\tau_0) \\ &+ \lambda_3(k_y s_x \sigma_x\tau_x - k_z s_y \sigma_0\tau_x + k_x s_z \sigma_x\tau_0) \\ &+ \lambda_4(k_x s_y \sigma_x\tau_z - k_y s_z \sigma_y\tau_y - k_z s_x \sigma_z\tau_x) \\ &+ \lambda_5(k_y s_x \sigma_x\tau_z - k_z s_y \sigma_y\tau_y - k_x s_z \sigma_z\tau_x) \\ &+ \lambda_6(k_x s_y \sigma_z\tau_0 + k_y s_z \sigma_0\tau_z + k_z s_x \sigma_z\tau_z) \\ &+ \lambda_7(k_y s_x \sigma_z\tau_0 + k_z s_y \sigma_0\tau_z + k_x s_z \sigma_z\tau_z). \quad \text{(A39)}\end{aligned}$$

Combining the SOC-free R model in Eq. (A24) with the SOC Hamiltonians in Eq. (A37) and Eq. (A39), we finally get the effective eight-band $\mathbf{k} \cdot \mathbf{p}$ Hamiltonian with SOC as

$$\mathcal{H}_R(\mathbf{k}) = s_0 \otimes [\mathcal{H}_1(\mathbf{k}) + \mathcal{H}_2(\mathbf{k})] + \mathcal{H}_{\text{soc}} + \mathcal{H}_{k,\text{soc}}(\mathbf{k}), \quad \text{(A40)}$$

which is called the eight-band R model with SOC for short in the following discussions. The basis for the R model is

made of the five d orbitals of the four Co atoms, whose details are shown in Appendix B. Since the SOC is relatively weak in CoSi, the linear k SOC terms are neglected in the main text. Nevertheless, their influence on the quasinodal planes will be addressed in the Supplemental Material [48] [see Appendix C].

4. The sixfold degenerate states at R point for spin-1/2 fermions

Next we briefly discuss the energy level splitting of the R model in Eq. (A40) at R point (i.e., $\mathbf{k} = 0$) due to the presence of the on-site SOC Hamiltonian $\mathcal{H}_{\text{soc}}$. Solving $\mathcal{H}_R(\mathbf{k} = 0)$ gives rise to a sixfold degeneracy (energy λ_0) and a twofold degeneracy (energy $-3\lambda_0$). The DFT calculation also implies that $\lambda_0 > 0$, so that the sixfold degenerate states have higher energy than the twofold states. And the sixfold is the double-valued $\bar{R}_6\bar{R}_7$ irrep while the twofold is the $\bar{R}_5\bar{R}_6$ irrep based on the irrep notations on the Bilbao [24–26]. Here we analytically solve the on-site SOC Hamiltonian. To do that, we first apply a unitary transformation

$$U = s_0 \otimes \sigma_0 \otimes \begin{pmatrix} i & 1 \\ -i & 1 \end{pmatrix}, \tag{A41}$$

which transforms $\mathcal{H}_{\text{soc}}$ into a block diagonal form

$$U[\mathcal{H}_{\text{soc}}]U^{\dagger} = \begin{pmatrix} \mathcal{H}_{+}(0) & 0 \\ 0 & \mathcal{H}_{-}(0) \end{pmatrix}, \tag{A42}$$

where the subscript $\pm$ labels the eigenvalues of τ_y and two blocks are given by

$$\mathcal{H}_{+}(0) = C_0 + \lambda_0(s_x\sigma_y + s_y\sigma_x - s_z\sigma_z) = C_0 + \lambda_0(\mathbf{s} \cdot \sigma'), \tag{A43}$$

$$\mathcal{H}_{-}(0) = C_0 + \lambda_0(s_x\sigma_y - s_y\sigma_x + s_z\sigma_z) = C_0 + \lambda_0(\mathbf{s} \cdot \sigma''), \tag{A44}$$

where σ' and σ'' are defined as $(\sigma_y, \sigma_x, -\sigma_z)$ and $(\sigma_y, -\sigma_x, \sigma_z)$, respectively. In fact, these two blocks, $\mathcal{H}_{+}(0)$ and $\mathcal{H}_{-}(0)$, are related by TR symmetry. To show it, please notice that the TR symmetry is presented as $\mathcal{T} = is_y\sigma_0\tau_0\mathcal{K}$ in the original basis. After the unitary transformation, it becomes $\mathcal{T}_U = is_y\sigma_0\tau_x\mathcal{K}$.

We take $\mathcal{H}_{+}(0)$ as an example, where σ' can be treated as pseudo-spin, so it preserves $\mathbf{J} = \frac{1}{2}\mathbf{s} + \frac{1}{2}\sigma'$. Therefore, the addition of two spin-1/2 naturally leads to one singlet state and three degenerate triplet states as $\frac{1}{2} \otimes \frac{1}{2} = 1 \oplus 0$. By using the identity

$$(\mathbf{s} \cdot \sigma') = 2\left[\mathbf{J}^2 - \left(\tfrac{1}{2}\mathbf{s}\right)^2 - \left(\tfrac{1}{2}\sigma'\right)^2\right] = 2\big(j(j+1) - \tfrac{1}{2} \times \tfrac{3}{2} \times 2\big), \tag{A45}$$

where $j = 0$ for singlet state and $j = 1$ for triplet states, we can solve the eigenenergies as $E_s = C_0 - 3\lambda_0$ for the singlet state and $E_t = C_0 + \lambda_0$ for the threefold triplet states. Similarly, the $\mathcal{H}_{-}(0)$ block also has one singlet state with energy $E_s = C_0 - 3\lambda_0$ and three triplet state with energy $E_t = C_0 + \lambda_0$. Therefore, the on-site SOC Hamiltonian splits the eight states at R point into a sixfold degeneracy and another twofold degeneracy.

Alternatively, the sixfold degeneracy can be viewed from the spin-1 excitation with its time-reversal (TR)-related partner. And we examine the sixfold degenerate states by symmetry arguments [27]. At the R point, we have the following commutation relations for spin-1/2 fermions:

$$G_3^3 = -1, \quad G_1^2 = G_2^2 = 1, \quad G_1G_2 = G_2G_1,$$

$$G_3^{-1}G_1G_3 = G_2, \quad G_3^{-1}G_2G_3 = G_1G_2, \tag{A46}$$

which provides the sufficient condition for a 3D Irrep at the R point. With $G_1\Psi = \lambda_1\Psi$ and $G_2\Psi = \lambda_2\Psi$, we have

$$G_1(G_3\Psi) = \lambda_2(G_3\Psi), \quad G_2(G_3\Psi) = \lambda_1\lambda_2(G_3\Psi),$$

$$G_1(G_3^2\Psi) = \lambda_1\lambda_2(G_3^2\Psi), \quad G_2(G_3^2\Psi) = \lambda_1(G_3^2\Psi). \tag{A47}$$

If either $\lambda_1 \neq 1$ or $\lambda_2 \neq 1$, Ψ, $G_3\Psi$, and $G_3^2\Psi$ all carry different eigenvalues under G_1 and G_2. Thus, it can lead to the basis for a 3D Irrep represented by $\{\Psi, G_3\Psi, G_3^2\Psi\}$, as proved in Ref. [27]. Next, let us discuss the effect of TR symmetry for the spin-1/2 system, and consider the eigenvalues of the states $\mathcal{T}\Psi_i$. Because $[\mathcal{T}, G_1] = [\mathcal{T}, G_2] = 0$ and the eigenvalues of G_1 and G_2 are real, $\mathcal{T}\Psi_i$ has the same eigenvalues of G_1 and G_2 as Ψ_i with $\Psi_i \in \{\Psi, G_3\Psi, G_3^2\Psi\}$. So, all these six basis functions are orthogonal with each other

$$\{\Psi, G_3\Psi, G_3^2\Psi\} \oplus \{\mathcal{T}\Psi, G_3\mathcal{T}\Psi, G_3^2\mathcal{T}\Psi\}, \tag{A48}$$

which generally forms the sixfold degeneracy [27].

APPENDIX B: THE JUSTIFICATION OF THE SOC HAMILTONIAN AND THE 3d-ORBITAL BASIS OF THE R MODEL

In this section, we justify the on-site SOC Hamiltonian obtained by the symmetry argument [see Eq. (A37)]. Based on the full tight-binding (TB) model based on the Wannier function method [49], we can obtain the exact wave functions and thus provide the 3d-orbital basis of the R model.

First of all, we discuss the four spinless degenerate wave functions (i.e., R_1R_3-Irrep) via a full TB model without SOC based on the Wannier function method from the DFT calculations. The model Hamiltonian (a 52-by-52 matrix) includes four Co atoms ($4s$, $4p$, $3d$ orbitals) and four Si atoms ($3s$, $3p$ orbitals) in one unit cell. In each simple cubic unit cell, these Co and Si atoms are located at

$$\mathbf{R}_{\text{Co}_1} = (0.14, 0.14, 0.14), \quad \mathbf{R}_{\text{Co}_2} = (-0.14, -0.36, 0.36),$$

$$\mathbf{R}_{\text{Co}_3} = (-0.36, 0.36, -0.14), \quad \mathbf{R}_{\text{Co}_4} = (0.36, -0.14, -0.36),$$

$$\mathbf{R}_{\text{Si}_1} = (-0.157, -0.157, -0.157), \quad \mathbf{R}_{\text{Si}_2} = (0.157, 0.343, -0.343),$$

$$\mathbf{R}_{\text{Si}_3} = (0.343, -0.343, 0.157), \quad \mathbf{R}_{\text{Si}_4} = (-0.343, 0.157, 0.343), \tag{B1}$$

which are in the unit of the lattice constant $a_0 = 4.45$ Å. The atomic orbitals of the full TB model are

$$\Psi_{\text{TB}} = \big\{ \phi_{\text{Co}_1,4s}, \phi_{\text{Co}_2,4s}, \phi_{\text{Co}_3,4s}, \phi_{\text{Co}_4,4s}, \phi_{\text{Co}_1,4p_y}, \phi_{\text{Co}_1,4p_z}, \phi_{\text{Co}_1,4p_x}, \phi_{\text{Co}_2,4p_y}, \phi_{\text{Co}_2,4p_z}, \phi_{\text{Co}_2,4p_x}, \phi_{\text{Co}_3,4p_y},$$

$$\phi_{\text{Co}_3,4p_z}, \phi_{\text{Co}_3,4p_x}, \phi_{\text{Co}_4,4p_y}, \phi_{\text{Co}_4,4p_z}, \phi_{\text{Co}_4,4p_x}, \phi_{\text{Co}_1,3d_{xy}}, \phi_{\text{Co}_1,3d_{yz}}, \phi_{\text{Co}_1,3d_{3z^2-1}}, \phi_{\text{Co}_1,3d_{xz}}, \phi_{\text{Co}_1,3d_{x^2-y^2}},$$

$$\phi_{\text{Co}_2,3d_{xy}}, \phi_{\text{Co}_2,3d_{yz}}, \phi_{\text{Co}_2,3d_{3z^2-1}}, \phi_{\text{Co}_2,3d_{xz}}, \phi_{\text{Co}_2,3d_{x^2-y^2}}, \phi_{\text{Co}_3,3d_{xy}}, \phi_{\text{Co}_3,3d_{yz}}, \phi_{\text{Co}_3,3d_{3z^2-1}}, \phi_{\text{Co}_3,3d_{xz}},$$

$$\phi_{\text{Co}_3,3d_{x^2-y^2}}, \phi_{\text{Co}_4,3d_{xy}}, \phi_{\text{Co}_4,3d_{yz}}, \phi_{\text{Co}_4,3d_{3z^2-1}}, \phi_{\text{Co}_4,3d_{xz}}, \phi_{\text{Co}_4,3d_{x^2-y^2}}, \phi_{\text{Si}_1,3s}, \phi_{\text{Si}_2,3s}, \phi_{\text{Si}_3,3s}, \phi_{\text{Si}_4,3s},$$

$$\phi_{\text{Si}_1,4p_y}, \phi_{\text{Si}_1,4p_z}, \phi_{\text{Si}_1,4p_x}, \phi_{\text{Si}_2,4p_y}, \phi_{\text{Si}_2,4p_z}, \phi_{\text{Si}_2,4p_x}, \phi_{\text{Si}_3,4p_y}, \phi_{\text{Si}_3,4p_z}, \phi_{\text{Si}_3,4p_x}, \phi_{\text{Si}_4,4p_y}, \phi_{\text{Si}_4,4p_z}, \phi_{\text{Si}_4,4p_x} \big\}. \tag{B2}$$

Here s, p, d are the real atomic orbitals. In the atomic orbital basis, we now discuss the crystal symmetries at R point. For instance, the spinless symmetry operator C_3 is constructed as

$$C_3 = [C_{3,\text{Co}}] \oplus [C_{3,\text{Co}} \otimes C_{3,p}] \oplus [C_{3,\text{Co}} \otimes C_{3,d}] \oplus [C_{3,\text{Si}}] \oplus [C_{3,\text{Si}} \otimes C_{3,p}], \tag{B3}$$

where

$$C_{3,\text{Co}} = C_{3,\text{Si}} = \begin{pmatrix} 1 & 0 & 0 & 0 \\ 0 & 0 & 0 & 1 \\ 0 & 1 & 0 & 0 \\ 0 & 0 & 1 & 0 \end{pmatrix}, \quad C_{3,p} = \begin{pmatrix} 0 & 1 & 0 \\ 0 & 0 & 1 \\ 1 & 0 & 0 \end{pmatrix}, \quad C_{3,d} = \begin{pmatrix} 0 & 1 & 0 & 0 & 0 \\ 0 & 0 & 0 & 1 & 0 \\ 0 & 0 & -\frac{1}{2} & 0 & \frac{\sqrt{3}}{2} \\ 1 & 0 & 0 & 0 & 0 \\ 0 & 0 & -\frac{\sqrt{3}}{2} & 0 & -\frac{1}{2} \end{pmatrix}. \tag{B4}$$

Similarly, at R point, the symmetry operator S_{2x} is represented by

$$S_{2x} = [C_{2x,\text{Co}}] \oplus [C_{2x,\text{Co}} \otimes C_{2x,p}] \oplus [C_{2x,\text{Co}} \otimes C_{2x,d}] \oplus [C_{2x,\text{Si}}] \oplus [C_{2x,\text{Si}} \otimes C_{2x,p}], \tag{B5}$$

where

$$C_{2x,\text{Co}} = C_{2x,\text{Si}} = \begin{pmatrix} 0 & 0 & 1 & 0 \\ 0 & 0 & 0 & 1 \\ -1 & 0 & 0 & 0 \\ 0 & -1 & 0 & 0 \end{pmatrix}, \quad C_{2x,p} = \begin{pmatrix} -1 & 0 & 0 \\ 0 & -1 & 0 \\ 0 & 0 & 1 \end{pmatrix}, \quad C_{2x,d} = \begin{pmatrix} -1 & 0 & 0 & 0 & 0 \\ 0 & 1 & 0 & 0 & 0 \\ 0 & 0 & 1 & 0 & 0 \\ 0 & 0 & 0 & -1 & 0 \\ 0 & 0 & 0 & 0 & 1 \end{pmatrix}. \tag{B6}$$

1. Atomic d-orbital basis: The complex wavefunctions for the single-valued $R_1 R_3$ Irrep

We then numerically solve the full SOC-free 52×52 TB model for the wavefunctions. At the R point, all states are fourfold degenerate. In this paper, we only focus on those four degenerate wave functions, whose energy is closest to the Fermi energy, as labeled by $|\Psi_{TB}\rangle$,

$$|\Psi_{TB}\rangle = \big\{ |\Psi_{R,1}^{TB}\rangle, |\Psi_{R,2}^{TB}\rangle, |\Psi_{R,3}^{TB}\rangle, |\Psi_{R,4}^{TB}\rangle \big\}. \tag{B7}$$

Other bands that are far away from the Fermi energy are neglected. Even though the dimension of each spinless wavefunction ($|\Psi_{R,i}^{TB}\rangle$) is 52, we notice that the $3d$ orbitals of Co contribute to 80% of total density of states. Then, it is reasonable to ignore the other contributions ($4s$ and $4p$ orbitals of the four Co atoms and all orbitals of the four Si atoms). The dimension is reduced to 20 since we only keep the five $3d$ orbitals of the four Co atoms. Therefore, the dimension-reduced subspace at the R point is expanded by

$$\{\text{Co}_1, \text{Co}_2, \text{Co}_3, \text{Co}_4\} \otimes \{d_{xy}, d_{yz}, d_{3z^2-1}, d_{xz}, d_{x^2-y^2}\}. \tag{B8}$$

The three-dimensional Cartesian coordinates are used for defining the d-orbitals of the cubic lattice CoSi, whose definitions are given in the Supplemental Material [48] [see Appendix A]. This convention is used throughout this paper.

This set of basis for these five d orbitals is used throughout this section. Therefore, the spinless basis in Eq. (B2) is reduced to

$$\big\{ \phi_{\text{Co}_1,3d_{xy}}, \phi_{\text{Co}_1,3d_{yz}}, \phi_{\text{Co}_1,3d_{3z^2-1}}, \phi_{\text{Co}_1,3d_{xz}}, \phi_{\text{Co}_1,3d_{x^2-y^2}}, \phi_{\text{Co}_2,3d_{xy}}, \phi_{\text{Co}_2,3d_{yz}}, \phi_{\text{Co}_2,3d_{3z^2-1}}, \phi_{\text{Co}_2,3d_{xz}}, \phi_{\text{Co}_2,3d_{x^2-y^2}},$$

$$\phi_{\text{Co}_3,3d_{xy}}, \phi_{\text{Co}_3,3d_{yz}}, \phi_{\text{Co}_3,3d_{3z^2-1}}, \phi_{\text{Co}_3,3d_{xz}}, \phi_{\text{Co}_3,3d_{x^2-y^2}}, \phi_{\text{Co}_4,3d_{xy}}, \phi_{\text{Co}_4,3d_{yz}}, \phi_{\text{Co}_4,3d_{3z^2-1}}, \phi_{\text{Co}_4,3d_{xz}}, \phi_{\text{Co}_4,3d_{x^2-y^2}}, \big\}. \tag{B9}$$

In this dimension-reduced basis, the symmetry operator C_3 in Eq. (B3) and S_{2x} in Eq. (B5) become

$$C_3 = C_{3,\text{Co}} \otimes C_{3,d}, \quad \text{and} \quad S_{2x} = C_{2x,\text{Co}} \otimes C_{2x,d}. \tag{B10}$$

These two are now 20×20 matrices. Correspondingly, the four degenerate states at the R point, $|\Psi_{R,i}^{TB}\rangle$ with $i = 1, 2, 3, 4$ are correspondingly reduced and renormalized (i.e., dimension 20). By symmetry principle, these four degenerate states

TABLE IV. The numerically calculated "complex" wavefunctions at the R point, where the first column represents the component number of the wavefunctions. Since these wave functions are made of the five $3d$ orbitals of the four Co atoms, shown in the second and third columns. These four wavefunctions $|\Psi_{R,i}^{TB}\rangle$ with $i = 1, 2, 3, 4$ are the common eigenstates of the Hamiltonian and the C_3^{TB} operators with the C_3^{TB} eigenvalues 1, $e^{i\omega_0}$, 1, $e^{-i\omega_0}$, respectively. These wavefunctions also show that time-reversal symmetry relates $\Psi_{R,1}^{TB}$ ($\Psi_{R,2}^{TB}$) and $\Psi_{R,3}^{TB}$ ($\Psi_{R,4}^{TB}$) by applying a complex conjugate.

Complex basis from TB			$\lvert\Psi_{R,1}^{TB}\rangle$	$\lvert\Psi_{R,2}^{TB}\rangle$	$\lvert\Psi_{R,3}^{TB}\rangle$	$\lvert\Psi_{R,4}^{TB}\rangle$
1		$3d_{xy}$	$0.065 - 0.038i$	$0.2773 - 0.2632i$	$0.065 + 0.038i$	$0.2773 + 0.2632i$
2		$3d_{yz}$	$0.065 - 0.038i$	$0.0893 + 0.3718i$	$0.065 + 0.038i$	$0.0893 - 0.3718i$
3	**Co$_1$**	$3d_{3z^2-1}$	0	$-0.1185 + 0.0901i$	0	$-0.1185 - 0.0901i$
4		$3d_{xz}$	$0.065 - 0.038i$	$-0.3666 - 0.1086i$	$0.065 + 0.038i$	$-0.3666 + 0.1086i$
5		$3d_{x^2-y^2}$	0	$-0.0901 - 0.1185i$	0	$-0.0901 + 0.1185i$
6		$3d_{xy}$	$0.3213 + 0.1262i$	$-0.1516 - 0.0986i$	$0.3213 - 0.1262i$	$-0.1516 + 0.0986i$
7		$3d_{yz}$	$-0.2045 + 0.2525i$	$0.215 + 0.0099i$	$-0.2045 - 0.2525i$	$0.215 - 0.0099i$
8	**Co$_2$**	$3d_{3z^2-1}$	$0.1121 + 0.047i$	$-0.052 - 0.0684i$	$0.1121 - 0.047i$	$-0.052 + 0.0684i$
9		$3d_{xz}$	$0.051 + 0.266i$	$0.0623 - 0.2732i$	$0.051 - 0.266i$	$0.0623 + 0.2732i$
10		$3d_{x^2-y^2}$	$-0.047 + 0.1121i$	$0.0684 - 0.052i$	$-0.047 - 0.1121i$	$0.0684 + 0.052i$
11		$3d_{xy}$	$-0.2045 + 0.2525i$	$-0.0989 - 0.1912i$	$-0.2045 - 0.2525i$	$-0.0989 + 0.1912i$
12		$3d_{yz}$	$0.051 + 0.266i$	$-0.2678 + 0.0826i$	$0.051 - 0.266i$	$-0.2678 - 0.0826i$
13	**Co$_3$**	$3d_{3z^2-1}$	$-0.0968 + 0.0736i$	$-0.052 - 0.0684i$	$-0.0968 - 0.0736i$	$-0.052 + 0.0684i$
14		$3d_{xz}$	$0.3213 + 0.1262i$	$-0.0096 + 0.1806i$	$0.3213 - 0.1262i$	$-0.0096 - 0.1806i$
15		$3d_{x^2-y^2}$	$-0.0736 - 0.0968i$	$0.0684 - 0.052i$	$-0.0736 + 0.0968i$	$0.0684 + 0.052i$
16		$3d_{xy}$	$0.051 + 0.266i$	$0.2054 + 0.1906i$	$0.051 - 0.266i$	$0.2054 - 0.1906i$
17		$3d_{yz}$	$0.3213 + 0.1262i$	$0.1612 - 0.082i$	$0.3213 - 0.1262i$	$0.1612 + 0.082i$
18	**Co$_4$**	$3d_{3z^2-1}$	$-0.0153 - 0.1206i$	$-0.052 - 0.0684i$	$-0.0153 + 0.1206i$	$-0.052 + 0.0684i$
19		$3d_{xz}$	$-0.2045 + 0.2525i$	$-0.1161 + 0.1812i$	$-0.2045 - 0.2525i$	$-0.1161 - 0.1812i$
20		$3d_{x^2-y^2}$	$0.1206 - 0.0153i$	$0.0684 - 0.052i$	$0.1206 + 0.0153i$	$0.0684 + 0.052i$

form a 4D single-valued irrep. Thus, they can be used to construct the matrix representations of the symmetry operators of SG 198 and time reversal. This can be helpful to check these fourfold degeneracy belongs to R_1R_3 Irrep or R_2R_2 Irrep. As we mentioned in Appendix A 1, the trace of G_3 for the R_1R_3-Irrep (R_2R_2-Irrep) is 1 (-2). For this purpose, the matrix representation G_3 for symmetry C_3 is calculated via

$$[G_3]_{i,j} = \langle \Psi_{R,i}^{TB} | C_3 | \Psi_{R,j}^{TB} \rangle, \tag{B11}$$

with $i, j = 1, 2, 3, 4$. Similarly, the matrix representation G_1 for S_{2x} is given by $\langle \Psi_{TB} | S_{2x} | \Psi_{TB} \rangle$. And the numerical results for the wavefunctions are listed in Table IV, which are orthogonal to each other

$$\langle \Psi_{R,i}^{TB} | \Psi_{R,j}^{TB} \rangle = \delta_{i,j}, \tag{B12}$$

here $\delta_{i,j}$ is the Kronecker delta function. This also leads to the following relations:

$$\mathrm{Tr}[G_3] = 1 \quad \text{and} \quad \mathrm{Tr}[G_1] = 0. \tag{B13}$$

This confirms these states form the R_1R_3 Irrep, as mentioned in the main text and Appendix A 1. Furthermore, it is also

ready to construct a basis under which the matrix representations of symmetry operators (C_3, S_{2x}, S_{2y}, and $\mathcal{T}$) are exactly given in Appendix A 3. Because the SOC Hamiltonian can be justified once the d-orbital basis is constructed. To do that, we first take a proper unitary transformation, i.e., linear combination of these states $|\Psi_{R,i}^{TB}\rangle$ with $i = 1, 2, 3, 4$, to make these states $|\Psi_{R,i}^{TB}\rangle$ are eigenstates of C_3. Under this d-orbital basis, the matrix representations are correspondingly constructed as follows. The G_3 is given by

$$G_3 = \mathrm{Diag}[1, e^{i\omega_0}, 1, e^{-i\omega_0}], \tag{B14}$$

where $\omega_0 = 2\pi/3$. These are complex wave functions and the TR symmetry requires $\Psi_{R,1}^{TB} = (\Psi_{R,3}^{TB})^*$ and $\Psi_{R,2}^{TB} = (\Psi_{R,4}^{TB})^*$. The time-reversal symmetry operator $\mathcal{T}$ is given by

$$\mathcal{T} = \begin{pmatrix} 0 & 0 & 1 & 0 \\ 0 & 0 & 0 & 1 \\ 1 & 0 & 0 & 0 \\ 0 & 1 & 0 & 0 \end{pmatrix} \mathcal{K}, \tag{B15}$$

where $\mathcal{K}$ is complex conjugate operator. Moreover, the matrix representation G_1 for S_{2x} is given by

$$G_1 = \begin{pmatrix} -i\sqrt{\frac{1}{3}} & -\sqrt{\frac{2}{3}} & 0 & 0 \\ \sqrt{\frac{2}{3}} & i\sqrt{\frac{1}{3}} & 0 & 0 \\ 0 & 0 & i\sqrt{\frac{1}{3}} & -\sqrt{\frac{2}{3}} \\ 0 & 0 & \sqrt{\frac{2}{3}} & -i\sqrt{\frac{1}{3}} \end{pmatrix}. \tag{B16}$$

In addition, one can also check that the matrix representation G_2 for the symmetry S_{2y} is obtained to obey the commutation relations in Eq. (A9).

We now consider the band splitting induced by the atomic SOC. For the full TB model at the R point, one can add the on-site atomic SOC Hamiltonian for the Co atoms,

$$\mathcal{H}_{3d,soc} = \lambda_{soc} \sum_{i=1}^{4} \mathbf{s}_i \cdot \mathbf{L}_{3d}^i, \tag{B17}$$

where i labels the four Co atoms, $\mathbf{L}_{3d}$ represents the three angular momentum operators based on the five d orbitals (i.e., $\{d_{xy}, d_{yz}, d_{3z^2-1}, d_{xz}, d_{x^2-y^2}\}$), and $\mathbf{s}$ are Pauli matrices acting on the spin subspace. We assume the SOC terms from other orbitals are small enough to be neglected. The explicit forms of operators $\mathbf{s}$ and $\mathbf{L}_{3d}$ are given by

$$s_+ = \frac{s_x + is_y}{2} = \begin{pmatrix} 0 & 1 \\ 0 & 0 \end{pmatrix}, \quad s_- = \frac{s_x - is_y}{2} = \begin{pmatrix} 0 & 0 \\ 1 & 0 \end{pmatrix},$$

$$s_z = \begin{pmatrix} 1/2 & 0 \\ 0 & -1/2 \end{pmatrix}, \tag{B18}$$

$$L_{3d,+} = \begin{pmatrix} 0 & -1 & 0 & -i & 0 \\ 1 & 0 & -i\sqrt{3} & 0 & -i \\ 0 & i\sqrt{3} & 0 & \sqrt{3} & 0 \\ i & 0 & -\sqrt{3} & 0 & 1 \\ 0 & i & 0 & -1 & 0 \end{pmatrix},$$

$$L_{3d,-} = \begin{pmatrix} 0 & 1 & 0 & -i & 0 \\ -1 & 0 & -i\sqrt{3} & 0 & -i \\ 0 & i\sqrt{3} & 0 & -\sqrt{3} & 0 \\ i & 0 & \sqrt{3} & 0 & -1 \\ 0 & i & 0 & 1 & 0 \end{pmatrix},$$

$$L_{3d,z} = \begin{pmatrix} 0 & 0 & 0 & 0 & 2i \\ 0 & 0 & 0 & i & 0 \\ 0 & 0 & 0 & 0 & 0 \\ 0 & -i & 0 & 0 & 0 \\ -2i & 0 & 0 & 0 & 0 \end{pmatrix}. \tag{B19}$$

Here we have defined $L_{3d,\pm} = (L_{3d,x} \pm iL_{3d,y})/2$. With this d-orbital basis ($R_1 R_3$ Irrep) shown in Table IV, we next project the atomic SOC terms into the effective $\mathbf{k} \cdot \mathbf{p}$ Hamiltonian to justify the k-independent SOC Hamiltonian in Eq. (A37). To do that, we consider the basis at the R point with spin degree

of freedom,

$$\{|\uparrow\rangle \otimes |\Psi_{TB}\rangle, |\downarrow\rangle \otimes |\Psi_{TB}\rangle\}$$

$$= \{|\uparrow\rangle \otimes |\Psi_{R,1}^{TB}\rangle, |\uparrow\rangle \otimes |\Psi_{R,2}^{TB}\rangle, |\uparrow\rangle \otimes |\Psi_{R,3}^{TB}\rangle, |\uparrow\rangle$$

$$\otimes |\Psi_{R,4}^{TB}\rangle, |\downarrow\rangle \otimes |\Psi_{R,1}^{TB}\rangle, |\downarrow\rangle \otimes |\Psi_{R,2}^{TB}\rangle, |\downarrow\rangle$$

$$\otimes |\Psi_{R,3}^{TB}\rangle, |\downarrow\rangle \otimes |\Psi_{R,4}^{TB}\rangle\} \tag{B20}$$

where $|\Psi_{R,i}^{TB}\rangle$ with $i = 1, 2, 3, 4$ have been shown in Table IV. After projecting $\mathcal{H}_{3d,soc}$ onto the spinfull basis at the R point in Eq. (B20), the effective SOC Hamiltonian at the R point reads

$$\mathcal{H}_{eff,soc} = \lambda_{eff,soc} \mathbf{s} \cdot \tilde{\mathbf{L}}. \tag{B21}$$

Here, the effective angular momentum operators, denoted as $\tilde{L}_x, \tilde{L}_y, \tilde{L}_z$, are given by

$$[\tilde{L}_a]_{ij} = \langle \Psi_{R,i}^{TB} | I_{4\times4} \otimes L_{3d,a} | \Psi_{R,j}^{TB}\rangle, \tag{B22}$$

where the index $a = \{x, y, z\}$, $i, j = 1, 2, 3, 4$, and $I_{4\times4}$ is a 4-by-4 identity matrix. And the numerical results of these 4-by-4 matrices are given by

$$\tilde{L}_x = \begin{pmatrix} -a_1 & ia_2 & 0 & 0 \\ -ia_2 & a_1 & 0 & 0 \\ 0 & 0 & a_1 & ia_2 \\ 0 & 0 & -ia_2 & -a_1 \end{pmatrix}, \tag{B23a}$$

$$\tilde{L}_y = \begin{pmatrix} -a_1 & -a_2 e^{i\omega_0'} & 0 & 0 \\ -a_2 e^{-i\omega_0'} & a_1 & 0 & 0 \\ 0 & 0 & a_1 & a_2 e^{-i\omega_0'} \\ 0 & 0 & a_2 e^{i\omega_0'} & -a_1 \end{pmatrix}, \tag{B23b}$$

$$\tilde{L}_z = \begin{pmatrix} -a_1 & a_2 e^{-i\omega_0'} & 0 & 0 \\ a_2 e^{i\omega_0'} & a_1 & 0 & 0 \\ 0 & 0 & a_1 & -a_2 e^{i\omega_0'} \\ 0 & 0 & -a_2 e^{-i\omega_0'} & -a_1 \end{pmatrix}, \tag{B23c}$$

where $\omega_0' = \pi/6$, $a_1 = 1/(2\sqrt{3})$ and $a_2 = 1/\sqrt{6}$. Moreover, the above effective angular momentum operators satisfy the standard (anti-)commutation relations

$$[\tilde{L}_i, \tilde{L}_j] = i\epsilon_{ijk} \tilde{L}_k, \tag{B24a}$$

$$\{\tilde{L}_i, \tilde{L}_j\} = \tfrac{1}{2}\delta_{ij}, \tag{B24b}$$

where $i, j, k = \{x, y, z\}$, δ_{ij} is the Kronecker delta function, and ϵ_{ijk} is the Levi-Civita symbol. Moreover, we also notice that the eigenvalues of $\mathcal{H}_{eff,soc}$ are $-3\lambda_{eff,soc}$ (twofold) and $\lambda_{eff,soc}$ (sixfold), by diagonalizing the SOC Hamiltonian (B21). This explains the energy splitting at the R due to the presence of SOC, indicting that the important role of SOC in the low-energy physics. This is consistent with the analysis in Appendix A 4.

2. The real wavefunctions: atomic d-orbital basis for the eight-band R model

In this section, we construct the d-orbital basis for the R model in the main text (details are shown in Appendix A 2 and Appendix A 3). Recall that the spinful eight-band R model in Eq. (A40) is constructed only by symmetry arguments, but

the corresponding "physical" basis has not been derived. To solve this issue, we take the following unitary transformation $\mathcal{U}$, which connects these two representations,

Matrix representations in the "complex" basis

$\longleftrightarrow$ Matrix representation for the eight-band R model. (B25)

Once this is proved, the important on-site SOC Hamiltonian $\mathcal{H}_{\text{soc}}$ can be easily justified. Practically, $\mathcal{U}$ needs to be mathematically constructed to make the matrix representations (G_1 for S_{2x} and G_3 for C_3) be transferred correspondingly as

$$\mathcal{U}^{-1}G_3\mathcal{U} = \begin{pmatrix} 1 & 0 & 0 & 0 \\ 0 & 0 & -1 & 0 \\ 0 & 0 & 0 & 1 \\ 0 & -1 & 0 & 0 \end{pmatrix}, \quad (B26)$$

$$\mathcal{U}^{-1}G_1\mathcal{U} = \begin{pmatrix} 0 & 0 & 1 & 0 \\ 0 & 0 & 0 & 1 \\ -1 & 0 & 0 & 0 \\ 0 & -1 & 0 & 0 \end{pmatrix}. \quad (B27)$$

where the matrices G_3 and G_1 are given by Eq. (B14) and Eq. (B16), respectively. The right side are the matrix representations used for the eight-band R model in Appendix A 1. Solving this problem is equivalently to define the following basis transformation based on the complex wavefunctions given by Table IV,

$$|\Psi_{R,1}^{TB}\rangle_{\text{real}} = \frac{1}{\sqrt{2}}\big[|\Psi_{R,1}^{TB}\rangle + |\Psi_{R,3}^{TB}\rangle\big], \quad (B28a)$$

$$|\Psi_{R,2}^{TB}\rangle_{\text{real}} = -i\frac{1}{\sqrt{6}}\big[|\Psi_{R,1}^{TB}\rangle - |\Psi_{R,3}^{TB}\rangle\big]$$
$$- \frac{1}{\sqrt{3}}\big[a_p^*|\Psi_{R,2}^{TB}\rangle + a_p|\Psi_{R,4}^{TB}\rangle\big], \quad (B28b)$$

$$|\Psi_{R,3}^{TB}\rangle_{\text{real}} = i\frac{1}{\sqrt{6}}\big[|\Psi_{R,1}^{TB}\rangle - |\Psi_{R,3}^{TB}\rangle\big]$$
$$- \frac{1}{\sqrt{3}}\big[|\Psi_{R,2}^{TB}\rangle + |\Psi_{R,4}^{TB}\rangle\big], \quad (B28c)$$

$$|\Psi_{R,4}^{TB}\rangle_{\text{real}} = i\frac{1}{\sqrt{6}}\big[|\Psi_{R,1}^{TB}\rangle - |\Psi_{R,3}^{TB}\rangle\big]$$
$$+ \frac{1}{\sqrt{3}}\big[a_p|\Psi_{R,2}^{TB}\rangle + a_p^*|\Psi_{R,4}^{TB}\rangle\big], \quad (B28d)$$

where $a_p = \exp(i\frac{\pi}{3})$. Please notice that time-reversal is just a complex conjugate used for the construction of the eight-band R model in Appendix A 1, we have to define the real wavefunctions by the above basis transformation. In other words, the time-reversal symmetry in the complex basis is given by Eq. (B15), which needs to be transformed to

$$\mathcal{T} = I_{4\times 4}\mathcal{K}, \quad (B29)$$

with $I_{4\times 4}$ a 4-by-4 identity matrix and $\mathcal{K}$ the complex conjugate. It is only possible for real basis wavefunctions. Therefore, the corresponding unitary transformation matrix $\mathcal{U}$

is represented as

$$\mathcal{U} = \begin{pmatrix} \frac{1}{\sqrt{2}} & -\frac{i}{\sqrt{6}} & \frac{i}{\sqrt{6}} & \frac{i}{\sqrt{6}} \\ 0 & -\frac{a_p^*}{\sqrt{3}} & -\frac{1}{\sqrt{3}} & \frac{a_p}{\sqrt{3}} \\ \frac{1}{\sqrt{2}} & \frac{i}{\sqrt{6}} & -\frac{i}{\sqrt{6}} & -\frac{i}{\sqrt{6}} \\ 0 & -\frac{a_p}{\sqrt{3}} & -\frac{1}{\sqrt{3}} & \frac{a_p^*}{\sqrt{3}} \end{pmatrix}, \quad (B30)$$

which is unitary transformation because of $\mathcal{U}\mathcal{U}^\dagger = \mathcal{U}\mathcal{U}^{-1} = I_{4\times 4}$ and it gives rise to

$$\big(|\Psi_{R,1}^{TB}\rangle, |\Psi_{R,2}^{TB}\rangle, |\Psi_{R,3}^{TB}\rangle, |\Psi_{R,4}^{TB}\rangle\big)\mathcal{U}$$
$$= \big(|\Psi_{R,1}^{TB}\rangle_{\text{real}}, |\Psi_{R,2}^{TB}\rangle_{\text{real}}, |\Psi_{R,3}^{TB}\rangle_{\text{real}}, |\Psi_{R,4}^{TB}\rangle_{\text{real}}\big), \quad (B31)$$

Therefore, the new wavefunctions are also orthogonal to each other, $_{\text{real}}\langle\Psi_{R,i}^{TB}|\Psi_{R,j}^{TB}\rangle_{\text{real}} = \delta_{i,j}$. Each component of the real wavefunctions are shown in Table V. For the R point, we can use this real d-orbital basis in Table V to construct the on-site SOC Hamiltonian in Appendix A 3. To show that, after the transformation, the projected angular momentum operators in Eq. (B23) become

$$\mathcal{U}^{-1}\tilde{L}_x\mathcal{U} = \frac{1}{2}\begin{pmatrix} 0 & 0 & -i & 0 \\ 0 & 0 & 0 & -i \\ i & 0 & 0 & 0 \\ 0 & i & 0 & 0 \end{pmatrix} \triangleq L_x, \quad (B32a)$$

$$\mathcal{U}^{-1}\tilde{L}_y\mathcal{U} = \frac{1}{2}\begin{pmatrix} 0 & 0 & 0 & -i \\ 0 & 0 & i & 0 \\ 0 & -i & 0 & 0 \\ i & 0 & 0 & 0 \end{pmatrix} \triangleq L_y, \quad (B32b)$$

$$\mathcal{U}^{-1}\tilde{L}_z\mathcal{U} = -\frac{1}{2}\begin{pmatrix} 0 & -i & 0 & 0 \\ i & 0 & 0 & 0 \\ 0 & 0 & 0 & i \\ 0 & 0 & -i & 0 \end{pmatrix} \triangleq L_z. \quad (B32c)$$

These matrices in the right side are $L_x = \frac{1}{2}\sigma_y\tau_0$, $L_y = \frac{1}{2}\sigma_x\tau_y$, $L_z = -\frac{1}{2}\sigma_z\tau_y$, which are just the angular momentum operators defined in Eq. (A17). According to Eq. (B21), the on-site SOC Hamiltonian becomes $\mathcal{U}^{-1}\mathcal{H}_{\text{eff,soc}}\mathcal{U} = 4\lambda_0(\mathbf{S}\cdot\mathbf{L})$, with $\mathbf{S} = \frac{1}{2}(s_x, s_y, s_z)$ and $\mathbf{L} = (L_x, L_y, L_z)$. The SU(2) algebra for the angular momentum is given by $[S_i, S_j] = i\epsilon_{ijk}S_k$, $\{S_i, S_j\} = \frac{1}{2}\delta_{ij}$ and $[L_i, L_j] = i\epsilon_{ijk}L_k$, $\{L_i, L_j\} = \frac{1}{2}\delta_{ij}$. As a brief conclusion, we have numerically found the real basis function for the eight-band R model, and also confirmed the form of the angular momentum operators, which are required for the construction of the on-site SOC Hamiltonian. The wavefunctions in Table V show that the mixing of t_{2g} and e_g orbitals are essential for the on-site SOC Hamiltonian in the spinful R model, as mentioned in the main text.

APPENDIX C: APPROACH I FOR THE HIERARCHY OF THE QUASI SYMMETRY

In this section, we use the perturbation theory to identify the hierarchy of quasisymmetry. This is Approach I mentioned in the main text. Here we explain the necessary details. The linear k-order SOC-free Hamiltonian $\mathcal{H}_1(\mathbf{k})$,

$$\mathcal{H}_1(\mathbf{k}) = C_0\sigma_0\tau_0 + 2A_1(\mathbf{k}\cdot\mathbf{L}), \quad (C1)$$

TABLE V. The numerically calculated "real" wavefunctions at the R point, the first column represents the component number of the wavefunctions. Since these wave functions are made of the five $3d$ orbitals of the four Co atoms, shown in the second and third columns. These real wavefunctions are obtained via a unitary transformation in Eq. (B30) on the complex wavefunctions in Table IV. In these new spinless basis, time-reversal symmetry is just a complex conjugate. This basis becomes the spinless basis for the eight-band R model after taking the spin degree of freedom into account, represented by $|\uparrow\rangle \otimes \{|\Psi_{R,1}^{TB}\rangle_{\text{real}}, |\Psi_{R,2}^{TB}\rangle_{\text{real}}, |\Psi_{R,3}^{TB}\rangle_{\text{real}}, |\Psi_{R,4}^{TB}\rangle_{\text{real}}\}, |\downarrow\rangle \otimes \{|\Psi_{R,1}^{TB}\rangle_{\text{real}}, |\Psi_{R,2}^{TB}\rangle_{\text{real}}, |\Psi_{R,3}^{TB}\rangle_{\text{real}}, |\Psi_{R,4}^{TB}\rangle_{\text{real}}\}$.

Real basis from TB			$\|\mathbf{\Psi}_{R,1}^{TB}\rangle_{\text{real}}$	$\|\mathbf{\Psi}_{R,2}^{TB}\rangle_{\text{real}}$	$\|\mathbf{\Psi}_{R,3}^{TB}\rangle_{\text{real}}$	$\|\mathbf{\Psi}_{R,4}^{TB}\rangle_{\text{real}}$
1		$3d_{xy}$	0.0920	0.0721	−0.2892	0.4544
2		$3d_{yz}$	0.0920	−0.4544	−0.0721	−0.2892
3	Co$_1$	$3d_{3z^2-1}$	0	−0.0217	0.1369	−0.1585
4		$3d_{xz}$	0.0920	0.2892	0.4544	−0.0721
5		$3d_{x^2-y^2}$	0	0.1706	0.1040	0.0665
6		$3d_{xy}$	0.4544	0.2892	0.0721	−0.0920
7		$3d_{yz}$	−0.2892	0.0721	−0.4544	−0.0920
8	Co$_2$	$3d_{3z^2-1}$	0.1585	0.1369	0.0217	0
9		$3d_{xz}$	0.0721	0.4544	−0.2892	0.0920
10		$3d_{x^2-y^2}$	−0.0665	0.1040	−0.1706	0
11		$3d_{xy}$	−0.2892	0.4544	−0.0920	−0.0721
12		$3d_{yz}$	0.0721	0.2892	0.0920	−0.4544
13	Co$_3$	$3d_{3z^2-1}$	−0.1369	0.1585	0	−0.0217
14		$3d_{xz}$	0.4544	−0.0721	−0.0920	−0.2892
15		$3d_{x^2-y^2}$	−0.1040	−0.0665	0	0.1706
16		$3d_{xy}$	0.0721	−0.0920	−0.4544	−0.2892
17		$3d_{yz}$	0.4544	0.0920	−0.2892	0.0721
18	Co$_4$	$3d_{3z^2-1}$	−0.0217	0	0.1585	0.1369
19		$3d_{xz}$	−0.2892	0.0920	−0.0721	−0.4544
20		$3d_{x^2-y^2}$	0.1706	0	−0.0665	0.1040

where the angular momentum operators are $L_x = \frac{1}{2}\sigma_y\tau_0$, $L_y = \frac{1}{2}\sigma_x\tau_y$, $L_z = -\frac{1}{2}\sigma_z\tau_y$ defined in Eq. (A18). Notice that $\mathcal{H}_1(\mathbf{k})$ is invariant under the spin SU$_s$(2) symmetry group. Moreover, we notice that an additional hidden SU$_o$(2) symmetry also exists for $\mathcal{H}_1(\mathbf{k})$ in the "orbital" space that can be generated by the following operators:

$$\mathcal{M}_{1,2,3} = \frac{1}{2}\{s_0\sigma_y\tau_z, s_0\sigma_y\tau_x, s_0\sigma_0\tau_y\}, \quad \text{(C2)}$$

which is shown in the main text [see Eq. (2)], and $\mathcal{M}_{1,2,3}$ all commute with $\mathcal{H}_1(\mathbf{k})$ and satisfy the commutation relations

$$[\mathcal{M}_i, \mathcal{M}_j] = i\epsilon_{i,j,k}\mathcal{M}_k, \quad \text{(C3a)}$$

$$\{\mathcal{M}_i, \mathcal{M}_j\} = \frac{1}{2}\delta_{i,j}. \quad \text{(C3b)}$$

Here $i, j = 1, 2, 3$, $\epsilon_{i,j,k}$ is the 3D Levi-Civita symbol, and $\delta_{i,j}$ is the Kronecker delta function. Thus, we refer to it as the orbital SU$_o$(2) quasisymmetry group for $\mathcal{H}_1(\mathbf{k}) + \mathcal{H}_{\text{soc}}$ because of

$$[\mathcal{M}_i, \mathcal{H}_1(\mathbf{k}) + \mathcal{H}_{\text{soc}}] = 0, \quad \text{(C4)}$$

where the on-site SOC Hamiltonian is given by Eq. (A37),

$$\mathcal{H}_{\text{soc}} = 4\lambda_0(\mathbf{S} \cdot \mathbf{L}), \quad \text{(C5)}$$

where we use $\mathbf{S} = \frac{1}{2}(s_x, s_y, s_z)$ for the spin-1/2 angular momentum operators. And $[S_i, S_j] = i\epsilon_{ijk}S_k$. In addition, we consider the k^2-order Hamiltonian that can be represented in a compact form,

$$\mathcal{H}_2(\mathbf{k}) = \mathcal{H}_{2,\mathcal{M}_1}(\mathbf{k}) + \mathcal{H}_{2,\mathcal{M}_2}(\mathbf{k}) + \mathcal{H}_{2,\mathcal{M}_3}(\mathbf{k}), \quad \text{(C6)}$$

where each part of $\mathcal{H}_2(\mathbf{k})$ is given by

$$\mathcal{H}_{2,\mathcal{M}_i}(\mathbf{k}) = \mathbf{g}_i \cdot \mathbf{J}_i, \quad \text{(C7)}$$

for $i = 1, 2, 3$. Here we define the k-dependent vectors as

$$\mathbf{g}_1(\mathbf{k}) = (C_2 k_x k_y, -C_3 k_x k_z, C_1 k_y k_z),$$
$$\mathbf{g}_2(\mathbf{k}) = (C_3 k_x k_y, C_1 k_x k_z, -C_2 k_y k_z),$$
$$\mathbf{g}_3(\mathbf{k}) = (C_1 k_x k_y, C_2 k_x k_z, -C_3 k_y k_z). \quad \text{(C8)}$$

And the corresponding vectors of operators

$$\mathbf{J}_1 = (\sigma_x\tau_x, -\sigma_z\tau_x, \sigma_0\tau_z),$$
$$\mathbf{J}_2 = (\sigma_x\tau_z, \sigma_z\tau_z, \sigma_0\tau_x),$$
$$\mathbf{J}_3 = (\sigma_z\tau_0, \sigma_x\tau_0, \sigma_y\tau_y). \quad \text{(C9)}$$

In addition, we also realize that the k^2 terms of $\mathcal{H}_2(\mathbf{k})$ break this orbital SU$_o$(2) quasisymmetry generated by $\{\mathcal{M}_{1,2,3}\}$ and

lead to the splitting of all bands. However, different parts of the entire k^2 terms can lead to the reduction from $SU_o(2)$ to a orbital U(1). To show that, as we discussed in the main text, we find that

$$[\mathbf{J}_i, \mathcal{M}_i] = 0 \quad \text{and} \quad \{\mathbf{J}_i, \mathcal{M}_j\} = 0 \quad \text{for} \quad i \neq j, \quad (C10)$$

which implies

$$[\mathcal{H}_{2,\mathcal{M}_i}(\mathbf{k}), \mathcal{M}_i] = 0. \quad (C11)$$

This can be also found in the main text and Appendix A 2. Below, we focus on how to identity the quasisymmetry based on the effective perturbation theory (Approach I). Note that alternative Approach II will be presented in Appendix D.

Furthermore, we notice there is a conservation of total angular momentum at fixed $\mathbf{k}$ for $\mathcal{H}_1(\mathbf{k}) + \mathcal{H}_{\text{soc}} = C_0 + 2A_1(\mathbf{k} \cdot \mathbf{L}) + 4\lambda_0(\mathbf{S} \cdot \mathbf{L})$. As we have discussed in Appendix A 4, the total angular momentum $\mathbf{S} + \mathbf{L}$ is conserved at $\mathbf{k} = 0$. But it does not commute with the Hamiltonian $\mathcal{H}_1(\mathbf{k}) + \mathcal{H}_{\text{soc}}$ at the nonzero $\mathbf{k}$. However, we notice that

$$[(\mathbf{S} + \mathbf{L}) \cdot \vec{n}_{\mathbf{k}}, \mathcal{H}_1(\mathbf{k}) + \mathcal{H}_{\text{soc}}] = 0, \quad (C12)$$

where $\vec{n}_{\mathbf{k}} = \frac{\mathbf{k}}{k}$ is the direction of the momentum $\mathbf{k}$. And $(\mathbf{S} + \mathbf{L}) \cdot \vec{n}_{\mathbf{k}}$ is physically similar to the helicity operator at nonzero $\mathbf{k}$. Also, Eq. (C12) can be proved as follows:

(i) Spin and orbital are independent degree of freedoms, so we have $[\mathbf{S}, \mathbf{L}] = 0$. Therefore, $[(\mathbf{S} + \mathbf{L}) \cdot \vec{n}_{\mathbf{k}}, \mathcal{H}_1(\mathbf{k})] = [\mathbf{L} \cdot \vec{n}_{\mathbf{k}}, C_0 + 2A_1(\mathbf{k} \cdot \mathbf{L})] = 0$.

(ii) We can define total angular momentum $\mathbf{L}_{\text{tot}} = \mathbf{S} + \mathbf{L}$, so that $\mathcal{H}_{\text{soc}} = 2\lambda_0(\mathbf{L}_{\text{tot}}^2 - \mathbf{S}^2 - \mathbf{L}^2) = 2\lambda_0(\mathbf{L}_{\text{tot}}^2 - \frac{3}{4} - \frac{3}{4})$.

Then one can check

$$[\mathbf{L}_{\text{tot},i}, \mathbf{L}_{\text{tot},j}] = [S_i, S_j] + [L_i, L_j] = i\epsilon_{ijk}S_k + i\epsilon_{ijk}L_k$$
$$= i\epsilon_{ijk}\mathbf{L}_{\text{tot},k}. \quad (C13)$$

Besides, we have $[\mathbf{L}_{\text{tot}}, \mathbf{L}_{\text{tot}}^2] = 0$ (i.e., the square of the angular momentum commutes with any of the components), which leads to $[\mathbf{L}_{\text{tot}}, \mathcal{H}_{\text{soc}}] = 0$. Therefore, we have

$$[\mathbf{L}_{\text{tot}} \cdot \vec{n}_{\mathbf{k}}, \mathbf{L}_{\text{tot}}^2] = 0. \quad (C14)$$

This proves that $\mathbf{L}_{\text{tot}} \cdot \vec{n}_{\mathbf{k}}$ is a symmetry operator of $\mathcal{H}_1(\mathbf{k}) + \mathcal{H}_{\text{soc}}$ at any nonzero $\mathbf{k}$.

1. Approach I: The U(1) quasi symmetry protected nodal planes

We solve the eigenproblem of the Hamiltonian $\mathcal{H}_1(\mathbf{k})$ in Eq. (A16) or Eq. (A18). Due to the full rotation symmetry, we choose the spherical coordinate with the momentum $\mathbf{k} = (k_x, k_y, k_z) = k(\sin\theta\cos\phi, \sin\theta\sin\phi, \cos\theta)$. The eigenenergies of $\mathcal{H}_1(\mathbf{k})$ have two branches $E_\pm = C_0 \pm A_1 k$ with each branch twofold degeneracy (fourfold if spin degeneracy is involved). In this paper, we assume $A_1 > 0$, and the two degenerate eigen wavefunctions $|\Psi_{A/B+}(\theta, \phi)\rangle$ of the positive energy branch (E_+) and $|\Psi_{A/B-}(\theta, \phi)\rangle$ of the negative energy branch (E_-) are given by

$$\mathcal{H}_1(\mathbf{k}) \begin{cases} |\Psi_{A/B+}(\theta, \phi)\rangle = E_+|\Psi_{A/B+}(\theta, \phi)\rangle, \\ |\Psi_{A/B-}(\theta, \phi)\rangle = E_-|\Psi_{A/B-}(\theta, \phi)\rangle, \end{cases} \quad (C15)$$

where the index $\pm$ represent the eigenvalues of $\mathbf{L} \cdot \vec{n}_{\mathbf{k}}$, and the eigenstates in the spherical coordinator are given by

$$|\Psi_{A+}(\theta, \phi)\rangle = \frac{1}{\sqrt{2}}(\cos\theta\cos\phi - i\sin\phi, -\cos\theta\sin\phi - i\cos\phi, 0, \sin\theta)^T,$$

$$|\Psi_{B+}(\theta, \phi)\rangle = \frac{1}{\sqrt{2}}(-i\sin\theta\cos\phi, i\sin\theta\sin\phi, 1, i\cos\theta)^T. \quad (C16a)$$

$$|\Psi_{A-}(\theta, \phi)\rangle = \frac{1}{\sqrt{2}}(i\sin\theta\cos\phi, -i\sin\theta\sin\phi, 1, -i\cos\theta)^T,$$

$$|\Psi_{B-}(\theta, \phi)\rangle = \frac{1}{\sqrt{2}}(\cos\theta\cos\phi + i\sin\phi, -\cos\theta\sin\phi + i\cos\phi, 0, \sin\theta)^T. \quad (C16b)$$

The solution is not unique, since there exists a twofold degeneracy between $|\Psi_{A+}(\theta, \phi)\rangle$ and $|\Psi_{B+}(\theta, \phi)\rangle$ at arbitrary $\mathbf{k}$, protected by the orbital SU(2) symmetry generated by $\{\mathcal{M}_1, \mathcal{M}_2, \mathcal{M}_3\}$ in Eq. (C2). Moreover, the subscript $A(B)$ can represent the eigenvalues of the quasisymmetry operator defined as $(\mathcal{M}_1, \mathcal{M}_2, \mathcal{M}_3) \cdot \vec{n}$ with a specific real normalized vector $\vec{n} = (n_1, n_2, n_3)$. For the basis in Eq. (C16a) and Eq. (C16b), the $\vec{n}$ vector reads

$$\vec{n} = (-\sin(\theta)\cos(\phi), \sin(\theta)\sin(\phi), -\cos(\theta)). \quad (C17)$$

And one can check

$$(\mathcal{M} \cdot \vec{n})|\Psi_{A+}(\theta, \phi)\rangle = |\Psi_{A+}(\theta, \phi)\rangle, \quad (C18a)$$

$$(\mathcal{M} \cdot \vec{n})|\Psi_{A-}(\theta, \phi)\rangle = |\Psi_{A-}(\theta, \phi)\rangle, \quad (C18b)$$

$$(\mathcal{M} \cdot \vec{n})|\Psi_{B+}(\theta, \phi)\rangle = -|\Psi_{B+}(\theta, \phi)\rangle, \quad (C18c)$$

$$(\mathcal{M} \cdot \vec{n})|\Psi_{B-}(\theta, \phi)\rangle = -|\Psi_{B-}(\theta, \phi)\rangle. \quad (C18d)$$

But $\vec{n}$ can be arbitrary due to this twofold degeneracy (fourfold if spin degeneracy is accounted). This means the

choice of eigenstates are not unique. Besides, another set of wavefunctions chosen as eigenstates of $\mathcal{M}_3$ will be shown in Appendix D 2 by fixing $\vec{n} = (0, 0, 1)$. Furthermore, we can project the angular momentum operator $\mathbf{L}$ into the eigenstate subspace,

$$\langle\Psi_{A\pm}(\theta, \phi)|\mathbf{L}|\Psi_{A\pm}(\theta, \phi)\rangle = \langle\Psi_{B\pm}(\theta, \phi)|\mathbf{L}|\Psi_{B\pm}(\theta, \phi)\rangle$$
$$= \pm\frac{\mathbf{k}}{2k}, \quad (C19)$$

$$\langle\Psi_{A\pm}(\theta, \phi)|\mathbf{L}|\Psi_{B\pm}(\theta, \phi)\rangle = \langle\Psi_{B\pm}(\theta, \phi)|\mathbf{L}|\Psi_{A\pm}(\theta, \phi)\rangle = 0. \quad (C20)$$

Here, Eqs. (C19) and (C20) mean the emergent angular momentum operator $\mathbf{L}$ is along the momentum direction after the projection. Besides, with involving the spin degree of freedom, the corresponding fourfold degenerate wavefunctions are labeled as

$$|\Psi_+\rangle = \{|\Psi_{A+\uparrow}(\theta, \phi)\rangle, |\Psi_{B+\uparrow}(\theta, \phi)\rangle, |\Psi_{A+\downarrow}(\theta, \phi)\rangle,$$
$$|\Psi_{B+\downarrow}(\theta, \phi)\rangle\}, \quad (C21)$$

where

$$|\Psi_{A+\uparrow}(\theta,\phi)\rangle = (1,0)^T \otimes |\Psi_{A+}(\theta,\phi)\rangle,$$

$$|\Psi_{B+\uparrow}(\theta,\phi)\rangle = (1,0)^T \otimes |\Psi_{B+}(\theta,\phi)\rangle,$$

$$|\Psi_{A+\downarrow}(\theta,\phi)\rangle = (0,1)^T \otimes |\Psi_{A+}(\theta,\phi)\rangle,$$

$$|\Psi_{B+\downarrow}(\theta,\phi)\rangle = (0,1)^T \otimes |\Psi_{B+}(\theta,\phi)\rangle,$$

(C22)

where $(1,0)^T$ and $(0,1)^T$ label the spin-up and spin-down wavefunctions, respectively. The above set of wavefunctions serves as the basis for the projected four-band perturbation model via the first-order perturbation theory, dubbed as "the P model". We treat both the on-site SOC in Eq. (A37) and the k^2 terms in Eq. (A19) as perturbations,

$$\mathcal{H}_{perb}(\mathbf{k}) = \mathcal{H}_{soc} + s_0 \otimes \mathcal{H}_2(\mathbf{k}). \quad (C23)$$

The projected Hamiltonian $\langle \Psi_+ | \mathcal{H}_{perb} | \Psi_+ \rangle$ is given by

$$\mathcal{H}_P^{\text{eff}(1)}(\mathbf{k}) = (E_+ + B_1 k^2)s_0\omega_0 + \mathcal{H}_{\text{soc},+}^{\text{eff}(1)}(\mathbf{k}) + \mathcal{H}_{k^2,+}^{\text{eff}(1)}(\mathbf{k}),$$

(C24)

which is marked as the P model around R point. And

$$\mathcal{H}_{\text{soc},+}^{\text{eff}(1)}(\mathbf{k}) = \lambda_0(\lambda_x s_x + \lambda_y s_y + \lambda_z s_z) \otimes \omega_0, \quad (C25a)$$

$$\mathcal{H}_{k^2,+}^{\text{eff}(1)}(\mathbf{k}) = \tilde{C}k^2 s_0 \otimes (d_x\omega_x + d_y\omega_y + d_z\omega_z), \quad (C25b)$$

where $\tilde{C} = C_1 - C_2 + C_3$, and $\omega_{x,y,z}$ are Pauli matrices for the $\{A+, B+\}$ band subspace. The coefficients $\lambda_{x,y,z}$ are defined as

$$(\lambda_x, \lambda_y, \lambda_z) = (\sin\theta\cos\phi, \sin\theta\sin\phi, \cos\theta) = \frac{\mathbf{k}}{|\mathbf{k}|}, \quad (C26)$$

On the other hand, the coefficients $d_{x,y,z}$ are given by

$$d_x = \tfrac{1}{4}\sin\theta\sin(2\theta)\sin(2\phi)(\cos\phi + \sin\phi),$$

$$d_y = \tfrac{1}{4}\sin\theta\sin(2\theta)\sin(2\phi)(\sin\phi + \cos\theta(\cos\phi - \sin\phi)),$$

$$d_z = \tfrac{1}{4}\sin\theta\sin(2\theta)\sin(2\phi)(\cos\theta - \sin\theta(\cos\phi - \sin\phi)).$$

(C27)

Furthermore, we use the symmetry to understand the above first-order perturbation Hamiltonian. The basis function in Eq. (C21) can be labeled by eigenvalues of symmetries,

$$|\Psi_{A+\uparrow}(\theta,\phi)\rangle = |\uparrow\rangle \otimes |p = +\tfrac{1}{2}, q = +1\rangle, \quad (C28a)$$

$$|\Psi_{B+\uparrow}(\theta,\phi)\rangle = |\uparrow\rangle \otimes |p = +\tfrac{1}{2}, q = -1\rangle, \quad (C28b)$$

$$|\Psi_{A+\downarrow}(\theta,\phi)\rangle = |\downarrow\rangle \otimes |p = +\tfrac{1}{2}, q = +1\rangle, \quad (C28c)$$

$$|\Psi_{B+\downarrow}(\theta,\phi)\rangle = |\downarrow\rangle \otimes |p = +\tfrac{1}{2}, q = -1\rangle, \quad (C28d)$$

Here we take $p = \pm 1/2$ as the eigenvalues of $\mathbf{L} \cdot \vec{n}_{\mathbf{k}}$ and $q = \pm 1$ as the eigenvalues of $\vec{\mathcal{M}} \cdot \vec{n}$. All these four states are degenerate with eigenenergy of $\mathcal{H}_1$ as $C_0 + A_1 k$. The linear k Hamiltonian has both orbital SU(2) symmetry and spin SU(2) symmetry. Specifically, the orbital SU(2) symmetry generated by $\{\mathcal{M}_{1,2,3}\}$ indicates that the vector $\vec{n}$ is arbitrary. And the spin SU(2) symmetry implies that $|\uparrow/\downarrow\rangle$ can be any direction in the spin subspace. Then, to show the origin of the hidden quasisymmetry of the P model, we individually do the projection for the on-site SOC and k^2-order Hamiltonian,

(i) Only do the projection of the on-site SOC Hamiltonian. In this case, the orbital SU(2) symmetry generated by

$\{\mathcal{M}_{1,2,3}\}$ preserves, because of $[\mathcal{M}_i, \mathcal{H}_1(\mathbf{k}) + \mathcal{H}_{\text{soc}}] = 0$ with $i = 1, 2, 3$. Thus, we obtain

$$\text{SU}_s(2) \times \text{SU}_o(2) \xrightarrow{\langle\mathcal{H}_{\text{soc}}\rangle_{\mathcal{H}_1}} \text{U}_s(1) \times \text{SU}_o(2), \quad (C29)$$

where the spin U(1) symmetry generator depends on $\mathbf{k}$. To understand this, we recall the conservation of $(\mathbf{S} + \mathbf{L}) \cdot \vec{n}_{\mathbf{k}}$ for $\mathcal{H}_1(\mathbf{k}) + \mathcal{H}_{\text{soc}} = C_0 + 2A_1\mathbf{k}\cdot\mathbf{L} + 4\lambda_0\mathbf{S}\cdot\mathbf{L}$. Then, for a fixed nonzero $\mathbf{k}$, one can take the eigenstates in Eq. (C28) as eigenstates of the helicity operator $(\mathbf{S} + \mathbf{L}) \cdot \vec{n}_{\mathbf{k}}$ by choosing

$$|\Psi_{A+\uparrow}(\theta,\phi)\rangle = |s = +\tfrac{1}{2}\rangle \otimes |p = +\tfrac{1}{2}, q = +1\rangle, \quad (C30a)$$

$$|\Psi_{B+\uparrow}(\theta,\phi)\rangle = |s = +\tfrac{1}{2}\rangle \otimes |p = +\tfrac{1}{2}, q = -1\rangle, \quad (C30b)$$

$$|\Psi_{A+\downarrow}(\theta,\phi)\rangle = |s = -\tfrac{1}{2}\rangle \otimes |p = +\tfrac{1}{2}, q = +1\rangle, \quad (C30c)$$

$$|\Psi_{B+\downarrow}(\theta,\phi)\rangle = |s = -\tfrac{1}{2}\rangle \otimes |p = +\tfrac{1}{2}, q = -1\rangle. \quad (C30d)$$

Here we use $s = \pm 1/2$ as eigenvalues of $\mathbf{S} \cdot \vec{n}_{\mathbf{k}}$. Here we use $\vec{n}_{\mathbf{k}}$, $\vec{n}'_{\mathbf{k}}$, and $\vec{n}''_{\mathbf{k}}$ to be the set of 3D orthogonal coordinates at the fixed $\mathbf{k}$ and $\vec{n}_{\mathbf{k}}$ is the direction of $\mathbf{k}$ [i.e., $\vec{n}_{\mathbf{k}} = (\sin\theta\cos\phi, \sin\theta\sin\phi, \cos\theta)$]. Namely, $|\vec{n}_{\mathbf{k}}| = |\vec{n}'_{\mathbf{k}}| = |\vec{n}''_{\mathbf{k}}| = 1$, and $\vec{n}_{\mathbf{k}} \cdot \vec{n}'_{\mathbf{k}} = \vec{n}_{\mathbf{k}} \cdot \vec{n}''_{\mathbf{k}} = \vec{n}'_{\mathbf{k}} \cdot \vec{n}''_{\mathbf{k}} = 0$. Then, the first-order projection of $\mathbf{S} \cdot \mathbf{L} = [(\mathbf{S}\cdot\vec{n}_{\mathbf{k}})(\mathbf{L}\cdot\vec{n}_{\mathbf{k}}) + (\mathbf{S}\cdot\vec{n}'_{\mathbf{k}})(\mathbf{L}\cdot\vec{n}'_{\mathbf{k}}) + (\mathbf{S}\cdot\vec{n}''_{\mathbf{k}})(\mathbf{L}\cdot\vec{n}''_{\mathbf{k}})]$ onto these four states in Eq. (C30) leads to

$$[\langle\mathcal{H}_{\text{soc}}\rangle_{\mathcal{H}_1}]_{i,j} = 4\lambda_0\langle\Psi_i(\theta,\phi)|\mathbf{S}\cdot\mathbf{L}|\Psi_j(\theta,\phi)\rangle,$$

$$= 4\lambda_0\langle\Psi_i(\theta,\phi)|(\mathbf{S}\cdot\vec{n}_{\mathbf{k}})(\mathbf{L}\cdot\vec{n}_{\mathbf{k}})$$

$$+ (\mathbf{S}\cdot\vec{n}'_{\mathbf{k}})(\mathbf{L}\cdot\vec{n}'_{\mathbf{k}}) + (\mathbf{S}\cdot\vec{n}''_{\mathbf{k}})$$

$$\times (\mathbf{L}\cdot\vec{n}''_{\mathbf{k}})|\Psi_j(\theta,\phi)\rangle,$$

$$= 4\lambda_0\langle\Psi_i(\theta,\phi)|(\mathbf{S}\cdot\vec{n}_{\mathbf{k}})(\mathbf{L}\cdot\vec{n}_{\mathbf{k}})|\Psi_j(\theta,\phi)\rangle,$$

(C31)

where $i, j = \{A+\uparrow, B+\uparrow, A+\downarrow, B+\downarrow\}$. Thus, the first-order perturbation for on-site SOC Hamiltonian is

$$\langle\mathcal{H}_{\text{soc}}\rangle_{\mathcal{H}_1} = \lambda_0 \begin{pmatrix} 1 & 0 & 0 & 0 \\ 0 & 1 & 0 & 0 \\ 0 & 0 & -1 & 0 \\ 0 & 0 & 0 & -1 \end{pmatrix}. \quad (C32)$$

Please notice that $\langle\mathcal{H}_{\text{soc}}\rangle_{\mathcal{H}_1}$ can be also obtained after diagonalizing $\mathcal{H}_{\text{soc},+}^{\text{eff}(1)}(\mathbf{k})$ in Eq. (C25). At nonzero $\mathbf{k}$, we find that the fourfold degenerate states [$C_0 + A_1 k$ for $\mathcal{H}_1(\mathbf{k})$] are split by the on-site SOC Hamiltonian $\mathcal{H}_{\text{soc}}$ into two states and each state has twofold degeneracy stemming from the orbital SU(2) symmetry, $E = C_0 + A_1 k \pm \lambda_0$. And the eigenstates are just Eq. (C30). And the spin-polarization along the direction of $\mathbf{k}$ represents the spin U(1) symmetry.

(ii) Only do the projection of the k^2-order Hamiltonian. In this case, the spin SU(2) symmetry preserves. Since the k^2-order Hamiltonian is spin independent. Thus,

$$\text{SU}_s(2) \times \text{SU}_o(2) \xrightarrow{\langle\mathcal{H}_2\rangle_{\mathcal{H}_1}} \text{SU}_s(2) \times \text{U}_o(1). \quad (C33)$$

We do not have an elegant picture for the $\langle\mathcal{H}_2\rangle_{\mathcal{H}_1}$. But we know it does not dependent on spin, as shown in Eq. (C25). The fourfold degeneracy is split into two states, and each state has twofold degeneracy (i.e., spin degeneracy). And, the

two-by-two matrix in the $\{A, B\}$-subspace itself severs as the orbital U(1) symmetry.

Therefore, up to the first-order perturbation, we obtain a hierarchy of quasisymmetry for CoSi mentioned in the main text [see Eq. (7)],

$$
\text{SU}_s(2) \times \text{SU}_o(2) \xrightarrow{\langle \mathcal{H}_{\text{soc}} + \mathcal{H}_2 \rangle_{\mathcal{H}_1}} \text{U}_s(1) \times \text{U}_o(1). \quad \text{(C34)}
$$

And $[\text{U}_s(1), \text{U}_o(1)] = 0$, as shown below.

2. The analytical properties of the effective perturbation four-band P model

The P model has the self-commuting structure at every $\mathbf{k}$. Explicitly,

$$
\begin{aligned}
&\left[\mathcal{H}_{\text{soc},+}^{\text{eff}(1)}(\mathbf{k}_1), \mathcal{H}_{k^2,+}^{\text{eff}(1)}(\mathbf{k}_2) \right] \\
&= 0, \quad \forall \mathbf{k}_1 \ \& \ \forall \mathbf{k}_2 \text{ in the whole momentum space,}
\end{aligned} \quad \text{(C35)}
$$

as discussed in the main text, which is known as the projected stabilizer code Hamiltonian and directly leads to the U(1) quasisymmetry group. Below, we provide some analytical study on the properties of the effective P model. The eigenenergies of the P model in Eq. (C24) are

$$
\begin{aligned}
E_{\alpha\beta}(k, \theta, \phi) &= C_0 + B_1 k^2 + A_1 k + \alpha \lambda_0 \\
&+ \beta \frac{\sqrt{3}}{4} \tilde{C} k^2 |\sin 2\phi \sin 2\theta \sin \theta|, \quad \text{(C36)}
\end{aligned}
$$

where $\alpha = \pm$ and $\beta = \pm$. Here $\sin 2\phi \sin 2\theta \sin \theta = 4 k_x k_y k_z / k^3$, indicating that there are twofold degeneracy on high symmetry planes ($k_x = 0$ or $k_y = 0$ or $k_z = 0$).

For the $\Gamma - R - M$ plane, $\phi = \pi/4$ so $\sin 2\phi = 1$. The eigenenergies along high symmetry lines are listed as follows:

(1) Along the $R - M$ line.

$\theta = 0$, so $E_\alpha = C_0 + B_1 k^2 + A_1 k + \alpha \lambda_0$. All the bands are twofold degenerate.

(2) Along the $R - Z$ line.

$\theta = \pi/2$, so $E_\alpha = C_0 + B_1 k^2 + A_1 k + \alpha \lambda_0$. All the bands are twofold degenerate.

We then analyze the perturbation along these two high symmetry lines (i.e., the $R - M$ line and the $R - Z$ line) to identify the band crossing types of the Fermi surface (linear or quadratic). For a given E_f, the Fermi surface shape of the momentum $k_\pm$ for the upper four bands is determined by the quadratic equation

$$
B_1 k^2 + A_1 k + C_\alpha = 0, \quad \text{(C37)}
$$

where $C_\alpha = \alpha \lambda_0 + C_0 - E_f$ with $\alpha = \pm$. This equation leads to the solution

$$
k_{\alpha,\theta=0} = k_{\alpha,\theta=\pi/2} = \frac{1}{2B_1} \left(-A_1 + \sqrt{A_1^2 - 4 B_1 C_\alpha} \right). \quad \text{(C38)}
$$

We firstly focus on the $R - M$ line by expanding Eq. (C36) around $\theta = 0$. In this case, we have $\theta = 0 + \delta_\theta$ and

$k = k_{\alpha,\theta=0} + \delta_k$. Then, the Eq. (C37) should be replaced by

$$
0 = C_\alpha + B_1 k^2 + A_1 k + \beta \frac{\sqrt{3}}{4} \tilde{C} k^2 |\sin 2\phi \sin 2\theta \sin \theta|, \quad \text{(C39)}
$$

which leads to

$$
\begin{aligned}
0 &= C_\alpha + B_1 (k_{\alpha,\theta=0} + \delta_k)^2 + A_1 (k_{\alpha,\theta=0} + \delta_k) \\
&+ \beta \frac{\sqrt{3}}{4} \tilde{C} (k_{\alpha,\theta=0} + \delta_k)^2 |\sin 2\phi| (2\delta_\theta^2). \quad \text{(C40)}
\end{aligned}
$$

After neglecting the δ_k^2 terms, we find

$$
\delta_{k,\beta} = -\beta \frac{\sqrt{3}}{2} \frac{\tilde{C} |\sin 2\phi| \delta_\theta^2 (k_{\alpha,\theta=0})^2}{2 B_1 k_{\alpha,\theta=0} + A_1 + \beta \sqrt{3} \tilde{C} |\sin 2\phi| \delta_\theta^2 k_{\alpha,\theta=0}}. \quad \text{(C41)}
$$

To the δ_θ^2 order, we have

$$
\delta_{k,\beta} = -\beta \frac{\sqrt{3}}{2} \frac{\tilde{C} |\sin 2\phi| (k_{\alpha,\theta=0})^2}{2 B_1 k_{\alpha,\theta=0} + A_1} \times \delta_\theta^2, \quad \text{(C42)}
$$

which indicates that the exact crossing along the $R - M$ line is quadratic in momentum $k = \sqrt{k_x^2 + k_y^2}$, as illustrated in Fig. 5(a) around the $R - M$ line.

For $\theta = \pi/2$ (i.e., the $R - Z$ line), we then expand Eq. (C36) around $\theta = \pi/2 + \delta_\theta$. Because

$$
\sin 2\theta \sin \theta \rightarrow \sin(\pi + 2\delta_\theta) \sin(\pi/2 + \delta_\theta) \rightarrow -2\delta_\theta + \mathcal{O}(\delta_\theta^3). \quad \text{(C43)}
$$

It leads to the solution for k at a fixed E_f,

$$
\delta_{k,\beta} = -\beta \frac{\sqrt{3}}{2} \frac{\tilde{C} |\sin 2\phi| (k_{\alpha,\theta=\pi/2})^2}{2 B_1 k_{\alpha,\theta=0} + A_1} \times |\delta_\theta|, \quad \text{(C44)}
$$

which indicate the exact crossing along k_z is linear, as illustrated in Fig. 5(b) around the $R - Z$ line.

In addition, we discuss the emergent nodal lines on Fermi surfaces for the P model. The comparison of the FSs between the eight-band $\mathbf{k} \cdot \mathbf{p}$ effective Hamiltonian, the R model [e.g., see Eq. (A40) in Appendix A 3] and the first-order-perturbation four-band Hamiltonian, the P model [e.g., see Eq. (C24) in Appendix C 1] are shown in Fig. 6. The P model shows exact degeneracy at non-high-symmetry points. The crossings from two bands can be obtained from the constraint equation

$$
E_{\alpha=+1,\beta=-1} = E_{\alpha=-1,\beta=+1}, \quad \text{(C45)}
$$

of which the solution

$$
\lambda_0 = \frac{\sqrt{3}}{4} \tilde{C} k^2 |\sin 2\phi \sin 2\theta \sin \theta| = \sqrt{3} \tilde{C} \frac{|k_x k_y k_z|}{k} \quad \text{(C46)}
$$

generally leads to nodal planes. The obtained nodal planes do not intersect with high-symmetry planes, e.g., $k_x = 0$ or $k_y = 0$ or $k_z = 0$. At the Fermi energy, we require an additional constraint equation

$$
E_f = E_{\alpha=+1,\beta=-1} = E_{\alpha=-1,\beta=+1}. \quad \text{(C47)}
$$

(a) The four Fermi surfaces in the $\Gamma - R - M$ plane

(b) The quadratic band splitting
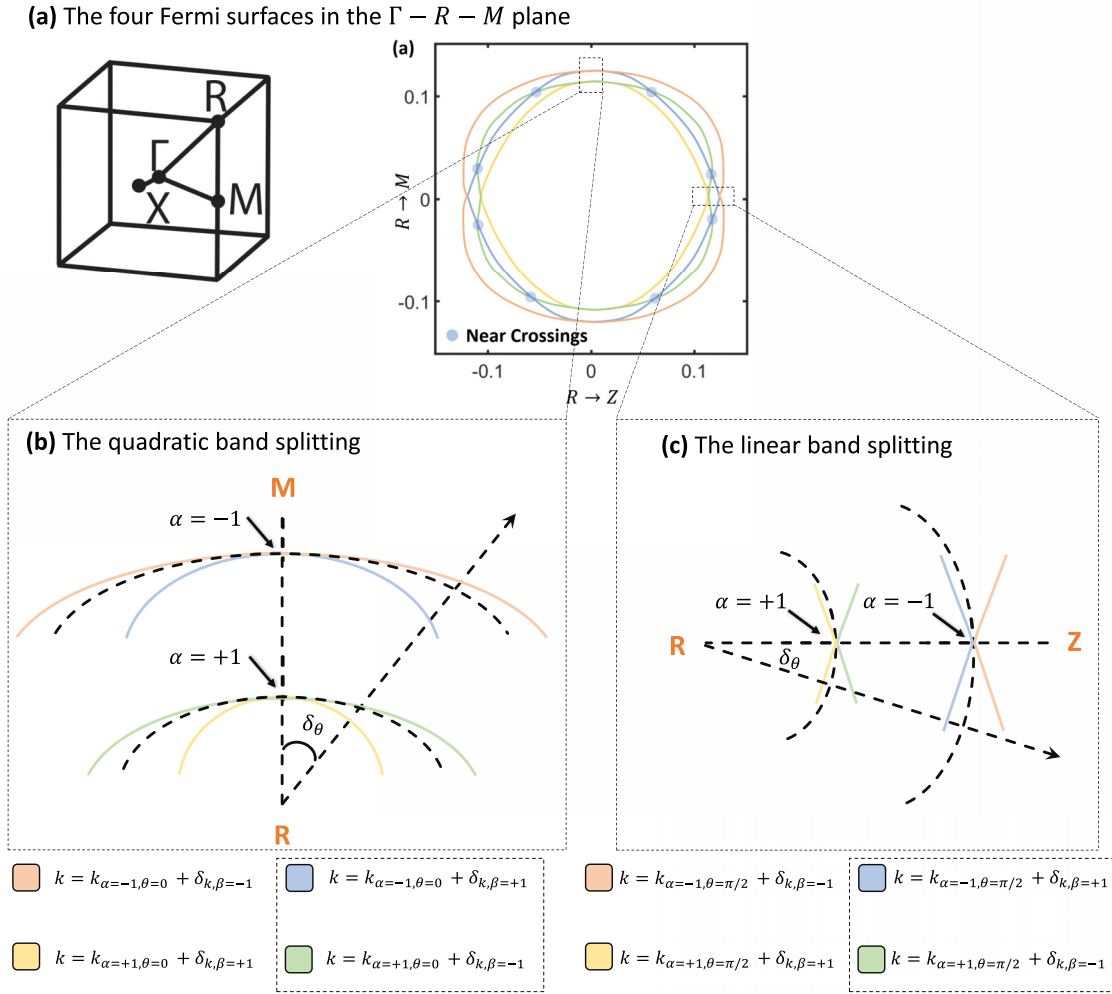
(c) The linear band splitting

FIG. 5. The four distinct Fermi surfaces of CoSi are numerically calculated, as shown in (a) for the $\Gamma - R - M$ plane. These high-symmetry points are marked in the first Brillouin zone [left panel in (a)]. And these four Fermi surfaces are labeled by four different colors. The middle two have a "crossing" behavior with a tiny gap. And the analytical results for the band dispersions [see Eq. (C36)] of the P model along the $R - M$ line in (b) and the $R - Z$ line in (c). The two dashed black lines represent the Fermi surfaces with $\alpha = \pm 1$ and $\beta = 0$. The β term leads to the quadratic band splitting around the $R - M$ line in (a) with $\delta_k \sim \delta_\theta^2$, and the linear band splitting around the $R - Z$ line in (b) with $\delta_k \sim \delta_\theta$. Here, the orange line is for $\alpha = -1$, $\beta = -1$, the blue line is for $\alpha = -1$, $\beta = +1$, the green line is for $\alpha = +1$, $\beta = -1$, and the yellow line is for $\alpha = +1$, $\beta = +1$. Once the band splitting caused by the β term is large enough, the band crossing between the blue line ($\beta = +1$) and the green line ($\beta = -1$) may happen at arbitrary momenta, which are exact and protected by the quasisymmetry.
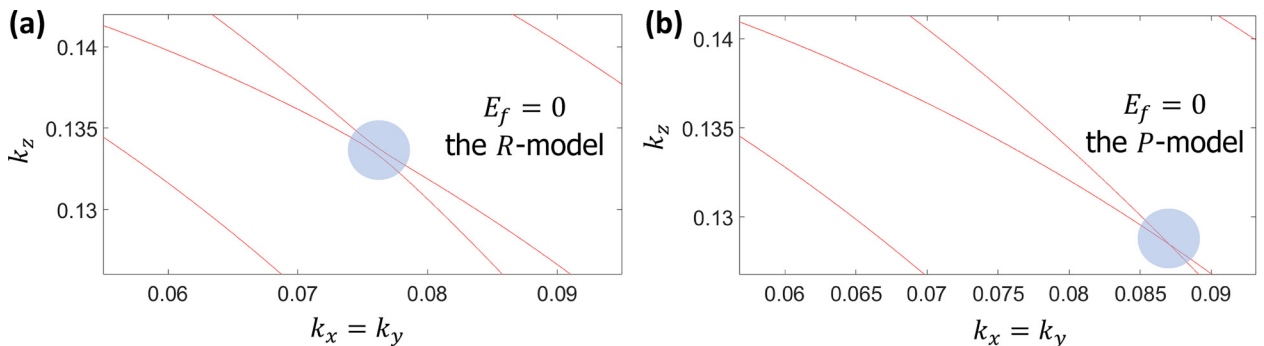

FIG. 6. Comparison of the Fermi surfaces with the R model in (a) and the P model in (b) around the quasinodal points in the $\Gamma - R - M$ plane. (a) Shows a tiny gap in the blue circle, and (b) shows the exact quasisymmetry protected degeneracy.

By solving the above equation, we find the curve equation for the emergent nodal lines at the Fermi energy

$$\sqrt{3}\tilde{C}\frac{|k_x k_y k_z|}{k^3} = \frac{\sqrt{3}}{4}\tilde{C}|\sin 2\phi \sin 2\theta \sin \theta|$$

$$= \frac{A_1^2 \lambda_0}{2(E_f - C_0)^2}\left[1 + \frac{2B_1(E_f - C_0)}{A_1^2}\right.$$

$$\left. + \sqrt{1 + \frac{4B_1(E_f - C_0)}{A_1^2}}\right]. \quad (C48)$$

For a fixed Fermi energy E_f, solving Eq. (C48) generally gives rise to a line solution in the $\theta - \phi$ plane. It represents a nodal line because of Eq. (C46): solving θ and ϕ at fixed E_f from Eq. (C48) will fix k simultaneously. However, the existence of such a line solution for Eq. (C48) depends on the value of E_f. For a critical E_f, there is no line solution from the curve equation (C48), instead, we can only get a point solution. To find this minimal E_f, we set $\phi = \pi/4$, and notice that the function $|\sin 2\theta \sin \theta|$ reaches its maximum

when $\theta \to \arcsin\sqrt{\frac{2}{3}}$, we find the minimal E_f as

$$E_{f,c} = \frac{A_1\sqrt{C_4 \lambda_0} + B_1\lambda_0 + C_0 C_4}{C_4}. \quad (C49)$$

Thus, $E_{f,c}$ is the energy for the single nodes with twofold degeneracy on the corresponding nodal planes. Based on this analysis, we realize that the quasinodal line will emerge into single nodes when decreasing the Fermi energy. For $E_f < E_{f,c}$, no solution of Eq. (C48) can be obtained anymore. Therefore, one can conclude that each nodal line emerges into a single point after decreasing E_f down to $E_{f,c}$. Moreover, when the nodal plane is split due to high-order perturbations, this point becomes a Weyl point pinned along the (111) axis. Thus we conclude that nodal lines exist only when $E_f \geqslant E_{f,c}$.

3. The second-order perturbation: Gap out the quasi nodal planes

Next we consider the second-order perturbation corrections for the four-band P model [e.g., see Eq. (C24) in Appendix C 1], which can open a tiny gap for the emergent nodal lines obtained from Eq. (C48) at generic momenta. Recall that the first-order perturbation Hamiltonian, the P model, is based on the basis in Eq. (C21),

$$|\Psi_+\rangle \triangleq |\Psi_{\text{upper}}\rangle = \{(1,0)^T \otimes |\Psi_{A+}(\theta,\phi)\rangle, (1,0)^T \otimes |\Psi_{B+}(\theta,\phi)\rangle, (0,1)^T \otimes |\Psi_{A+}(\theta,\phi)\rangle, (0,1)^T \otimes |\Psi_{B+}(\theta,\phi)\rangle\}, \quad (C50)$$

which are all eigenstates of $\mathcal{H}_1$ with the same eigenenergy $E_+ = C_0 + A_1 k$. And the spinless wavefunctions $|\Psi_{A/B+}(\theta,\phi)\rangle$ are given by Eq. (C16a),

$$|\Psi_{A+}(\theta,\phi)\rangle = \frac{1}{\sqrt{2}}(\cos\theta\cos\phi - i\sin\phi, -\cos\theta\sin\phi - i\cos\phi, 0, \sin\theta)^T, \quad (C51a)$$

$$|\Psi_{B+}(\theta,\phi)\rangle = \frac{1}{\sqrt{2}}(-i\sin\theta\cos\phi, i\sin\theta\sin\phi, 1, i\cos\theta)^T, \quad (C51b)$$

where A/B represent the eigenvalues of $\vec{\mathcal{M}} \cdot \vec{n}$. The second-order perturbation theory has been presented in the Supplemental Material in Ref. [16]. To make sure the completeness of this Appendix, we repeat the discussion of the second-order perturbation in this subsection. Here, we consider the inter-band correction via second-order perturbation. The fourfold degenerate eigenstates of $\mathcal{H}_1$ with lower energy ($E_- = C_0 - A_1 k$) are given by

$$|\Psi_{\text{lower}}\rangle = \{(1,0)^T \otimes |\Psi_{B-}(\theta,\phi)\rangle, (1,0)^T \otimes |\Psi_{A-}(\theta,\phi)\rangle, (0,1)^T \otimes |\Psi_{B-}(\theta,\phi)\rangle, (0,1)^T \otimes |\Psi_{A-}(\theta,\phi)\rangle\}, \quad (C52)$$

which are all eigenstates of of $\mathcal{H}_1$ with the same eigenenergy $E_- = C_0 - A_1 k$. And the spinless wavefunctions $|\Psi_{A/B-}(\theta,\phi)\rangle$ are given by Eq. (C16b),

$$|\Psi_{A-}(\theta,\phi)\rangle = \frac{1}{\sqrt{2}}(i\sin\theta\cos\phi, -i\sin\theta\sin\phi, 1, -i\cos\theta), \quad (C53a)$$

$$|\Psi_{B-}(\theta,\phi)\rangle = \frac{1}{\sqrt{2}}(\cos\theta\cos\phi + i\sin\phi, -\cos\theta\sin\phi + i\cos\phi, 0, \sin\theta)^T. \quad (C53b)$$

Therefore, the second-order perturbed Hamiltonian is given by

$$\Delta\mathcal{H}_P^{\text{eff}(2)}(\mathbf{k}) = \frac{1}{\Delta E}(\langle\Psi_{\text{upper}}|(\mathcal{H}_{\text{soc}} + \mathcal{H}_2(\mathbf{k}))\hat{P}_{\text{lower}}(\mathcal{H}_{\text{soc}} + \mathcal{H}_2(\mathbf{k}))|\Psi_{\text{upper}}\rangle), \quad (C54)$$

where $\Delta E = E_+ - E_- = 2A_1 k$ is the energy difference between the upper-energy band the lower-energy band, and the projection operator $\hat{P}_{\text{lower}} = |\Psi_{\text{lower}}\rangle\langle\Psi_{\text{lower}}|$ onto the lower four bands in Eq. (C52). The mixed terms of $\mathcal{H}_{\text{soc}}$ and $\mathcal{H}_2(\mathbf{k})$ for the second-order perturbation are given by

$$\Delta\mathcal{H}_P^{\text{eff}(2)}(\mathbf{k}) = \frac{1}{\Delta E}(\langle\Psi_{\text{upper}}|\mathcal{H}_{\text{soc}}|\Psi_{\text{lower}}\rangle\langle\Psi_{\text{lower}}|\mathcal{H}_2(\mathbf{k})|\Psi_{\text{upper}}\rangle) + \text{H.c.,} \quad (C55)$$

with the matrix elements of $\Delta \mathcal{H}_P^{\text{eff}(2)}$

$$\left[\Delta \mathcal{H}_P^{\text{eff}(2)}\right]_{1,1} = 2\sin^2(\theta)\sin(\phi)\cos(\phi)(\sin^3(\theta)\sin(\phi) + \sin(\theta)\cos^2(\theta)\cos(\phi) - \cos^3(\theta)), \tag{C56}$$

$$\left[\Delta \mathcal{H}_P^{\text{eff}(2)}\right]_{1,2} = \sin^2(\theta)\cos(\phi)(\sin^2(\theta)\sin(2\phi) + 2i\cos(\theta)\sin(\phi)(\cos(\theta)(\cos(\theta)\cos(\phi)$$
$$+ \sin(\theta)) + \sin(\phi)(\sin^2(\theta) + i\cos(\theta)))), \tag{C57}$$

$$\left[\Delta \mathcal{H}_P^{\text{eff}(2)}\right]_{1,3} = \frac{1}{4}e^{-i\phi}\sin(\theta)\cos(\theta)(\sin(2\phi)(\sin(3\theta)\sin(\phi) + 4\cos^3(\theta)) - 8\sin(\theta)\cos^2(\theta)$$
$$\times \sin(\phi)\cos^2(\phi) + 8i\cos(\theta)\sin^2(\phi) + \left(-\frac{3}{2} + 6i\right)\sin(\theta)\cos(\phi) + \left(\frac{3}{2} + 2i\right)\sin(\theta)\cos(3\phi)), \tag{C58}$$

$$\left[\Delta \mathcal{H}_P^{\text{eff}(2)}\right]_{1,4} = e^{-i\phi}\sin(\theta)\bigg((\cos(\theta) - 1)(\cos^2(\theta)\cos(\phi) + i\sin(\theta)\sin(\phi)\cos(\phi)(-\cos^2(\theta)$$
$$+ \sin(\theta)(\cos(\theta) + i)\cos(\phi)) + \sin(\theta)\cos(\theta)\sin^2(\phi)(-1 - i\sin(\theta)\cos(\phi)))$$
$$- 2i\cos^2\left(\frac{\theta}{2}\right)(-i\cos^2(\theta)\cos(\phi)\cos(2\phi) + \sin(\phi)\cos(\phi)((\cos^3(\theta) + \cos(\theta))$$
$$\times \cos(\phi) - i\sin^2(\theta)\cos(\phi) + \sin(\theta)\cos^2(\theta)) + \sin(\theta)\cos(\theta)\sin^2(\phi)(\sin(\theta)\cos(\phi) + i))\bigg) \tag{C59}$$

and

$$\left[\Delta \mathcal{H}_P^{\text{eff}(2)}\right]_{2,2} = -\frac{1}{4}\sin^5(\theta)\sin(\phi)\sin(2\phi)(\cot^2(\theta)(-4\cot(\theta)\csc(\phi) + 4\cot(\phi) - 1) + \csc^2(\theta) + 3), \tag{C60}$$

$$\left[\Delta \mathcal{H}_P^{\text{eff}(2)}\right]_{2,3} = \frac{1}{2}e^{-i\phi}\sin(\theta)\cos(\theta)\bigg(-4\sin(\phi)(\sin(\theta)\sin(\phi) + (2 + 2i)\sin^2\left(\frac{\theta}{2}\right)\cos^2(\phi))$$
$$+ \cos^2(\theta)\sin(2\phi)\bigg(-4i\sin^2\left(\frac{\theta}{2}\right)\cos(\phi) + 2i\sin(\theta) + \csc(\phi)\bigg) + \cos(\theta)\csc(\phi)$$
$$\times \bigg(-(2 + 2i)\sin^2\left(\frac{\theta}{2}\right)\sin^2(2\phi) + \sin^2\left(\frac{\theta}{2}\right)\sin(4\phi) + 4i\sin^2(\theta)\sin^3(\phi)\cos(\phi) + \sin(2\phi)\bigg)\bigg), \tag{C61}$$

$$\left[\Delta \mathcal{H}_P^{\text{eff}(2)}\right]_{2,4} = -\frac{1}{8}e^{-i\phi}\sin(\theta)\cos(\theta)(8\cos^3(\theta)\sin(2\phi) - 16\sin(\theta)\cos^2(\theta)\sin(\phi)\cos^2(\phi)$$
$$+ 16i\cos(\theta)\sin^2(\phi) + \cos(\phi)(4\sin(3\theta)\sin^2(\phi) + (-3 + 12i)\sin(\theta))$$
$$+ (3 + 4i)\sin(\theta)\cos(3\phi)), \tag{C62}$$

and

$$\left[\Delta \mathcal{H}_P^{\text{eff}(2)}\right]_{3,3} = -\frac{1}{4}\sin^5(\theta)\sin(\phi)\sin(2\phi)(\cot^2(\theta)(-4\cot(\theta)\csc(\phi) + 4\cot(\phi) - 1) + \csc^2(\theta) + 3), \tag{C63}$$

$$\left[\Delta \mathcal{H}_P^{\text{eff}(2)}\right]_{3,4} = -i\sin^2(\theta)\sin(\phi)\cos(\phi)(2\cos^3(\theta)\cos(\phi) + 2\cos^2(\theta)(\sin(\theta) + i\sin(\phi))$$
$$+ \sin(\theta)(\sin(2\theta)\sin(\phi) - 2i\sin(\theta)\cos(\phi))), \tag{C64}$$

and

$$\left[\Delta \mathcal{H}_P^{\text{eff}(2)}\right]_{4,4} = 2\sin^2(\theta)\sin(\phi)\cos(\phi)(\sin^3(\theta)\sin(\phi) + \sin(\theta)\cos^2(\theta)\cos(\phi) - \cos^3(\theta)). \tag{C65}$$

The other parts are related by complex conjugation $[\Delta \mathcal{H}_P^{\text{eff}(2)}]_{i,j} = [\Delta \mathcal{H}_P^{\text{eff}(2)}]_{j,i}^*$.

APPENDIX D: APPROACH II FOR THE HIERARCHY OF THE QUASI SYMMETRY

In this section, we discuss the Approach II for the hierarchy of the quasisymmetry and the perturbation theory based on the solution of $\mathcal{H}_1(\mathbf{k}) + \mathcal{H}_{\text{soc}}$ for the $\mathcal{H}_2(\mathbf{k})$. Please note that

the algebra of the orbital SU(2) quasisymmetry defined in Eq. (C2) in Appendix D 1,

$$\mathcal{M}_{1,2,3} = \tfrac{1}{2}\{s_0\sigma_y\tau_z, s_0\sigma_y\tau_x, s_0\sigma_0\tau_y\}, \tag{D1}$$

which all commute with $\mathcal{H}_1(\mathbf{k}) + \mathcal{H}_{\text{soc}}$, but do not commute between themselves. And $[\mathcal{M}_i, \mathcal{M}_j] = i\epsilon_{i,j,k}\mathcal{M}_k$. Moreover, we can also defined the rotation for this orbital SU(2)

quasisymmetry group

$$\mathcal{U}(\theta, \phi)$$

$$= e^{i\theta\mathcal{M}_3} e^{i\phi\mathcal{M}_2}$$

$$= \cos\left(\frac{\theta}{2}\right)\cos\left(\frac{\phi}{2}\right)s_0\sigma_0\tau_0 + i\sin\left(\frac{\theta}{2}\right)\cos\left(\frac{\phi}{2}\right)\mathcal{M}_3$$

$$+ i\cos\left(\frac{\theta}{2}\right)\sin\left(\frac{\phi}{2}\right)\mathcal{M}_2 + i\sin\left(\frac{\theta}{2}\right)\sin\left(\frac{\phi}{2}\right)\mathcal{M}_1.$$
(D2)

Clearly, $\mathcal{U}(\theta, \phi)$ commutes with $s_0 \otimes \mathcal{H}_1(\mathbf{k}) + \mathcal{H}_{\text{soc}}$ for any values of θ and ϕ. The $\mathcal{U}(0, \frac{\pi}{2})$ can rotate $\mathcal{M}_1$ to $\mathcal{M}_3$,

$$\mathcal{U}\left(0, \frac{\pi}{2}\right) = e^{i\frac{\pi}{2}\mathcal{M}_2} = \frac{\sqrt{2}}{2}s_0 \otimes (\sigma_0\tau_0 + i\sigma_y\tau_x)$$

$$\Rightarrow \mathcal{U}\left(0, \frac{\pi}{2}\right)\mathcal{M}_1\mathcal{U}^\dagger\left(0, \frac{\pi}{2}\right) = \mathcal{M}_3. \quad \text{(D3)}$$

For better readability of this section, here, we first repeat the linear k Hamiltonian, on-site SOC Hamiltonian and k^2-order Hamiltonian,

$$\mathcal{H}_1(\mathbf{k}) = C_0\sigma_0\tau_0 + 2A_1(\mathbf{k} \cdot \mathbf{L}), \quad \text{(D4a)}$$

$$\mathcal{H}_{\text{soc}} = 4\lambda_0(\mathbf{S} \cdot \mathbf{L}), \quad \text{(D4b)}$$

$$\mathcal{H}_2(\mathbf{k}) = \mathcal{H}_{2,\mathcal{M}_1}(\mathbf{k}) + \mathcal{H}_{2,\mathcal{M}_2}(\mathbf{k}) + \mathcal{H}_{2,\mathcal{M}_3}(\mathbf{k}), \quad \text{(D4c)}$$

where the spin angular momentum $\mathbf{S} = \frac{1}{2}(s_x, s_y, s_z)$, and the orbital angular momentum operators are $\mathbf{L} = (\frac{1}{2}\sigma_y\tau_0, \frac{1}{2}\sigma_x\tau_y, -\frac{1}{2}\sigma_z\tau_y)$. And each part of $\mathcal{H}_2(\mathbf{k})$ is given by

$$\mathcal{H}_{2,\mathcal{M}_i}(\mathbf{k}) = \mathbf{g}_i(\mathbf{k}) \cdot \mathbf{J}_i, \quad \text{(D5)}$$

for $i = 1, 2, 3$. Here we define the k-dependent vectors as

$$\mathbf{g}_1(\mathbf{k}) = (C_2k_xk_y, -C_3k_xk_z, C_1k_yk_z),$$
$$\mathbf{g}_2(\mathbf{k}) = (C_3k_xk_y, C_1k_xk_z, -C_2k_yk_z),$$
$$\mathbf{g}_3(\mathbf{k}) = (C_1k_xk_y, C_2k_xk_z, -C_3k_yk_z). \quad \text{(D6)}$$

and the corresponding vectors of operators

$$\mathbf{J}_1 = (\sigma_x\tau_x, -\sigma_z\tau_x, \sigma_0\tau_z),$$
$$\mathbf{J}_2 = (\sigma_x\tau_z, \sigma_z\tau_z, \sigma_0\tau_x),$$
$$\mathbf{J}_3 = (\sigma_z\tau_0, \sigma_x\tau_0, \sigma_y\tau_y). \quad \text{(D7)}$$

In addition, we also realize that the k^2 terms of $\mathcal{H}_2(\mathbf{k})$ break this orbital $\text{SU}_o(2)$ quasisymmetry generated by $\{\mathcal{M}_{1,2,3}\}$ and lead to the splitting of all bands. However, different parts of the entire k^2 terms can lead to the reduction from $\text{SU}_o(2)$ to a orbital $\text{U}(1)$. To show that, as we discussed in the main text, we find that

$$[\mathbf{J}_i, \mathcal{M}_i] = 0 \quad \text{and} \quad \{\mathbf{J}_i, \mathcal{M}_j\} = 0 \quad \text{for } i \neq j, \quad \text{(D8)}$$

which implies

$$[\mathcal{H}_{2,\mathcal{M}_i}(\mathbf{k}), \mathcal{M}_i] = 0. \quad \text{(D9)}$$

1. The algebra for the orbital SU(2) quasi symmetry for the k^2-order Hamiltonian

In this subsection, we discuss the algebra of the orbital SU(2) quasisymmetry in Eq. (C2). To show the generality of the breaking of the orbital SU(2) quasisymmetry down to U(1) quasisymmetry by the k^2-order Hamiltonian. We can rewrite the $\mathcal{H}_2(\mathbf{k})$ into the form

$$\mathcal{H}_2(\mathbf{k}) = k_xk_y(\vec{C}_\mathcal{J} \cdot \vec{\mathcal{J}}) + k_xk_z(\vec{C}_\mathcal{P} \cdot \vec{\mathcal{P}}) + k_yk_z(\vec{C}_\mathcal{Q} \cdot \vec{\mathcal{Q}}), \quad \text{(D10)}$$

where the three $\mathbf{k}$-independent parameter vectors are

$$\vec{C}_\mathcal{J} = (C_2, -C_3, C_1),$$
$$\vec{C}_\mathcal{P} = (-C_3, C_1, C_2), \quad \text{(D11)}$$
$$\vec{C}_\mathcal{Q} = (C_1, -C_2, -C_3),$$

and the corresponding operator vectors are given by

$$\vec{\mathcal{J}} = (\sigma_x\tau_x, -\sigma_x\tau_z, \sigma_z\tau_0),$$
$$\vec{\mathcal{P}} = (-\sigma_z\tau_x, \sigma_z\tau_z, \sigma_x\tau_0),$$
$$\vec{\mathcal{Q}} = (\sigma_0\tau_z, \sigma_0\tau_x, \sigma_y\tau_y). \quad \text{(D12)}$$

Moreover, we notice that

$$[\mathcal{J}_a, \mathcal{M}_b] = i\epsilon_{\text{abc}}\mathcal{J}_c,$$
$$[\mathcal{P}_a, \mathcal{M}_b] = i\epsilon_{\text{abc}}\mathcal{P}_c,$$
$$[\mathcal{Q}_a, \mathcal{M}_b] = i\epsilon_{\text{abc}}\mathcal{Q}_c, \quad \text{(D13)}$$

where ϵ_{abc} is the three-dimensional Levi-Civita symbol with $a, b, c = 1, 2, 3$. Therefore, for arbitrary real normalized vector $\vec{n} = (n_1, n_2, n_3)$, we have the following commutation relations:

$$[\vec{\mathcal{J}} \cdot \vec{n}, \vec{\mathcal{M}} \cdot \vec{n}] = [\vec{\mathcal{P}} \cdot \vec{n}, \vec{\mathcal{M}} \cdot \vec{n}] = [\vec{\mathcal{Q}} \cdot \vec{n}, \vec{\mathcal{M}} \cdot \vec{n}] = 0. \quad \text{(D14)}$$

These can be easily shown, for example,

$$[\vec{\mathcal{J}} \cdot \vec{n}, \vec{\mathcal{M}} \cdot \vec{n}] = \sum_{a=1}^{3}\sum_{b=1}^{3} n_an_b[\mathcal{J}_a, \mathcal{M}_b]$$

$$= \sum_{a=1}^{3}\sum_{b=1}^{3} n_an_b(i\epsilon_{\text{abc}}\mathcal{J}_c)$$

$$= \sum_{a=1}^{3}\sum_{b=a+1}^{3} n_an_b(i\epsilon_{\text{abc}}\mathcal{J}_c + i\epsilon_{bac}\mathcal{J}_c) = 0. \quad \text{(D15)}$$

Here we have used $\epsilon_{\text{abc}} + \epsilon_{bac} = 0$. Therefore, we find a general symmetry-breaking case with the orbital SU(2) quasisymmetry down to the U(1) quasisymmetry. For any three normalized and orthogonal vector, $\vec{n}$, $\vec{n}'$, and $\vec{n}''$, satisfy $|\vec{n}| = |\vec{n}'| = |\vec{n}''| = 1$ and $\vec{n} \perp \vec{n}'$, $\vec{n} \perp \vec{n}''$ and $\vec{n}' \perp \vec{n}''$. Then we can do the projection for the k^2-order Hamiltonian,

$$\mathcal{H}_2(\mathbf{k}) = \mathcal{H}_{2,\vec{n}}(\mathbf{k}) + \mathcal{H}_{2,\vec{n}'}(\mathbf{k}) + \mathcal{H}_{2,\vec{n}''}(\mathbf{k}), \quad \text{(D16)}$$

where we project the parameter-vectors $(\vec{C}_\mathcal{J}, \vec{C}_\mathcal{P}, \vec{C}_\mathcal{Q})$ into the $\{\vec{n}, \vec{n}', \vec{n}''\}$ space,

$$\vec{C}_\mathcal{J} = \vec{n}(\vec{C}_\mathcal{J} \cdot \vec{n}) + \vec{n}'(\vec{C}_\mathcal{J} \cdot \vec{n}') + \vec{n}''(\vec{C}_\mathcal{J} \cdot \vec{n}''), \quad \text{(D17a)}$$

$$\vec{C}_{\mathcal{P}} = \vec{n}(\vec{C}_{\mathcal{P}} \cdot \vec{n}) + \vec{n}'(\vec{C}_{\mathcal{P}} \cdot \vec{n}') + \vec{n}''(\vec{C}_{\mathcal{P}} \cdot \vec{n}''), \quad \text{(D17b)}$$

$$\vec{C}_{\mathcal{Q}} = \vec{n}(\vec{C}_{\mathcal{Q}} \cdot \vec{n}) + \vec{n}'(\vec{C}_{\mathcal{Q}} \cdot \vec{n}') + \vec{n}''(\vec{C}_{\mathcal{Q}} \cdot \vec{n}''), \quad \text{(D17c)}$$

Therefore, the first term in Eq. (D16) is given by

$$\mathcal{H}_{2,\vec{n}}(\mathbf{k}) = k_x k_y (\vec{C}_{\mathcal{J}} \cdot \vec{n}) \times (\vec{n} \cdot \vec{\mathcal{J}}) + k_x k_z (\vec{C}_{\mathcal{P}} \cdot \vec{n})$$
$$\times (\vec{n} \cdot \vec{\mathcal{P}}) + k_y k_z (\vec{C}_{\mathcal{Q}} \cdot \vec{n})(\vec{n} \cdot \vec{\mathcal{Q}}), \quad \text{(D18)}$$

which commutes with $\mathcal{M} \cdot \vec{n}$,

$$[\mathcal{M} \cdot \vec{n}, \mathcal{H}_{2,\vec{n}}(\mathbf{k})] = 0. \quad \text{(D19)}$$

Especially, in the main text, we have mentioned three cases:

(i) $\vec{n} = (1, 0, 0)$. The $\mathcal{H}_{2,\vec{n}}(\mathbf{k})$ Hamiltonian is given by $\mathcal{H}_{2,\mathcal{M}_1}(\mathbf{k})$ in Eq. (C6).

(ii) $\vec{n} = (0, 1, 0)$. The $\mathcal{H}_{2,\vec{n}}(\mathbf{k})$ Hamiltonian is given by $\mathcal{H}_{2,\mathcal{M}_2}(\mathbf{k})$ in Eq. (C6).

(iii) $\vec{n} = (0, 0, 1)$. The $\mathcal{H}_{2,\vec{n}}(\mathbf{k})$ Hamiltonian is given by $\mathcal{H}_{2,\mathcal{M}_3}(\mathbf{k})$ in Eq. (C6).

Moreover, the U(1) quasisymmetry protected nodal-plane for $\mathcal{H}_{2,\mathcal{M}_1}$ is discussed in the main text. More details will be discussed in the following Appendices D 2, D 3, and D 4.

2. Analytical solutions by using the U(1) quasi symmetry

Furthermore, we show the important role of the orbital SU(2) quasisymmetry operators (i.e., $\mathcal{M}_{1,2,3}$) in analytically solving the eigenstate problem. Here, we take $\mathcal{H}_1(\mathbf{k})$ in Eq. (A16) or Eq. (A18) as an example,

$$\mathcal{H}_1(\mathbf{k}) = C_0 + A_1(k_x \sigma_y \tau_0 + k_y \sigma_x \tau_y - k_z \sigma_z \tau_y), \quad \text{(D20)}$$

which commutes with the orbital SU(2) quasisymmetry. Here we choose the eigenstates of $\mathcal{H}_1(\mathbf{k})$ to be the common eigenstate of $\mathcal{M}_3 = \sigma_0 \tau_y$ in Eq. (C2). It is equivalently to apply a unitary transformation

$$\mathcal{U} = \frac{1}{\sqrt{2}} s_0 \otimes \sigma_0 \otimes \begin{pmatrix} 1 & -i \\ 1 & i \end{pmatrix}, \quad \text{(D21)}$$

to the R model, which only leads to a rotation in the (τ_x, τ_y, τ_z) subspace

$$\mathcal{U}\tau_0\mathcal{U}^\dagger = \tau_0, \mathcal{U}\tau_x\mathcal{U}^\dagger = \tau_y, \mathcal{U}\tau_y\mathcal{U}^\dagger = \tau_z, \mathcal{U}\tau_z\mathcal{U}^\dagger = \tau_x. \quad \text{(D22)}$$

Therefore, the quasisymmetry $\mathcal{M}_3$ becomes $\mathcal{U}\mathcal{M}_3\mathcal{U}^\dagger = \sigma_0\tau_z$. Note that the spin Pauli matrix is dropped here. As a result, the linear k Hamiltonian becomes

$$\mathcal{U}[\mathcal{H}_1(\mathbf{k}) - C_0]\mathcal{U}^\dagger = [\mathcal{H}_{1,\mathcal{M}_3=+1}(\mathbf{k})]_{2\times2} \oplus [\mathcal{H}_{1,\mathcal{M}_3=-1}(\mathbf{k})]_{2\times2}$$
$$= \begin{pmatrix} \mathcal{H}_{1,\mathcal{M}_3=+1}(\mathbf{k}) & 0 \\ 0 & \mathcal{H}_{1,\mathcal{M}_3=-1}(\mathbf{k}) \end{pmatrix}, \quad \text{(D23a)}$$

$$\mathcal{H}_{1,\mathcal{M}_3=+1}(\mathbf{k}) = A_1(k_x\sigma_y + k_y\sigma_x - k_z\sigma_z), \quad \text{(D23b)}$$

$$\mathcal{H}_{1,\mathcal{M}_3=-1}(\mathbf{k}) = A_1(k_x\sigma_y - k_y\sigma_x + k_z\sigma_z). \quad \text{(D23c)}$$

It is easy to analytically find the eigenstates of the 2-by-2 Hamiltonian $\mathcal{H}_{1,\mathcal{M}_3=\pm1}(\mathbf{k})$, in the spherical coordinate with the momentum $\mathbf{k} = (k_x, k_y, k_z) = k(\sin\theta\cos\phi, \sin\theta\sin\phi, \cos\theta)$. The eigenstates are given by

$$\mathcal{H}_{1,\mathcal{M}_3=+1}(\mathbf{k})|A-\rangle = -A_1 k|A-\rangle, \quad \text{with } |A-\rangle = \frac{1}{\sqrt{2}\sqrt{1+\cos\theta}}(i(\cos\theta + 1), e^{-i\phi}\sin\theta)^T, \quad \text{(D24a)}$$

$$\mathcal{H}_{1,\mathcal{M}_3=+1}(\mathbf{k})|A+\rangle = A_1 k|A+\rangle, \quad \text{with } |A+\rangle = \frac{1}{\sqrt{2}\sqrt{1-\cos\theta}}(i(\cos\theta - 1), e^{-i\phi}\sin\theta)^T, \quad \text{(D24b)}$$

and by substituting the replacement $(k_x, k_y, k_z) \to (k_x, -k_y, -k_z)$ [i.e., $(\theta, \phi) \to (\theta + \pi, \pi - \phi)$], then $\cos\theta \to -\cos\theta, \sin\theta \to -\sin\theta, e^{-i\phi} \to -e^{i\phi}$ into the above solution, it results in

$$\mathcal{H}_{1,\mathcal{M}_3=-1}(\mathbf{k})|B-\rangle = -A_1 k|B-\rangle, \quad \text{with } |B-\rangle = \frac{1}{\sqrt{2}\sqrt{1-\cos\theta}}(i(-\cos\theta + 1), e^{i\phi}\sin\theta)^T, \quad \text{(D25a)}$$

$$\mathcal{H}_{1,\mathcal{M}_3=-1}(\mathbf{k})|B+\rangle = A_1 k|B+\rangle, \quad \text{with } |B+\rangle = \frac{1}{\sqrt{2}\sqrt{1+\cos\theta}}(i(-\cos\theta - 1), e^{i\phi}\sin\theta)^T, \quad \text{(D25b)}$$

where the subscripts $A(B)$ represent the eigenvalues $+1(-1)$ of the quasisymmetry $\mathcal{M}_3$. Therefore, the eigenstate of $\mathcal{H}_1(\mathbf{k})$ are given by

$$\mathcal{H}_1(\mathbf{k})|\Psi_{A/B+}(\theta, \phi)\rangle = E_+|\Psi_{A/B+}(\theta, \phi)\rangle, \quad \text{(D26a)}$$

$$\mathcal{H}_1(\mathbf{k})|\Psi_{A/B-}(\theta, \phi)\rangle = E_-|\Psi_{A/B-}(\theta, \phi)\rangle, \quad \text{(D26b)}$$

where $E_\pm = \pm A_1 k$ and the corresponding eigenstates are given by

$$|\Psi_{A-}(\theta, \phi)\rangle = |A-\rangle \otimes \left(-\frac{i}{\sqrt{2}}, \frac{1}{\sqrt{2}}\right)^T, \quad \text{(D27a)}$$

$$|\Psi_{A+}(\theta, \phi)\rangle = |A+\rangle \otimes \left(-\frac{i}{\sqrt{2}}, \frac{1}{\sqrt{2}}\right)^T, \quad \text{(D27b)}$$

$$|\Psi_{B-}(\theta, \phi)\rangle = |B-\rangle \otimes \left(\frac{i}{\sqrt{2}}, \frac{1}{\sqrt{2}}\right)^T, \quad \text{(D27c)}$$

$$|\Psi_{B+}(\theta, \phi)\rangle = |B+\rangle \otimes \left(\frac{i}{\sqrt{2}}, \frac{1}{\sqrt{2}}\right)^T. \quad \text{(D27d)}$$

Due to the presence of the orbital SU(2) symmetry, one can also find the common eigenstates of $\mathcal{H}_1(\mathbf{k})$ and $\mathcal{M} \cdot \vec{n}$ for arbitrary real vector $\vec{n}$, which is a rotation acting on the solution in Eq. (D27). Thus, the eigenstate solution is not unique

due to this twofold degeneracy, protected by the orbital SU(2) symmetry. Note that the degeneracy will be doubled if spin degeneracy is taken into account.

Similarly, we can further analytically solve $\mathcal{H}_1(\mathbf{k}) + \mathcal{H}_{\mathrm{soc}}$ by using the U(1) quasisymmetry generator $\mathcal{M}_3$. The R model in Eq. (A40) becomes

$$\mathcal{U}\mathcal{H}_R\mathcal{U}^\dagger = \mathcal{U}[s_0 \otimes \mathcal{H}_1(\mathbf{k}) + \mathcal{H}_{\mathrm{soc}} + s_0 \otimes \mathcal{H}_2(\mathbf{k})]\mathcal{U}^\dagger. \quad (D28)$$

The first two parts, $s_0 \otimes \mathcal{H}_1(\mathbf{k}) + \mathcal{H}_{\mathrm{soc}}$, preserve the orbital SU(2) symmetry, while some specific terms of the k^2-order Hamiltonian can break the SU(2) quasisymmetry down to U(1). This shows the hierarchy structure of the quasisymmetry, which will be discussed in details in Appendix D 3. Here we focus on $s_0 \otimes \mathcal{H}_1(\mathbf{k}) + \mathcal{H}_{\mathrm{soc}}$, which becomes block-diagonal after this unitary transformation defined in Eq. (D21),

$$\mathcal{U}[s_0 \otimes \mathcal{H}_1(\mathbf{k}) + \mathcal{H}_{\mathrm{soc}}]\mathcal{U}^\dagger = C_0 + \begin{pmatrix} \mathcal{H}_A(\mathbf{k}) & 0 \\ 0 & \mathcal{H}_B(\mathbf{k}) \end{pmatrix}, \quad (D29)$$

where the index $A(B)$ represent the eigenvalues $+1(-1)$ of quasisymmetry $\mathcal{M}_3$, and $\mathcal{H}_A(\mathbf{k})$ and $\mathcal{H}_B(\mathbf{k})$ are given by

$$\mathcal{H}_A(\mathbf{k}) = A_1 s_0 \otimes (k_x\sigma_y + k_y\sigma_x - k_z\sigma_z) \\ + \lambda_0(s_x\sigma_y + s_y\sigma_x - s_z\sigma_z), \quad (D30)$$

$$\mathcal{H}_B(\mathbf{k}) = A_1 s_0 \otimes (k_x\sigma_y - k_y\sigma_x + k_z\sigma_z) \\ + \lambda_0(s_x\sigma_y - s_y\sigma_x + s_z\sigma_z). \quad (D31)$$

First, one can check that the Hamiltonian can be reduced back to that in Eq. (D23) by setting $\lambda_0 = 0$. In addition, $\mathcal{H}_A(\mathbf{k})$ and $\mathcal{H}_B(\mathbf{k})$ are related to each other by time-reversal symmetry,

$$\mathcal{H}_B(\mathbf{k}) = \mathcal{T}[\mathcal{H}_A(-\mathbf{k})]\mathcal{T}^\dagger. \quad (D32)$$

Here $\mathcal{T} = is_y\mathcal{K}$ with $\mathcal{K}$ the complex conjugate. Therefore, we only need to solve the four eigenstates for $\mathcal{H}_A(\mathbf{k})$. After straightforward calculation, the four eigenenergies of $\mathcal{H}_A(\mathbf{k})$ are given by

$$E(\mathbf{k}) = C_0 + \{\pm A_1 k + \lambda_0, \pm\sqrt{A_1^2 k^2 + 4\lambda_0^2} - \lambda_0\}. \quad (D33)$$

Drop the constant C_0 for short, the two positive upper bands are

$$E_{A,+}(\mathbf{k}) = A_1 k + \lambda_0, \quad (D34a)$$

$$E_{A,-}(\mathbf{k}) = \sqrt{A_1^2 k^2 + 4\lambda_0^2} - \lambda_0, \quad (D34b)$$

which both have increasing energy as k increases, and $\pm$ are the band index. Note we have assumed $A_1 > 0$. And we notice that $E_{A,+}(\mathbf{k} = 0) = E_{A,-}(\mathbf{k} = 0)$ and $E_{A,+}(\mathbf{k}) > E_{A,-}(\mathbf{k})$ for any nonzero $\mathbf{k}$. It indicates that the SOC-induced gap between them, $E_{A,+}(\mathbf{k}) - E_{A,-}(\mathbf{k})$, approaches to $2\lambda_0$ as $k \to \infty$. By time-reversal symmetry, the four eigenenergies of $\mathcal{H}_B(\mathbf{k})$ are the same. Therefore, each state has twofold degeneracy at any nonzero $\mathbf{k}$. This is due to the presence of the orbital SU(2) symmetry.

Moreover, we can also solve the eigen wavefunctions of $\mathcal{U}[s_0 \otimes \mathcal{H}_1(\mathbf{k}) + \mathcal{H}_{\mathrm{soc}}]\mathcal{U}^\dagger$. For instance, for the two positive upper bands of $\mathcal{H}_A(\mathbf{k})$, the corresponding wavefunctions are

given by

$$\mathcal{H}_A(\mathbf{k}) \begin{cases} |E_{A,+}(\mathbf{k})\rangle = E_{A,+}(\mathbf{k})|E_{A,+}(\mathbf{k})\rangle, \\ |E_{A,-}(\mathbf{k})\rangle = E_{A,-}(\mathbf{k})|E_{A,-}(\mathbf{k})\rangle. \end{cases} \quad (D35)$$

And the corresponding eigen wavefunctions are given by

$$|E_{A,+}(\mathbf{k})\rangle = \frac{1}{\mathcal{N}_{A,+}(\mathbf{k})} \left(-i, \frac{k_x - ik_y}{k - k_z}, \frac{-ik_x + k_y}{k + k_z}, 1 \right)^T, \quad (D36a)$$

$$|E_{A,-}(\mathbf{k})\rangle = \frac{1}{\mathcal{N}_{A,-}(\mathbf{k})} (i(-A_1k_z - \lambda_0 + E_{A,-}(\mathbf{k})), \\ \times A_1(-k_x + ik_y), A_1(-ik_x + k_y), A_1k_z - \lambda_0 \\ + E_{A,-}(\mathbf{k}))^T, \quad (D36b)$$

where the normalization factors are

$$\mathcal{N}_{A,+}(\mathbf{k}) = 2k/\sqrt{k_x^2 + k_y^2}, \quad (D37a)$$

$$\mathcal{N}_{A,-}(\mathbf{k}) = 2\sqrt{(E_{A,-}(\mathbf{k}))^2 - \lambda_0^2}. \quad (D37b)$$

In addition, we discuss the band index $\pm$ that are actually eigenvalues of symmetry. To show that, we emphasize that one can also obtain the common eigenstates for $\mathcal{H}_1(\mathbf{k}) + \mathcal{H}_{\mathrm{soc}}$ and $\mathcal{M} \cdot \vec{n}$. As we discussed in Eq. (C12), there is a helicity-type symmetry operator that commutes with $\mathcal{H}_1(\mathbf{k}) + \mathcal{H}_{\mathrm{soc}}$, which indicates the index $\pm$ in the eigenstate solution $|E_{A,\pm}(\mathbf{k})\rangle$ are eigenvalues of $(\mathbf{S} + \mathbf{L}) \cdot \vec{n}_\mathbf{k}$. Explicitly, one can check that

$$[(\mathbf{S} + \mathbf{L}) \cdot \vec{n}_\mathbf{k}]|E_{A,+}(\mathbf{k})\rangle = |E_{A,+}(\mathbf{k})\rangle, \quad (D38a)$$

$$[(\mathbf{S} + \mathbf{L}) \cdot \vec{n}_\mathbf{k}]|E_{A,-}(\mathbf{k})\rangle = 0. \quad (D38b)$$

It represents the eigenvalues of the z-component angular moment of the total angular momentum at nonzero $\mathbf{k}$.

3. Approach II: The U(1) quasi symmetry protected nodal planes

As discussed in Appendix D 1, parts of the entire k^2-order Hamiltonian break the SU(2) quasisymmetry down to the U(1) quasisymmetry. For example, we consider

$$\mathcal{H}_{2,\vec{n}}(\mathbf{k}) = k_xk_y(\vec{C}_{\mathcal{J}} \cdot \vec{n}) \times (\vec{n} \cdot \vec{\mathcal{J}}) + k_xk_z(\vec{C}_{\mathcal{P}} \cdot \vec{n}) \\ \times (\vec{n} \cdot \vec{\mathcal{P}}) + k_yk_z(\vec{C}_{\mathcal{Q}} \cdot \vec{n})(\vec{n} \cdot \vec{\mathcal{Q}}), \quad (D39)$$

which commutes with $\mathcal{M} \cdot \vec{n}$,

$$[\mathcal{M} \cdot \vec{n}, \mathcal{H}_{2,\vec{n}}(\mathbf{k})] = 0. \quad (D40)$$

For an illustration, we can choose $\vec{n} = (0, 0, 1)$ without loss of generality, so that $\mathcal{M}_3$ is the symmetry generator for the remaining U(1) quasisymmetry. Therefore, we consider the Hamiltonian $\mathcal{H}_{qsR}(\mathbf{k})$ that commute with $\mathcal{M}_3$ as

$$\mathcal{H}_{qsR}(\mathbf{k}) = \mathcal{H}_1(\mathbf{k}) + \mathcal{H}_{\mathrm{soc}} + \mathcal{H}_{2,\mathcal{M}_3}(\mathbf{k}), \quad (D41a)$$

$$\mathcal{H}_1(\mathbf{k}) = C_0\sigma_0\tau_0 + 2A_1(\mathbf{k} \cdot \mathbf{L}), \quad (D41b)$$

$$\mathcal{H}_{\mathrm{soc}} = 4\lambda_0(\mathbf{S} \cdot \mathbf{L}), \quad (D41c)$$

$$\mathcal{H}_{2,\mathcal{M}_3}(\mathbf{k}) = \mathbf{g}_3 \cdot \mathbf{J}_3 = (C_1k_xk_y, C_2k_xk_z, -C_3k_yk_z) \\ \cdot (\sigma_z\tau_0, \sigma_x\tau_0, \sigma_y\tau_y), \quad (D41d)$$

where $L_x = \frac{1}{2}\sigma_y\tau_0$, $L_y = \frac{1}{2}\sigma_x\tau_y$, $L_z = -\frac{1}{2}\sigma_z\tau_y$. Notice that $\mathcal{M}_3 = \sigma_0\tau_y$ is the quasisymmetry operator. It is easy to check $[\mathcal{M}_3, \mathcal{H}_{qsR}(\mathbf{k})] = 0$. We next solve the common eigenstates of $\mathcal{M}_3$ and $\mathcal{H}_{qsR}(\mathbf{k})$. To do that, we only need to diagonalize the τ_y term for $\mathcal{H}_{qsR}(\mathbf{k})$. In other words, we apply a unitary transformation

$$\mathcal{U}_{\mathcal{M}_3} = \frac{1}{\sqrt{2}}s_0 \otimes \sigma_0 \otimes \begin{pmatrix} 1 & -i \\ 1 & i \end{pmatrix}, \qquad \text{(D42)}$$

which leads to the rotating in the (τ_x, τ_y, τ_z) subspace

$$\mathcal{U}_{\mathcal{M}_3}\tau_0\mathcal{U}_{\mathcal{M}_3}^\dagger = \tau_0, \mathcal{U}_{\mathcal{M}_3}\tau_x\mathcal{U}_{\mathcal{M}_3}^\dagger = \tau_y,$$
$$\mathcal{U}_{\mathcal{M}_3}\tau_y\mathcal{U}_{\mathcal{M}_3}^\dagger = \tau_z, \mathcal{U}_{\mathcal{M}_3}\tau_z\mathcal{U}_{\mathcal{M}_3}^\dagger = \tau_x. \qquad \text{(D43)}$$

Therefore, after this unitary transformation, the U(1) quasisymmetry generator $\mathcal{M}_3$ becomes

$$\mathcal{U}_{\mathcal{M}_3}\mathcal{M}_3\mathcal{U}_{\mathcal{M}_3}^\dagger \triangleq \mathcal{M}_{qs} = \begin{pmatrix} \sigma_0 & 0 \\ 0 & -\sigma_0 \end{pmatrix}. \qquad \text{(D44)}$$

And we take this unitary transformation on the $\mathcal{H}_{qsR}(\mathbf{k})$ Hamiltonian and obtain

$$\mathcal{U}_{\mathcal{M}_3}\mathcal{H}_{qsR}(\mathbf{k})\mathcal{U}_{\mathcal{M}_3}^\dagger \triangleq \mathcal{H}_{qsR}(\mathbf{k})$$

$$= C_0 + B_1k^2 + \begin{pmatrix} \mathcal{H}'_+(\mathbf{k}) & 0 \\ 0 & \mathcal{H}'_-(\mathbf{k}) \end{pmatrix}, \qquad \text{(D45a)}$$

where

$$\mathcal{H}'_+(\mathbf{k}) = s_0 \otimes [(A_1k_x - C_3k_yk_z)\sigma_y + (A_1k_y + C_2k_xk_z)\sigma_x - (A_1k_z - C_1k_xk_y)\sigma_z] + \lambda_0(s_x\sigma_y + s_y\sigma_x - s_z\sigma_z), \qquad \text{(D46)}$$

$$\mathcal{H}'_-(\mathbf{k}) = s_0 \otimes [(A_1k_x + C_3k_yk_z)\sigma_y - (A_1k_y - C_2k_xk_z)\sigma_x + (A_1k_z + C_1k_xk_y)\sigma_z] + \lambda_0(s_x\sigma_y - s_y\sigma_x + s_z\sigma_z). \qquad \text{(D47)}$$

This means that we have chosen the eigenstates of $\mathcal{H}_{qsR}(\mathbf{k})$ to be the common eigenstate of $\mathcal{M}_3$ or $\mathcal{M}_{qs}$. Due to the presence of the U(1) quasisymmetry, we dubbed $\mathcal{H}_{qsR}$ as the quasisymmetric R model ("qsR"). Therefore, the subscript $\pm$ for $\mathcal{H}'_\pm(\mathbf{k})$ represent the different eigenvalues of $\mathcal{M}_3$ or $\mathcal{M}_{qs}$. Besides, $\mathcal{H}'_+(\mathbf{k})$ and $\mathcal{H}'_-(\mathbf{k})$ are related to each other by TR $\mathcal{T} = is_y\mathcal{K}$ with $\mathcal{K}$ complex conjugate,

$$\mathcal{H}'_-(\mathbf{k}) = \mathcal{T}\mathcal{H}'_+(-\mathbf{k})\mathcal{T}^\dagger. \qquad \text{(D48)}$$

Next, we compute the eigenenergy of the qsR model. The energy of the upper four bands are given by

$$E_{+,1}(\mathbf{k}) = C_0 + B_1k^2 + \sqrt{A_1^2k^2 + C_1^2k_x^2k_y^2 + C_2^2k_x^2k_z^2 + C_3^2k_y^2k_z^2 - 2A_1\tilde{C}k_xk_yk_z} + \lambda_0, \qquad \text{(D49)}$$

$$E_{+,2}(\mathbf{k}) = C_0 + B_1k^2 + \sqrt{A_1^2k^2 + C_1^2k_x^2k_y^2 + C_2^2k_x^2k_z^2 + C_3^2k_y^2k_z^2 - 2A_1\tilde{C}k_xk_yk_z + 4\lambda_0^2} - \lambda_0, \qquad \text{(D50)}$$

$$E_{-,1}(\mathbf{k}) = C_0 + B_1k^2 + \sqrt{A_1^2k^2 + C_1^2k_x^2k_y^2 + C_2^2k_x^2k_z^2 + C_3^2k_y^2k_z^2 + 2A_1\tilde{C}k_xk_yk_z} + \lambda_0, \qquad \text{(D51)}$$

$$E_{-,2}(\mathbf{k}) = C_0 + B_1k^2 + \sqrt{A_1^2k^2 + C_1^2k_x^2k_y^2 + C_2^2k_x^2k_z^2 + C_3^2k_y^2k_z^2 + 2A_1\tilde{C}k_xk_yk_z + 4\lambda_0^2} - \lambda_0, \qquad \text{(D52)}$$

where $\tilde{C} = C_1 - C_2 + C_3$. The qsR model breaks the $C_{3,(111)}$ rotation symmetry because of $C_1 \neq C_2 \neq C_3$. Moreover, the $\pm$ index for $E_{\pm,i}$ means the eigenvalues of $\mathcal{M}_{qs}$,

$$\mathcal{H}_{qsR}(\mathbf{k})|E_{\pm,i}(\mathbf{k})\rangle = E_{\pm,i}(\mathbf{k})|E_{\pm,i}(\mathbf{k})\rangle, \quad \mathcal{M}_{qs}|E_{\pm,i}(\mathbf{k})\rangle = \pm|E_{\pm,i}(\mathbf{k})\rangle, \qquad \text{(D53)}$$

where $i = 1, 2$ is the band index. $E_{+,i}(\mathbf{k}) = E_{-,i}(-\mathbf{k})$ is required by TR symmetry. The quasisymmetry protected nodal planes are given by

$$k_xk_yk_z > 0, E_{+,1}(\mathbf{k}) = E_{-,2}(\mathbf{k}),$$
$$k_xk_yk_z < 0, E_{+,2}(\mathbf{k}) = E_{-,1}(\mathbf{k}). \qquad \text{(D54)}$$

The crossings are between the bands with different eigenvalue of quasisymmetry $\mathcal{M}_3$ or $\mathcal{M}_{qs}$, and thus we find nodal planes at generic momenta with the protection from the quasisymmetry $\mathcal{M}_{qs}$. By further imposing the Fermi energy constraint, there will be nodal lines on the Fermi surface, shown in Fig. 7. In Fig. 7(a), the four Fermi surfaces are plotted in the $\Gamma - R - M$ plane, where two inner FSs intersect with each other and generate the quasisymmetry protected exact crossings (marked as purple circles). In Figs. 7(b) and 7(c), the solution of Eq. (D54) are explicitly depicted, showing the exact nodal lines on the FSs.

Next, let us discuss the terms that break the quasisymmetry. By including the remaining k^2-order Hamiltonian $\mathcal{H}_{2,\mathcal{M}_1}(\mathbf{k}) + \mathcal{H}_{2,\mathcal{M}_2}(\mathbf{k})$, the full Hamiltonian is given by

$$\mathcal{H}_R(\mathbf{k}) = \mathcal{H}_{qsR}(\mathbf{k}) + \mathcal{U}_{\mathcal{M}_3}[\mathcal{H}_{2,\mathcal{M}_1}(\mathbf{k}) + \mathcal{H}_{2,\mathcal{M}_2}(\mathbf{k})]\mathcal{U}_{\mathcal{M}_3}^\dagger, \qquad \text{(D55)}$$

where the U(1) quasisymmetry breaking terms are given by

$$\mathcal{H}_{2,qsb}(\mathbf{k}) = \mathcal{U}_{\mathcal{M}_3}[\mathcal{H}_{2,\mathcal{M}_1}(\mathbf{k}) + \mathcal{H}_{2,\mathcal{M}_2}(\mathbf{k})]\mathcal{U}_{\mathcal{M}_3}^\dagger = \begin{pmatrix} 0 & s_0 \otimes H_{(2)} \\ s_0 \otimes H_{(2)}^\dagger & 0 \end{pmatrix}, \qquad \text{(D56a)}$$

$$H_{(2)} = C_1(k_yk_z\sigma_0 + k_xk_z\sigma_z) + C_2(-ik_xk_y\sigma_x + ik_yk_z\sigma_0) + C_3(k_xk_y\sigma_x + ik_xk_z\sigma_z)$$
$$+ (C_1 + iC_2)k_yk_z\sigma_0 + (C_1 + iC_3)k_xk_z\sigma_z + (-iC_2 + C_3)k_xk_y\sigma_x. \qquad \text{(D56b)}$$
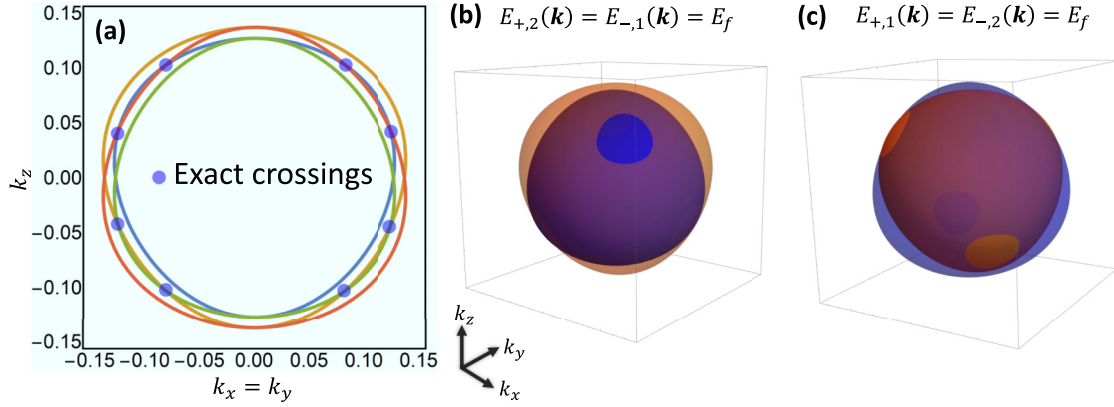
FIG. 7. The exact crossings of the eight-band qsR model. In (a), the Fermi surfaces with exact crossing are shown in the $\Gamma - R - M$ plane. In (b) and (c), we show the exact nodal lines on the FSs. These nodal lines are protected by the U(1) quasisymmetry.

Therefore, we have

$$[\mathcal{M}_{qs}, \mathcal{H}_{2,qsb}(\mathbf{k})] = 2\begin{pmatrix} 0 & h_{(2)}(\mathbf{k}) \\ -h_{(2)}^{\dagger}(\mathbf{k}) & 0 \end{pmatrix} \neq 0, \quad (D57)$$

where

$$h_{(2)} = (C_1 + iC_2)k_y k_z \sigma_0 + (C_1 + iC_3)k_x k_z \sigma_z \\ + (-iC_2 + C_3)k_x k_y \sigma_x. \quad (D58)$$

For this Hamiltonian, $[\mathcal{M}_{qs}, \mathcal{H}_{2,qsb}(\mathbf{k})] = 0$ only occurs for $\mathbf{k} = (0, 0, 0)$ (the R point). Therefore, for any Fermi surface that does not cross the R point, the nodal planes will be gapped. This leads to the quasisymmetry hierarchy mentioned in the main text [see Eq. (10)],

$$SU_s(2) \times SU_o(2) \xrightarrow{\mathcal{H}_{\text{soc}}} SU_o(2) \xrightarrow{\mathcal{H}_{2,\mathcal{M}_i}} U_o(1). \quad (D59)$$

More interestingly, as we discussed in Appendix D 1, we have shown that the choice of $\mathcal{H}_{2,\mathcal{M}_3}$ is just one specific case, instead, for any real vector $\vec{n}$ of $\mathcal{H}_{2,\vec{n}}$ that commute with $\mathcal{M} \cdot \vec{n}$ (see Appendix D 1 for details) can generally lead to the same quasisymmetry hierarchy results. Because we have

$$[\mathcal{M} \cdot \vec{n}, s_0 \otimes \mathcal{H}_1(\mathbf{k}) + \mathcal{H}_{\text{soc}} + s_0 \otimes \mathcal{H}_{2,\vec{n}}(\mathbf{k})] = 0. \quad (D60)$$

Thus, one can conclude that this analysis for the reduction from SU(2) quasisymmetry down to U(1) quasisymmetry is general, which can help to protect quasinodal plane at generic momenta.

To show this nodal plane due to the remaining U(1) quasisymmetry in our Approach II more explicitly, we next consider the perturbation to $\mathcal{H}_{2,\vec{n}}(\mathbf{k})$. Here we emphasize that one can also obtain the common eigenstates for $\mathcal{H}_1(\mathbf{k}) + \mathcal{H}_{\text{soc}}$ and $\mathcal{M} \cdot \vec{n}$. Different from Approach I in Appendix C, here we take the eigenstate solution of $s_0 \otimes \mathcal{H}_1(\mathbf{k}) + \mathcal{H}_{\text{soc}}$, and do the perturbation for the k^2-order Hamiltonian. Below we choose $\vec{n} = (0, 0, 1)$ and the corresponding U(1) quasisymmetry opeator is $\mathcal{M} \cdot \vec{n} = \mathcal{M}_3$. Recall that $\mathcal{H}_1(\mathbf{k}) + \mathcal{H}_{\text{soc}}$ becomes block diagonal after this unitary transformation defined in Eq. (D21),

$$\mathcal{U}[s_0 \otimes \mathcal{H}_1(\mathbf{k}) + \mathcal{H}_{\text{soc}}]\mathcal{U}^{\dagger} = C_0 + \begin{pmatrix} \mathcal{H}_A(\mathbf{k}) & 0 \\ 0 & \mathcal{H}_B(\mathbf{k}) \end{pmatrix}, \quad (D61)$$

where $\mathcal{H}_{A/B}(\mathbf{k})$ are given by

$$\mathcal{H}_A(\mathbf{k}) = A_1 s_0 \otimes (k_x \sigma_y + k_y \sigma_x - k_z \sigma_z) \\ + \lambda_0(s_x \sigma_y + s_y \sigma_x - s_z \sigma_z), \quad (D62)$$

$$\mathcal{H}_B(\mathbf{k}) = A_1 s_0 \otimes (k_x \sigma_y - k_y \sigma_x + k_z \sigma_z) \\ + \lambda_0(s_x \sigma_y - s_y \sigma_x + s_z \sigma_z). \quad (D63)$$

Again, note that the index $A(B)$ represent the eigenvalues $+1(-1)$ of the quasisymmetry $\mathcal{M}_3$. Therefore, after this unitary transformation, the U(1) quasisymmetry generator $\mathcal{M}_3$ becomes

$$\mathcal{U}_{\mathcal{M}_3} \mathcal{M}_3 \mathcal{U}_{\mathcal{M}_3}^{\dagger} \triangleq \mathcal{M}_{qs} = \begin{pmatrix} \sigma_0 & 0 \\ 0 & -\sigma_0 \end{pmatrix}. \quad (D64)$$

The analytical solution for the two upper bands [i.e., Eq. (D36a)] of $\mathcal{H}_1(\mathbf{k}) + \mathcal{H}_{\text{soc}}$ in Appendix D 2 are given by

$$|E_{A,+}(\mathbf{k})\rangle = \frac{1}{\mathcal{N}_{A,+}(\mathbf{k})}\left(-i, \frac{k_x - ik_y}{k - k_z}, \frac{-ik_x + k_y}{k + k_z}, 1\right)^T, \quad (D65a)$$

$$|E_{A,-}(\mathbf{k})\rangle = \frac{1}{\mathcal{N}_{A,-}(\mathbf{k})}(i(-A_1 k_z - \lambda_0 + E_{A,-}(\mathbf{k})), \\ \times A_1(-k_x + ik_y), A_1(-ik_x + k_y), \\ \times A_1 k_z - \lambda_0 + E_{A,-}(\mathbf{k}))^T. \quad (D65b)$$

where the index $\pm$ in the eigenstate solution $|E_{A,\pm}(\mathbf{k})\rangle$ are eigenvalues of $(\mathbf{S} + \mathbf{L}) \cdot \vec{n}_{\mathbf{k}}$ for nonzero $\mathbf{k}$. And the normalization factors are given by $\mathcal{N}_{A,+}(\mathbf{k}) = 2k/\sqrt{k_x^2 + k_y^2}$, and $\mathcal{N}_{A,-}(\mathbf{k}) = 2\sqrt{(E_{A,-}(\mathbf{k}))^2 - \lambda_0^2}$. Moreover, note that they are the two positive upper bands with eigenenergies,

$$E_{A,+}(\mathbf{k}) = A_1 k + \lambda_0, \quad (D66a)$$

$$E_{A,-}(\mathbf{k}) = \sqrt{A_1^2 k^2 + 4\lambda_0^2} - \lambda_0, \quad (D66b)$$

which have increasing energy as k increases. And, the eigenstates of the $\mathcal{H}_B(\mathbf{k})$ block can be related to those of $\mathcal{H}_A(\mathbf{k})$ by time-reversal symmetry,

$$|E_{B,+}(\mathbf{k})\rangle = \mathcal{T}|E_{A,+}(-\mathbf{k})\rangle, \tag{D67a}$$

$$|E_{B,-}(\mathbf{k})\rangle = \mathcal{T}|E_{A,-}(-\mathbf{k})\rangle, \tag{D67b}$$

and

$$\mathcal{H}_B(\mathbf{k})|E_{B,\pm}(\mathbf{k})\rangle = E_{A,\pm}(\mathbf{k})|E_{B,\pm}(\mathbf{k})\rangle, \tag{D68}$$

where $E_{A,\pm}(-\mathbf{k}) = E_{A,\pm}(\mathbf{k})$ has been used. Therefore, we have the four bands as a basis,

$$\{|\Psi_+(\mathbf{k})\rangle\} = \{(1,0)^T \otimes |E_{A,+}(\mathbf{k})\rangle, (1,0)^T \otimes |E_{A,-}(\mathbf{k})\rangle, (0,1)^T \otimes |E_{B,+}(\mathbf{k})\rangle, (0,1)^T \otimes |E_{B,-}(\mathbf{k})\rangle\}. \tag{D69}$$

In this basis, the $\mathcal{H}_1(\mathbf{k}) + \mathcal{H}_{\text{soc}}$ is diagonal,

$$\mathcal{H}_1(\mathbf{k}) + \mathcal{H}_{\text{soc}} = C_0 + \text{Diag}[E_{A,+}(\mathbf{k}), E_{A,-}(\mathbf{k}), E_{A,+}(\mathbf{k}), E_{A,-}(\mathbf{k})]. \tag{D70}$$

After straightforward calculation, we next project the k^2 term $\mathcal{H}_{2,\mathcal{M}_3}(\mathbf{k})$ onto the basis in Eq. (D69), and we arrive at the quasisymmetry P model (qsP model) as

$$\mathcal{H}_{qsP}(\mathbf{k}) = \begin{pmatrix} E'_{A,+}(\mathbf{k}) + f_1(\mathbf{k}) & d_1(\mathbf{k}) - id_2(\mathbf{k}) & 0 & 0 \\ d_1(\mathbf{k}) + id_2(\mathbf{k}) & E'_{A,-}(\mathbf{k}) + f_2(\mathbf{k}) & 0 & 0 \\ 0 & 0 & E'_{A,+}(\mathbf{k}) - f_1(\mathbf{k}) & d_1(\mathbf{k}) - id_2(\mathbf{k}) \\ 0 & 0 & d_1(\mathbf{k}) + id_2(\mathbf{k}) & E'_{A,-}(\mathbf{k}) - f_2(\mathbf{k}) \end{pmatrix}, \tag{D71}$$

where $E'_{A,\pm}(\mathbf{k}) = C_0 + B_1 k^2 + E_{A,\pm}(\mathbf{k})$. For the projected four-band qsP model, we check the protection from quasisymmetry as

$$[\mathcal{M}_{sq}, \mathcal{H}_{qsP}(\mathbf{k})] = 0. \tag{D72}$$

And all the other components are given by

$$f_1(\mathbf{k}) = -\tilde{C}\frac{k_x k_y k_z}{k}, \tag{D73a}$$

$$f_2(\mathbf{k}) = -A_1 \tilde{C}\frac{k_x k_y k_z}{\sqrt{A_1^2 k^2 + 4\lambda_0^2}}, \tag{D73b}$$

$$d_1(\mathbf{k}) = \frac{2(E_{A,+}(\mathbf{k}) - E_{A,-}(\mathbf{k}))k_x k_y}{\mathcal{N}_{A,+}\mathcal{N}_{A,-}}\left(C_1 + (C_2 - C_3)\frac{k_z^2}{k_x^2 + k_y^2}\right), \tag{D73c}$$

$$d_2(\mathbf{k}) = \frac{2(E_{A,+}(\mathbf{k}) - E_{A,-}(\mathbf{k}))k_z k}{\mathcal{N}_{A,+}\mathcal{N}_{A,-}}\frac{C_2 k_x^2 + C_3 k_y^2}{k_x^2 + k_y^2}. \tag{D73d}$$

The eigenenergies of the qsP model are given by

$$E_{\alpha,\beta}(\mathbf{k}) = \frac{1}{2}\left[\Delta E_+(\alpha\mathbf{k}) + \beta\sqrt{(\Delta E_-(\alpha\mathbf{k}))^2 + E_{d_{12}}}\right], \tag{D74}$$

with $\alpha, \beta = \pm$. And $\alpha = \pm$ are eigenvalues of $\mathcal{M}_{qs}$ and $\beta = \pm$ are for the band index. Here we have defined

$$E_{d_{12}}(\mathbf{k}) = 4[(d_1(\mathbf{k}))^2 + (d_2(\mathbf{k}))^2], \tag{D75a}$$

$$\Delta E_\pm(\mathbf{k}) = E'_{A,+}(\mathbf{k}) + f_1(\mathbf{k}) \pm (E'_{A,-}(\mathbf{k}) + f_2(\mathbf{k})). \tag{D75b}$$

Similar to the discussion for the nodal plane of the qsR model [see Eq. (D54)], the quasisymmetry protected nodal planes of the qsP model are give by

$$k_x k_y k_z < 0, \ E_{+,-}(\mathbf{k}) = E_{-,+}(\mathbf{k}),$$
$$k_x k_y k_z > 0, \ E_{+,+}(\mathbf{k}) = E_{-,-}(\mathbf{k}). \tag{D76}$$

The crossings happen for bands with different eigenvalue of quasisymmetry $\mathcal{M}_{qs}$. We numerically check these exact crossings on the $\Gamma - R - M$ planes, which is consistent with the results in Fig. 7(a).

4. Perturbation theory for tiny gap of the nodal plane in Approach II

The above discussion on the nodal planes in the Approach II requires a choice of specific k^2-order terms, but in real materials, all the coefficients before the k^2-order terms can generally be nonzero and at the same order. Thus, our current approach does not directly explain the near nodal plane seen in real materials. We notice that we treat the SOC terms accurately in our Approach II without any approximation, while the existence of near nodal planes in real materials actually require the SOC strength to be

much smaller than the Fermi energy. Therefore, we below consider the limit of the SOC strength $\lambda_0 \ll A_1 k_F$ (k_F is the Fermi momentum) in our Approach II, taking into account all nonzero k^2-order terms.

Following the same procedure of the perturbation projection as in the last section, we project all the k^2-order terms $\mathcal{H}_{2,\mathcal{M}_1}(\mathbf{k}) + \mathcal{H}_{2,\mathcal{M}_2}(\mathbf{k}) + \mathcal{H}_{2,\mathcal{M}_3}(\mathbf{k})$ onto the basis in Eq. (D69), and get the entire perturbation Hamiltonian,

$$
\mathcal{H}_{qsP+qsB}(\mathbf{k}) = \begin{pmatrix} E'_{A,+}(\mathbf{k}) + f_1(\mathbf{k}) & d_1(\mathbf{k}) - id_2(\mathbf{k}) & g_1(\mathbf{k}) & g_2(\mathbf{k}) \\ d_1(\mathbf{k}) + id_2(\mathbf{k}) & E'_{A,-}(\mathbf{k}) + f_2(\mathbf{k}) & g_3(\mathbf{k}) & g_4(\mathbf{k}) \\ g_1^*(\mathbf{k}) & g_3^*(\mathbf{k}) & E'_{A,+}(\mathbf{k}) - f_1(\mathbf{k}) & d_1(\mathbf{k}) - id_2(\mathbf{k}) \\ g_2^*(\mathbf{k}) & g_4^*(\mathbf{k}) & d_1(\mathbf{k}) + id_2(\mathbf{k}) & E'_{A,-}(\mathbf{k}) - f_2(\mathbf{k}) \end{pmatrix}.
\tag{D77}
$$

Here the terms d_1, d_2, f_1, f_2 have been given by Eq. (D73). In addition, the off-diagonal terms $g_{1,2,3,4}$ are generally to open a gap for the quasinodal plane. Because these off-diagonal terms break the quasisymmetry $\mathcal{M}_{qs}$. And, they are given by

$$
g_1(\mathbf{k}) = (1 - i)\tilde{C}\frac{k_x k_y k_z}{k},
\tag{D78a}
$$

$$
g_4(\mathbf{k}) = (i - 1)A_1\tilde{C}\frac{k_x k_y k_z}{E_{A,-}(\mathbf{k}) + \lambda_0},
\tag{D78b}
$$

$$
g_2(\mathbf{k}) = \frac{2}{(k_x^2 + k_y^2)\mathcal{N}_{A,+}(\mathbf{k})\mathcal{N}_{A,-}(\mathbf{k})}(C_2 + iC_3)k_x k_y(k_x^2 + k_y^2)(E_{A,-}(\mathbf{k}) - E_{A,+}(\mathbf{k}))
$$

$$
+ (C_1 + iC_3)k_x k_z(A_1 k_x k^2 - ik_y k_z(E_{A,-}(\mathbf{k}) - E_{A,+}(\mathbf{k})) - k_x k(E_{A,-}(\mathbf{k}) - \lambda_0))
$$

$$
+ (C_2 - iC_1)k_y k_z(A_1 k_y k^2 + ik_x k_z(E_{A,-}(\mathbf{k}) - E_{A,+}(\mathbf{k})) - k_y k(E_{A,-}(\mathbf{k}) - \lambda_0)),
\tag{D78c}
$$

$$
g_3(\mathbf{k}) = \frac{2}{(k_x^2 + k_y^2)\mathcal{N}_{A,+}(\mathbf{k})\mathcal{N}_{A,-}(\mathbf{k})}\{-(C_2 + iC_3)k_x k_y(k_x^2 + k_y^2)(E_{A,-}(\mathbf{k}) - E_{A,+}(\mathbf{k}))
$$

$$
+ (C_1 + iC_3)k_x k_z(A_1 k_x k^2 + ik_y k_z(E_{A,-}(\mathbf{k}) - E_{A,+}(\mathbf{k})) - k_x k(E_{A,-}(\mathbf{k}) - \lambda_0))
$$

$$
+ (C_2 - iC_1)k_y k_z(A_1 k_y k^2 - ik_x k_z(E_{A,-}(\mathbf{k}) - E_{A,+}(\mathbf{k})) - k_y k(E_{A,-}(\mathbf{k}) - \lambda_0))\}.
\tag{D78d}
$$

Here $g_3(\mathbf{k}) = -g_2(-\mathbf{k})$. The nodal planes are completely gapped out. Now we use perturbation to explain why the gap is tiny by realizing that the SOC in CoSi is weak enough for doing a perturbation expansion for the coefficients $f_{1,2}(\mathbf{k})$, $d_{1,2}(\mathbf{k})$, and $g_{1,2,3,4}(\mathbf{k})$. By setting $\lambda_0/A_1 k_F \to 0$, we obtain

$$
f_1(\mathbf{k}) = f_2(\mathbf{k}) = -\tilde{C}\frac{k_x k_y k_z}{k},
\tag{D79a}
$$

$$
d_1(\mathbf{k}) = d_2(\mathbf{k}) = 0,
\tag{D79b}
$$

$$
g_1(\mathbf{k}) = -g_2(\mathbf{k}) = (1 - i)\tilde{C}\frac{k_x k_y k_z}{k},
\tag{D79c}
$$

$$
g_2(\mathbf{k}) = g_3(\mathbf{k}) = 0,
\tag{D79d}
$$

for the zeroth-order terms. Please notice that only the diagonal energies $E'_{A,\pm}$ that are eigenenergies of $s_0 \otimes \mathcal{H}_1 + \mathcal{H}_{SOC}$ involve the SOC λ_0. As a result, the perturbation Hamiltonian in Eq. (D77) to the zeroth-order in λ_0 becomes

$$
\mathcal{H}_{qsP+qsB}^{(0)}(\mathbf{k}) = \begin{pmatrix} E'_{A,+}(\mathbf{k}) + f_1(\mathbf{k}) & 0 & g_1(\mathbf{k}) & 0 \\ 0 & E'_{A,-}(\mathbf{k}) + f_1(\mathbf{k}) & 0 & -g_1(\mathbf{k}) \\ g_1^*(\mathbf{k}) & 0 & E'_{A,+}(\mathbf{k}) - f_1(\mathbf{k}) & 0 \\ 0 & -g_1^*(\mathbf{k}) & 0 & E'_{A,-}(\mathbf{k}) - f_1(\mathbf{k}) \end{pmatrix},
\tag{D80a}
$$

$$
= \begin{pmatrix} E'_{A,+}(\mathbf{k}) + f_1(\mathbf{k}) & g_1(\mathbf{k}) \\ g_1^*(\mathbf{k}) & E'_{A,+}(\mathbf{k}) - f_1(\mathbf{k}) \end{pmatrix} \oplus \begin{pmatrix} E'_{A,-}(\mathbf{k}) + f_1(\mathbf{k}) & -g_1(\mathbf{k}) \\ -g_1^*(\mathbf{k}) & E'_{A,-}(\mathbf{k}) - f_1(\mathbf{k}) \end{pmatrix}
\tag{D80b}
$$

where the diagonal terms are $E'_{A,+}(\mathbf{k}) = C_0 + B_1 k^2 + A_1 k + \lambda_0$ and $E'_{A,-}(\mathbf{k}) = C_0 + B_1 k^2 + \sqrt{A_1^2 k^2 + 4\lambda_0^2} - \lambda_0$. Thus, the eigenenergies are given by

$$
E_{1,\pm}(\mathbf{k}) = C_0 + B_1 k^2 + A_1 k + \lambda_0 \pm \sqrt{|f_1(\mathbf{k})|^2 + |g_1(\mathbf{k})|^2},
\tag{D81a}
$$

$$
E_{2,\pm}(\mathbf{k}) = C_0 + B_1 k^2 + \sqrt{A_1^2 k^2 + 4\lambda_0^2} - \lambda_0 \pm \sqrt{|f_1(\mathbf{k})|^2 + |g_1(\mathbf{k})|^2},
\tag{D81b}
$$

which leads to the equation for the nodal-plane solution

$$
E_{1,-}(\mathbf{k}) = E_{2,+}(\mathbf{k}) \Rightarrow A_1 k - \sqrt{A_1^2 k^2 + 4\lambda_0^2} + 2\lambda_0 = 2\sqrt{|f_1(\mathbf{k})|^2 + |g_1(\mathbf{k})|^2}.
\tag{D82}
$$

In the $k \to \infty$ limit, this equation becomes

$$\lambda_0 = \sqrt{|f_1(\mathbf{k})|^2 + |g_1(\mathbf{k})|^2} = \sqrt{3}\tilde{C}\left|\frac{k_x k_y k_z}{k}\right|. \tag{D83}$$

Note that $\tilde{C} > 0$ in this paper. And it is exactly the same Eq. (C46) obtained from the Approach I in Appendix C. At small $\mathbf{k}$, they differs from each other. Moreover, the first-order correction from λ_0 will open a tiny gap for the nodal planes, which is actually the second-order perturbation theory in Approach I. Based on this analysis, we conclude that the results of Approach II is equivalent from those of Approach I.

[1] N. Goldenfeld, *Lectures on Phase Transitions and the Renormalization Group* (CRC Press, Boca Raton, FL, 2018).

[2] D. C. Mattis, *Theory Of Magnetism Made Simple, The: An Introduction To Physical Concepts And To Some Useful Mathematical Methods* (World Scientific, Singapore, 2006).

[3] G. E. Volovik, *The Universe in a Helium Droplet* (Oxford University Press, Oxford, 2003), Vol. 117.

[4] G. E. Volovik, Phys. Rep. **351**, 195 (2001).

[5] A. H. Castro Neto, F. Guinea, N. M. R. Peres, K. S. Novoselov, and A. K. Geim, Rev. Mod. Phys. **81**, 109 (2009).

[6] D. N. Basov, M. M. Fogler, A. Lanzara, F. Wang, and Y. Zhang, Rev. Mod. Phys. **86**, 959 (2014).

[7] M. Z. Hasan and C. L. Kane, Rev. Mod. Phys. **82**, 3045 (2010).

[8] X.-L. Qi and S.-C. Zhang, Rev. Mod. Phys. **83**, 1057 (2011).

[9] B. A. Bernevig, *Topological Insulators and Topological Superconductors* (Princeton University Press, Princeton, 2013).

[10] M. Franz and L. Molenkamp, *Topological Insulators* (Elsevier, Amsterdam, 2013).

[11] S.-Q. Shen, *Topological Insulators: Dirac Equation in Condensed Matter* (Springer, New York, 2018).

[12] A. K. Geim and K. S. Novoselov, Nat. Mater. **6**, 183 (2007).

[13] K. Yang, S. Das Sarma, and A. H. MacDonald, Phys. Rev. B **74**, 075423 (2006).

[14] K. Nomura and A. H. MacDonald, Phys. Rev. Lett. **96**, 256602 (2006).

[15] A. F. Young, C. R. Dean, L. Wang, H. Ren, P. Cadden-Zimansky, K. Watanabe, T. Taniguchi, J. Hone, K. L. Shepard, and P. Kim, Nat. Phys. **8**, 550 (2012).

[16] C. Guo, L. Hu, C. Putzke, J. Diaz, X. Huang, K. Manna, F.-R. Fan, C. Shekhar, Y. Sun, C. Felser *et al.*, Nat. Phys. **18**, 813 (2022).

[17] M. S. Dresselhaus, G. Dresselhaus, and A. Jorio, *Group Theory: Application to the Physics of Condensed Matter* (Springer Science & Business Media, New York, 2007).

[18] F. Tang and X. Wan, Phys. Rev. B **104**, 085137 (2021).

[19] Z.-M. Yu, Z. Zhang, G.-B. Liu, W. Wu, X.-P. Li, R.-W. Zhang, S. A. Yang, and Y. Yao, Sci. Bull. **67**, 375 (2022).

[20] Z. Zhang, G.-B. Liu, Z.-M. Yu, S. A. Yang, and Y. Yao, Phys. Rev. B **105**, 104426 (2022).

[21] F. Tang and X. Wan, Phys. Rev. B **105**, 155156 (2022).

[22] R. Winkler, *Spin-Orbit Coupling Effects in Two-Dimensional Electron and Hole Systems* (Springer, Berlin, 2003), Vol. 191.

[23] P. Tang, Q. Zhou, and S.-C. Zhang, Phys. Rev. Lett. **119**, 206402 (2017).

[24] B. Bradlyn, L. Elcoro, J. Cano, M. G. Vergniory, Z. Wang, C. Felser, M. I. Aroyo, and B. A. Bernevig, Nature (London) **547**, 298 (2017).

[25] Y. Xu, L. Elcoro, Z.-D. Song, B. J. Wieder, M. G. Vergniory, N. Regnault, Y. Chen, C. Felser, and B. A. Bernevig, Nature (London) **586**, 702 (2020).

[26] L. Elcoro, B. J. Wieder, Z. Song, Y. Xu, B. Bradlyn, and B. A. Bernevig, Nat. Commun. **12**, 5965 (2021).

[27] B. Bradlyn, J. Cano, Z. Wang, M. Vergniory, C. Felser, R. J. Cava, and B. A. Bernevig, Science **353**, aaf5037 (2016).

[28] N. Huber, K. Alpin, G. L. Causer, L. Worch, A. Bauer, G. Benka, M. M. Hirschmann, A. P. Schnyder, C. Pfleiderer, and M. A. Wilde, Phys. Rev. Lett. **129**, 026401 (2022).

[29] A. Leonhardt, M. M. Hirschmann, N. Heinsdorf, X. Wu, D. H. Fabini, and A. P. Schnyder, Phys. Rev. Mater. **5**, 124202 (2021).

[30] D. Gottesman, Phys. Rev. A **54**, 1862 (1996).

[31] D. Gottesman, Stabilizer codes and quantum error correction, Ph.D. thesis, California Institute of Technology, 1997.

[32] B. A. Bernevig, Z.-D. Song, N. Regnault, and B. Lian, Phys. Rev. B **103**, 205413 (2021).

[33] B. Lian, Z.-D. Song, N. Regnault, D. K. Efetov, A. Yazdani, and B. A. Bernevig, Phys. Rev. B **103**, 205414 (2021).

[34] E. Wigner and H. Margenau, Am. J. Phys. **35**, 1169 (1967).

[35] S. Murakami, S. Iso, Y. Avishai, M. Onoda, and N. Nagaosa, Phys. Rev. B **76**, 205304 (2007).

[36] X. Xu, X. Wang, T. A. Cochran, D. S. Sanchez, G. Chang, I. Belopolski, G. Wang, Y. Liu, H.-J. Tien, X. Gui, W. Xie, M. Z. Hasan, T.-R. Chang, and S. Jia, Phys. Rev. B **100**, 045104 (2019).

[37] D. S. Wu, Z. Y. Mi, Y. J. Li, W. Wu, P. L. Li, Y. T. Song, G. T. Liu, G. Li, and J. L. Luo, Chin. Phys. Lett. **36**, 077102 (2019).

[38] H. Wang, S. Xu, X.-Q. Lu, X.-Y. Wang, X.-Y. Zeng, J.-F. Lin, K. Liu, Z.-Y. Lu, and T.-L. Xia, Phys. Rev. B **102**, 115129 (2020).

[39] Z. Ni, K. Wang, Y. Zhang, O. Pozo, B. Xu, X. Han, K. Manna, J. Paglione, C. Felser, A. G. Grushin *et al.*, Nat. Commun. **12**, 154 (2021).

[40] M. Yao, K. Manna, Q. Yang, A. Fedorov, V. Voroshnin, B. V. Schwarze, J. Hornung, S. Chattopadhyay, Z. Sun, S. N. Guin *et al.*, Nat. Commun. **11**, 2033 (2020).

[41] J.-Z. Ma, Q.-S. Wu, M. Song, S.-N. Zhang, E. B. Guedes, S. A. Ekahana, M. Krivenkov, M. Y. Yao, S.-Y. Gao, W.-H. Fan *et al.*, Nat. Commun. **12**, 3994 (2021).

[42] S. Xu, L. Zhou, X.-Y. Wang, H. Wang, J.-F. Lin, X.-Y. Zeng, P. Cheng, H. Weng, and T.-L. Xia, Chin. Phys. Lett. **37**, 107504 (2020).

[43] N. B. M. Schröter, D. Pei, M. G. Vergniory, Y. Sun, K. Manna, F. de Juan, J. A. Krieger, V. Süss, M. Schmidt, P. Dudin *et al.*, Nat. Phys. **15**, 759 (2019).

[44] N. B. M. Schröter, S. Stolz, K. Manna, F. de Juan, M. G. Vergniory, J. A. Krieger, D. Pei, T. Schmitt, P. Dudin, T. K. Kim *et al.*, Science **369**, 179 (2020).

[45] P. Sessi, F.-R. Fan, F. Küster, K. Manna, N. B. M. Schröter, J.-R. Ji, S. Stolz, J. A. Krieger, D. Pei, T. K. Kim *et al.*, Nat. Commun. **11**, 3507 (2020).

[46] G. Chang, S.-Y. Xu, B. J. Wieder, D. S. Sanchez, S.-M. Huang, I. Belopolski, T.-R. Chang, S. Zhang, A. Bansil, H. Lin, and M. Z. Hasan, Phys. Rev. Lett. **119**, 206401 (2017).

[47] D. Rees, K. Manna, B. Lu, T. Morimoto, H. Borrmann, C. Felser, J. E. Moore, D. H. Torchinsky, and J. Orenstein, Sci. Adv. **6**, eaba0509 (2020).

[48] See Supplemental Material at http://link.aps.org/supplemental/10.1103/PhysRevB.107.125145 for more details of the construction of the 4D irreducible representations, perturbations for linear k SOC terms and projected two-band model, which includes Refs. [16,24–27,49].

[49] N. Marzari, A. A. Mostofi, J. R. Yates, I. Souza, and D. Vanderbilt, Rev. Mod. Phys. **84**, 1419 (2012).